COMENIUS UNIVERSITY BRATISLAVA
FACULTY OF PHARMACY

INTERACTION OF MODEL MEMBRANES WITH SURFACTANTS AND ANTIMICROBIAL PEPTIDES

Dissertation thesis

Bratislava 2022
Mgr. Katarína Želinská

COMENIUS UNIVERSITY BRATISLAVA
FACULTY OF PHARMACY

INTERACTION OF MODEL MEMBRANES WITH SURFACTANTS AND ANTIMICROBIAL PEPTIDES

Dissertation thesis

Study programme:	Pharmaceutical chemistry
Department:	Department of Physical Chemistry of Drugs
Tutor:	doc. RNDr. Jana Gallová, CSc.
Consultants:	Mgr. Bruno Demé, PhD., Mgr. Norbert Kučerka, DrSc.

Bratislava 2022
Mgr. Katarína Želinská

Comenius University Bratislava
Faculty of Pharmacy

THESIS ASSIGNMENT

Name and Surname:	Mgr. Katarína Želinská
Study programme:	Pharmaceutical Chemistry (Single degree study, Ph.D. III. deg., external form)
Field of Study:	Pharmacy
Type of Thesis:	Dissertation thesis
Language of Thesis:	English
Secondary language:	Slovak

Title: Interaction of model membranes with surfactants and antimicrobial peptides.

Tutor:	doc. RNDr. Jana Gallová, CSc.
Consultant:	Mgr. Norbert Kučerka, DrSc.
Consultant:	Mgr. Bruno Demé, PhD.
Department:	FaF.KFChL - Department of Physical Chemistry of Drugs
Head of Department:	prof. RNDr. Daniela Uhríková, CSc.

Electronic version available:
dočasne neprístupná, po uplynutí bez obmedzenia

Assigned: 07.09.2020

Approved: 09.09.2020

prof. RNDr. Peter Mikuš, PhD.
Guarantor of Main Study Field

.....
Student

.....
Tutor

Univerzita Komenského v Bratislave
Farmaceutická fakulta

ZADANIE ZÁVEREČNEJ PRÁCE

Meno a priezvisko študenta: Mgr. Katarína Želinská
Študijný program: farmaceutická chémia (Jednoodborové štúdium, doktorandské III. st., externá forma)
Študijný odbor: farmácia
Typ záverečnej práce: dizertačná
Jazyk záverečnej práce: anglický
Sekundárny jazyk: slovenský

Názov: Interaction of model membranes with surfactants and antimicrobial peptides.
Interakcia modelových membrán s tenzidmi a antimikrobiálnymi peptidmi.

Školiteľ: doc. RNDr. Jana Gallová, CSc.
Konzultant: Mgr. Norbert Kučerka, DrSc.
Konzultant: Mgr. Bruno Demé, PhD.
Katedra: FaF.KFChL - Katedra fyzikálnej chémie liečiv
FaF vedúci katedry: prof. RNDr. Daniela Uhríková, CSc.

Spôsob sprístupnenia elektronickej verzie práce:
dočasne neprístupná, po uplynutí bez obmedzenia

Dátum zadania: 07.09.2020

Dátum schválenia: 09.09.2020

prof. RNDr. Peter Mikuš, PhD.
osoba zodpovedná za realizáciu študijného programu

.....
študent

.....
školiteľ

ACKNOWLEDGEMENTS

I would like to take this opportunity to thank

doc. RNDr. Jana Gallová, CSc., my supervisor, for all the professional guidance, valuable advice, patience and her human approach even outside the professional field throughout my whole study,

prof. RNDr. Daniela Uhríková, CSc., head of the Department of Physical Chemistry of Drugs, Faculty of Pharmacy, for help with the evaluation of SANS data, funding, all her valuable advice and work opportunity,

prof. Ing. Vladimír Frecer, CSc., for help with the funding of our experiments and help with the mathematics courses,

Mgr. Bruno Demé, PhD., Mgr. Norbert Kučerka, DrSc., for their help with measurements and evaluation of the SANS and SAND experiments,

thanks to ILL for neutron beamtime on D16 diffractometer (DOI: 10.5291/ILL-DATA.8-02-862) and JINR for neutron beamtime on small-angle neutron spectrometer YuMO,

to the entire team of the Department of Physical Chemistry of Drugs, Faculty of Pharmacy and Large-Scale Structure Group at ILL, for creating a pleasant and friendly environment, with special thanks to my colleagues and friends Mgr. Silvia Huláková, PhD., Mgr. Lukáš Hubčík, PhD. and Mgr. Loreto Misuraca, PhD.,

and last but not least, the biggest thanks to my family and my fiancé for their immense love and support.

DECLARATION OF HONOUR

I declare that I have prepared this dissertation thesis independently under the guidance of my supervisor, doc. RNDr. Jana Gallová, CSc., using the cited references.

In Bratislava, ……

ABSTRACT

This thesis examines the interaction of surfactant *N*,*N*-dimethyl-1-dodecanamine-*N*-oxide (DDAO) with various mammalian and bacterial model membranes. This thesis also explores the effect of antimicrobial peptide dermaseptin S1 (DS1) on the permeability of bacterial model membrane. Mixtures of palmitoyloleoylphosphatidylcholine (POPC) or dioleoylphosphatidyl-choline (DOPC) with cholesterol (CHOL) were used as models of mammalian model membrane. Lipids palmitoyloleoylphosphatidylethanolamine (POPE), palmitoyloleoyl-phosphatidylglycerol (POPG) and tetraoleoylcardiolipin (TOCL) were used in bacterial model membranes to mimic the inner membrane of *Escherichia coli*. The solubilisation process is a complex process describing membrane-surfactant interaction in a wide range of surfactant concentration, from the partitioning and pore formation in the initial stage, to saturation of the membrane by surfactant and subsequent transition of liposomes into lipid-surfactant mixed aggregates. Disruption of bacterial membranes is the mechanism of antimicrobial effect of surfactants. The solubilisation process was studied nephelometrically on unilamellar liposomes (ULLs). Less DDAO was needed to solubilise the mammalian model membrane (POPC-CHOL) when compared to the bacterial model membranes. The TOCL containing bacterial model membrane (POPE-POPG-TOCL) was more stable against the DDAO-induced solubilisation than POPE-POPG. Creation of membrane pores was studied using the fluorescent probe leakage method. We found that the bacterial model membrane (POPE-POPG) was more resistant against the DDAO-induced leakage of the fluorescent probe than the mammalian model (POPC-CHOL). The complete release of the probe occurred at a concentration of DDAO that was lower than the concentration causing liposome disintegration. We calculated the partition coefficients of DDAO between the lipid bilayers and the water phase, 2300 ± 300 for POPC-CHOL, 4800 ± 500 for POPE-POPG and 6500 ± 500 for POPE-POPG-TOCL. Our data show that the partitioning coefficient of DDAO is higher when interacting with bacterial model membranes and the bacterial model membranes need more incorporated surfactant to undergo solubilisation. The leakage of the fluorescent probe was also observed after the addition of the antimicrobial peptide DS1. DS1 proved to be highly effective in releasing of the probe even at small molar ratios of n_{DS1}:n_{LIPID}, even though the DS1 was not able to completely release the probe. The small-angle neutron scattering method was used to study the structural parameters of the bilayers in ULLs made of DOPC, DOPC-CHOL and POPE-POPG and the geometry of the aggregates created after the addition of DDAO. With the increase of the molar ratio n_{DDAO}:n_{LIPID}, we have observed decreasing bilayer thickness, followed by a transition from liposomes into cylinders with elliptical cross section. In case

of POPE-POPG, the transition occurred at higher n_{DDAO}:n_{LIPID} molar ratio than for the two mammalian models. The cross-sectional dimensions of the cylinders suggested that the longitudinal part of the ellipse is formed by LIPID-DDAO mixed bilayer that is stabilised by a DDAO-rich rim. Small-angle neutron diffraction experiments on oriented stacks of lipid bilayers at 97% relative humidity were carried out with the intention of reconstructing the neutron scattering length density (NSLD) profiles of mammalian and bacterial model membranes with the addition of DDAO and DS1. Similar results were obtained for both types of model membrane – POPC-CHOL and POPE-POPG. We observed decrease in the bilayer thickness with increasing amount of DDAO incorporated into the membrane, accompanied by an increase in the area per lipid molecule. Membrane-incorporated DDAO did not prove to have an effect on the water distribution probability, as the water layer thickness and the width of the lipid/water interface stayed approximately the same. Samples containing DS1 showed unstable repeat spacing in different contrasts, preventing us from being able to calculate the NSLD profiles.

Key words: surfactant, antimicrobial peptide, liposome, solubilisation, static light scattering, fluorescence spectroscopy, SANS, SAND

ABSTRAKT

Táto práca skúma interakciu tenzidu *N*,*N*-dimetyl-1-dodekánamín-*N*-oxidu (DDAO) s rôznymi cicavčími a bakteriálnymi modelovými membránami. Táto práca tiež skúma vplyv antimikrobiálneho peptidu dermaseptínu S1 (DS1) na permeabilitu membrány bakteriálneho modelu. Zmesi palmitoyloleoylfosfatidylcholínu (POPC) alebo dioleoylfosfatidylcholínu (DOPC) s cholesterolom (CHOL) boli použité ako modely membrány cicavčieho modelu. Lipidy palmitoyloleoylfosfatidyletanolamín (POPE), palmitoyloleoylfosfatidylglycerol (POPG) a tetraoleoylkardiolipín (TOCL) boli použité v bakteriálnych modelových membránach na napodobenie vnútornej membrány *Escherichia coli*. Solubilizácia je komplexný proces opisujúci interakciu membrána-tenzid v širokom rozmedzí koncentrácie tenzidu, od rozdeľovania a tvorby pórov v počiatočnej fáze, po saturáciu membrány tenzidom a následnú premenu lipozómov na zmesné lipid-tenzid agregáty. Narušenie bakteriálnych membrán je mechanizmom antimikrobiálneho účinku tenzidov. Proces solubilizácie unilamelárnych lipozómov bol študovaný nefelometricky. Na solubilizáciu membrány cicavčieho modelu (POPC-CHOL) bolo potrebné menej DDAO v porovnaní s bakteriálnymi membránami. Bakteriálna modelová membrána obsahujúca TOCL (POPE-POPG-TOCL) bola v porovnaní s POPE-POPG stabilnejšia voči solubilizácii indukovanej DDAO. Tvorba pórov v modelových membránach bola študovaná pomocou metódy uvoľňovania fluorescenčnej sondy. Zistili sme, že membrána bakteriálneho modelu (POPE-POPG) bola odolnejšia voči úniku fluorescenčnej sondy vyvolanému DDAO ako cicavčí model (POPC-CHOL). K úplnému uvoľneniu sondy došlo pri nižšej koncentrácii DDAO ako je koncentrácia spôsobujúca rozpad lipozómov. Vypočítali sme rozdeľovacie koeficienty DDAO medzi lipidovými dvojvrstvami a vodnou fázou, 2300 ± 300 pre POPC-CHOL, 4800 ± 500 pre POPE-POPG a 6500 ± 500 pre POPE-POPG-TOCL. Naše údaje ukazujú, že rozdeľovací koeficient DDAO je vyšší pri interakcii s bakteriálnymi modelovými membránami a že bakteriálne modelové membrány potrebujú na solubilizáciu viac inkorporovaného tenzidu. Únik fluorescenčnej sondy bol tiež pozorovaný po pridaní antimikrobiálneho peptidu DS1. DS1 sa preukázal byť vysoko účinný pri uvoľňovaní sondy aj pri malých mólových pomeroch n_{DS1}:n_{LIPID}, aj keď DS1 nebol schopný sondu kompletne uvoľniť. Metóda rozptylu neutrónov pod malými uhlami bola použitá na štúdium štruktúrnych parametrov dvojvrstiev unilamelárnych lipozómov pripravených z DOPC, DOPC-CHOL a POPE-POPG a geometrie agregátov vytvorených po pridaní DDAO. So zvýšením mólového pomeru n_{DDAO}:n_{LIPID} sme pozorovali klesajúcu hrúbku dvojvrstvy, nasledovala premena lipozómov na cylindre s eliptickým prierezom. V prípade POPE-POPG sa prechod vyskytol pri vyššom mólovom pomere n_{DDAO}:n_{LIPID} ako v prípade oboch

cicavčích modelov. Prierezové rozmery cylindrov naznačovali, že pozdĺžna časť elipsy je tvorená zmiešanou dvojvrstvou LIPID-DDAO, ktorá je stabilizovaná okrajom bohatým na molekuly DDAO. Experimenty s difrakciou neutrónov pod malými uhlami na orientovaných vzorkách pri 97% relatívnej vlhkosti sa uskutočnili so zámerom rekonštruovať profily hustoty rozptylovej dĺžky neutrónov cicavčích a bakteriálnych modelových membrán s prídavkom DDAO a DS1. Podobné výsledky boli získané pre oba typy modelovej membrány – POPC-CHOL a POPE-POPG. Pozorovali sme pokles hrúbky dvojvrstvy so zvyšujúcim sa množstvom DDAO inkorporovaného do membrány, sprevádzaný nárastom plochy pripadajúcej na jednu molekulu lipidu. DDAO začlenené do membrány nepreukázalo vplyv na pravdepodobnosť distribúcie vody, pretože hrúbka vodnej vrstvy a šírka rozhrania lipid/voda zostali približne rovnaké. Vzorky obsahujúce DS1 vykazovali nestabilné mriežkové parametre pri meraniach v rôznych kontrastoch, čo nám zabránilo v možnosti vypočítať profily hustoty rozptylovej dĺžky neutrónov.

Kľúčové slová: tenzid, antimikrobiálny peptid, lipozóm, solubilizácia, statický rozptyl svetla, fluorescenčná spektroskopia, SANS, SAND

INTRODUCTION

Biological membranes are complex macromolecular aggregates necessary for cell function. Fundamental part of biological membrane is the lipid bilayer, which is a fluid system that provides structural support for other membrane components. Due to the structural complexity of biological membranes, it is more suitable to study model phospholipid membranes in the form of spherical liposomes.

Research on bacterial model membranes and their interactions with potential new pharmacotherapeutics is currently of great importance due to the alarming increase in the number of cases of multidrug-resistant bacterial infections. In particular, infections caused by multi-resistant G^- pathogenic bacteria pose a serious public health threat. Bactericidal surfactants, such as *N*-oxides, and antimicrobial peptides are promising substances exhibiting antimicrobial effects. In this thesis we are studying the interactions of surfactant *N,N*-dimethyl-1-dodecanamine-*N*-oxide (DDAO) and antimicrobial peptide dermaseptin S1 (DS1) with various mammalian and bacterial model membranes.

DDAO is often used in pharmaceutical and cosmetic formulations, as surfactants in cleaning products and also for research in membrane and protein studies. Due to its non-specific interaction with the membranes, it also exhibits haemolytic effect. Therefore, it is necessary to study its effect on mammalian membranes as well, to ensure it does not exert toxic actions on animals and humans. The goal of this thesis was to study the complex process of solubilisation of mammalian and bacterial model membranes by DDAO, from the partitioning and pore creation to the transition of liposomes into lipid-surfactant mixed aggregates.

Dermaseptins interact with the lipid bilayer of the target organism. This interaction leads to permeabilization and eventual cell lysis. Despite intensive research dedicated to antimicrobial peptides, we still do not know all about their interactions. The goal of this thesis was to study the effect of DS1 on the permeability and stability of model membranes.

This thesis was created at the Department of physical chemistry of drugs, Faculty of Pharmacy, Comenius University in Bratislava, supported by the VEGA grants 1/0916/16 (prof. RNDr. Daniela Uhríková, CSc.) and 1/0228/17, APVV project 17-0239 (prof. Ing. Vladimír Frecer, CSc.), FaF UK grants FaF-30-2017, FaF-21-2018 (Mgr. Katarína Želinská) and JINR topical themes 04-4-1121-2015/2020, 04-4-1142-2021/2025. This work benefited from the use of the SasView application, originally developed under NSF award DMR-0520547. Part of this work was created during a student internship at Institut Laue-Langevin, Grenoble, France, under the supervision of Mgr. Bruno Demé, PhD.

TABLE OF CONTENTS

LIST OF ABBREVIATIONS

acetyl-CoA	acetyl coenzyme A
AA, AAs	amino acid, amino acids
CHOL	cholesterol
CL, CLs	cardiolipin, cardiolipins
DDAO	*N*,*N*-dimethyl-1-dodecanamine-*N*-oxide
DOPC	dioleoylphosphatidylcholine
DOPE	dioleoylphosphatidylethanolamine
DS1	dermaseptin S1
E. coli	*Escherichia coli*
EYPC	egg yolk phosphatidylcholine
EYSM	egg yolk sphingomyelin
FA, FAs	fatty acid, fatty acids
G^+, G^-	gram-positive, gram-negative
GLs	glycolipids
GULs	giant unilamellar liposomes
L_α, L_d	liquid-crystalline phase, liquid-disordered phase
L_β, S_o	lamellar gel phase, solid-ordered phase
L_C	lamellar crystalline phase
L_o	liquid-ordered phase
LPS	lipopolysaccharide
LULs	large unilamellar liposomes
MLLs	multilamellar liposomes
MVLs	multivesicular liposomes
NSLD	neutron scattering length density
$P_{\beta'}$	rippled gel phase
PA, PAs	phosphatidic acid, phosphatidic acids
PC, PCs	phosphatidylcholine, phosphatidylcholines
PE, PEs	phosphatidylethanolamine, phosphatidylethanolamines
PG, PGs	phosphatidylglycerol, phosphatidylglycerols
PI, PIs	phosphatidylinositol, phosphatidylinositols
POPC	palmitoyloleoylphosphatidylcholine
POPE	palmitoyloleoylphosphatidylethanolamine
POPG	palmitoyloleoylphosphatidylglycerol
PS, PSs	phosphatidylserine, phosphatidylserines
PSM	palmitoylsphingomyelin
SAND	small-angle neutron diffraction
SANS	small-angle neutron scattering
SDS	sodium dodecylsulphate
SM, SMs	sphingomyelin, sphingomyelins
SULs	small unilamellar liposomes
TOCL	tetraoleoylcardiolipin
TX-100	triton X-100
ULLs	unilamellar liposomes
w%	weight percentage

1 THE CURRENT KNOWLEDGE

1.1 Biological membrane: function and composition

Biological membranes play an irreplaceable function in cell protection – they form selective barriers that separate, communicate and define cells and their internal organelles. They receive and promote important signals that control the behaviour of the cell (Escribá and Nicolson, 2014). The currently accepted model of biological membrane is called the ***fluid mosaic model***, proposed in 1972 by Singer and Nicolson. The membrane has been described as an oriented, two-dimensional, viscous solution of amphiphilic proteins (or lipoproteins) and lipids in instant thermodynamic equilibrium (Singer and Nicolson, 1972). Its modifications have been suggested in 1997, in the works of Simons and Ikonen (1997) and Brown and London, (1997). It has been pointed out that biological membranes do not form a homogeneous fluid lipid phase, but it was proposed that the lipids are organized into phase – separated microdomains, called ***lipid rafts***, characterized by specific composition and molecular dynamics different from their surroundings in the liquid-crystalline phase.

Biological membranes are very complex structures composed of lipids, proteins and oligosaccharides. Membrane proteins are dispersed in the membrane at low concentrations, some pass through the entire lipid bilayer (transmembrane proteins), and others are found only on its surface (peripheral proteins). Some proteins occupy a small space in the biological membrane, but have large ectodomains that cover lipids, thereby creating steric hindrances. The fluidity of the lipid bilayer makes it possible to adapt to relatively rigid protein molecules (Engelman, 2005).

1.1.1 Lipids

Lipids are a large and heterogeneous group of substances of biological origin, characterized by their good solubility in organic solvents, methanol, acetone, chloroform and benzene. In contrast, they are either insoluble or only very poorly soluble in water (Koolman and Roehm, 2005). They are usually divided into three classes: ***simple lipids*** (higher hydrocarbons, higher alcohols, higher carboxylic acids, triacylglycerols etc.), ***complex lipids*** (also called polar lipids, e.g. phospholipids, glycolipids etc.) and ***derived lipids*** (also known as isoprenoids, for example terpenes or steroids) (Dobrota, 2012).

Higher carboxylic acids (fatty acids, FAs) consist of the unbranched hydrocarbon chain (in the figures often marked with R–) and the terminal carboxyl group (–COOH). In cells, they occur rarely on their own, only transiently during biochemical reactions or during

transport from cell to cell, while bound to certain transport proteins (lipoproteins). However, they are fundamental components of complex lipids. The most commonly occurring FAs have chains with lengths from 14 to 22 carbons. The organism produces saturated FAs as a result of the activity of a multienzyme complex, called fatty acid synthase. Since the precursor of the synthesis is a 2-carbon fragment (acetyl-CoA), odd number of carbon atoms rarely occurs.

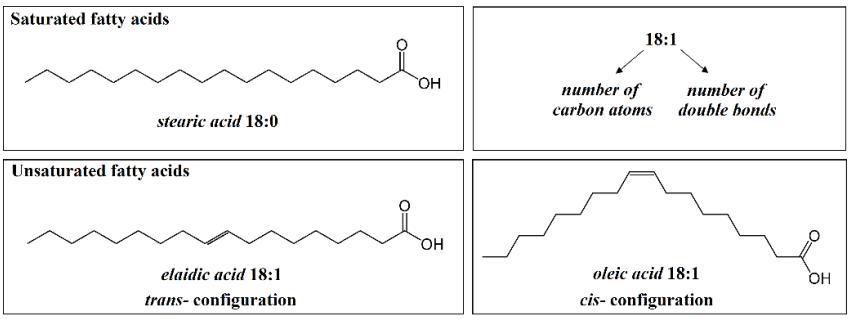

Figure 1: Saturated and unsaturated fatty acids

Saturated FAs are usually drawn in the conformation with the lowest energy, where all the C–C–C bonds are in an *all-trans* arrangement (Figure 1). However, isomerisation occurs around the single bonds in the FAs molecules, leading to more disordered conformations, which affects the hydrocarbon chain length and consequentially the thickness of the bilayers. ***Unsaturated FAs*** are created by oxidation process at specific places in the hydrocarbon chain. Most commonly, monounsaturated FAs occur. The first double bond is located at the ω-9 position (nomenclature calculates from the last carbon of the hydrocarbon chain, which is labelled ω) and the following desaturations can be found at the ω-6 and ω-3 position. Desaturations at the ω-6 and ω-3 positions occur only in plant cells, therefore, polyunsaturated linoleic acid (18:2, ω-6) and α-linolenic acid (18:3, ω-3) are essential for animals. The mammals are able to prolong these ***essential FAs*** in the liver cells and desaturate them to create other important derivatives such as arachidonic acid (20:4, ω-6), eicosapentaenoic acid (20:5, ω-3) and docosahexaenoic acid (22:6, ω-3). From arachidonic acid derivatives called eicosanoids are produced in cascade enzymatic oxidation. Eicosanoids are substances with significant, hormone-like, biological activity. Unsaturated FAs can vary in their spatial arrangement. The double bond between the two carbon atoms (C=C) may take two different stereoisomeric configurations called *cis*- or *trans*-. In the *cis*-isomers, the methylene groups (–CH_2–) next to the double bond are located on one side in the FA molecule (Figure 1, oleic acid). The methylene groups are located on the opposite sides in the *trans*-isomers (Figure 1, elaidic acid). The naturally occurring FAs occur almost always in the *cis*- configuration. Bending of the hydrocarbon chain of FAs molecule leads

to a reduction in hydrophobic interactions between neighbouring lipid molecules in the biological membrane. (Quinn, 2011; Mouritsen, 2005; Dobrota, 2012; Roche, 1999)

Polar lipids are the basic building blocks of cell membranes. As the name suggests, polar lipids contain polar components in their molecule: phospholipids (phosphoric acid residue), glycolipids (carbohydrate component), sulpholipids (sulphuric acid residue), lipoproteins (lipid complexes with specific proteins). The simultaneous presence of hydrophobic FAs and a hydrophilic fragment in the molecule of complex lipid gives them an amphiphilic character, which allows them to spontaneously create different aggregates (discussed in chapter 1.2.1 Spatial geometry of lipid molecules and supramolecular arrangements) in aqueous solutions (Dobrota, 2012).

Phospholipids are chemically esters of alcohols (glycerol → glycerophospholipids or sphingosine → sphingophospholipids) with FAs and ester-bound phosphoric acid. ***Glycerophospholipids*** include phosphatidic acids (PAs) and their esters, named phosphatidylcholines (lecithins, PCs), phosphatidylethanolamines (PEs), phosphatidylserines (PSs), phosphatidylglycerols (PGs) and phosphatidylinositols (PIs). While PCs and PEs are zwitterions (electroneutral net charge), PSs, PGs and PIs are carriers of negative charge. In the PC molecule, amino alcohol choline, is bound via an ester linkage. Choline is an important part of the acetylcholine neurotransmitter, also serves as a supply of methyl groups and is part of a lung surfactant (especially dipalmitoylphosphatidylcholine). The presence of PI is necessary to transmit signals in the cell. Through phospholipase C, the secondary messengers of diacylglycerol (DAG) and inositol-1,4,5-triphosphate (IP_3) are released from PI. The dimeric phospholipid, which contains 4 FAs in its molecule, is called cardiolipin (diphosphatidylglycerol, CL) (Dobrota, 2012; Mouritsen, 2005). Among the ***sphingophospholipids*** we list the sphingomyelins (SMs), which are predominantly found in myelin neurons. SM molecules consists of alcohol sphingosine, choline bound via the phosphoric acid residue to the primary alcohol group of sphingosine and a fatty acid (most commonly C_{24}) attached to its amino group (Dobrota, 2012).

Glycolipids are present in all tissues on the outside of the plasma membrane. In their molecule they contain the oligosaccharide, the alcohol component and the rest of the FA. According to the alcohol content, we divide the group into glycosphingolipids, present in animal membranes, and glycoglycerolipids, typical of plant and bacterial membranes. By attaching the hexose molecule (C_6 sugar, e.g. β-D-glucose or β-D-galactose) to the ceramide (N-acylsphingosine), the simplest glycolipids, cerebrosides, are formed. Galactocerebrosides are typically found in neuronal membranes, and in other tissues, predominantly glucocerebrosides are present. More complex glycolipids, gangliosides, include a branched or unbranched oligosaccharide chain consisting of up to 7 neutral sugars

or amino sugars attached to the ceramide molecule. Gangliosides, whose carbohydrate component from the membrane protrudes into the extracellular space, serve as specific receptors regulating several physiological functions, e.g., as pituitary receptors for certain glycoprotein hormones. They are also important for cell recognition among themselves, which is likely to play an important role in tissue growth and differentiation, as well as carcinogenesis (Quinn, 2011; Voet and Voet, 2010).

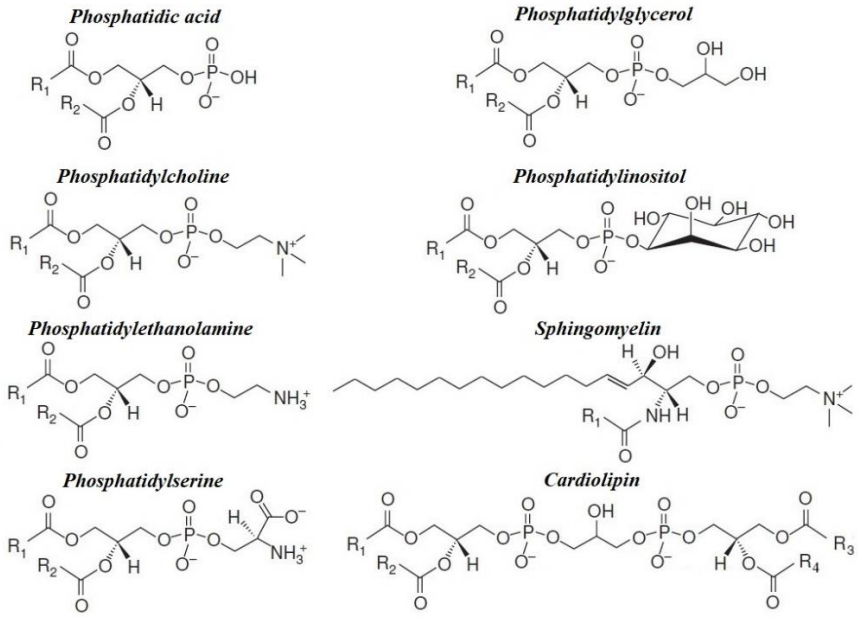

Figure 2: Membrane polar lipids

Sterols are derivatives of isoprene of considerable biological importance. The presence of cholesterol is typical in the biological membranes of animal cells, while in plant cells there are various sterols, e.g. stigmasterol, *β*-sitosterol, campesterol and others. Sterol present in microorganisms is called ergosterol (Quinn, 2011). The presence of cholesterol in the phospholipid bilayer alters its structural and dynamic properties by affecting freedom of movement and hydrophobicity. Its molecule consists of a rigid polycyclic skeleton with a side hydrocarbon chain and a hydroxyl group representing the polar part of the molecule. The amphiphilic character allows it to be incorporated into the membrane. Depending on the cell type, cholesterol is present in the animal cell membrane in the range of 20 – 50% of all lipids. Cholesterol has an unusual dual effect on membranes. It makes the membranes firmer, but leave the fluidity necessary for their proper function (Mouritsen, 2005). The solid cholesterol steroid skeleton, after incorporation into the membrane in the gel state, creates a defect in the bilayer. The defect allows for greater freedom in the movement of the acyl chains, thereby reducing the amount of heat required to pass into the liquid-crystalline phase. In the liquid-crystalline phase, cholesterol has the opposite effect. The rigid skeleton of

cholesterol prevents the increase of *trans-gauche* isomerization of the acyl chains, thereby maintaining their order (Uhríková, 2015). A mixture of lipid and cholesterol melts at a slightly lower temperature and a wider range of transition temperatures than is observed for pure lipid (Edidin, 2003). Cholesterol is an important component of cell membranes and myelin. It also serves as a precursor to oxysterols, steroid hormones, vitamin D and bile acids. It is an important part of the human brain (an adult human brain contains approximately 35 g of cholesterol) (Orth and Bellosta, 2012). Cholesterol and lipids with saturated chains are preferentially distributed in the membrane in microdomains called ***lipid rafts***. Cholesterol exhibits a lower affinity for the surrounding, fluid disordered membrane, consisting in particular of lipids with unsaturated acyl chains. Saturated chains acquire the *all-trans* configuration to facilitate closer contact with the rigid steroid skeleton, while unsaturated chains exhibit high conformational disorder, that is caused by a low energy barrier for rotation around single bonds separating multiple bonds (repeat pattern = C – C =) (Harroun et al., 2008). Lipid rafts are comprised in a ratio of about 1:1:1 of glycerophospholipids, sphingophospholipids and cholesterol. Lipid rafts are not formed in both layers of the bilayer randomly. They occur close to each other in the outer and inner layer of the membrane, despite various factors such as, higher degree of FA unsaturation in the inner bilayer or asymmetry of distribution of SMs and cholesterol in bilayer (Edidin, 2003).

1.2 Properties of biological membranes

1.2.1 Spatial geometry of lipid molecules and supramolecular arrangements

The lipids contain both the hydrophilic and the hydrophobic parts of the molecule. In the aqueous medium they form supramolecular arrangements, which are the most energy efficient state (Balazs and Godbey, 2011). These self-assemblies, which differ in morphology and size (nm to μm), are maintained by weak, non-covalent interactions. The arrangement of molecules is highly dependent on the geometry of the molecule (Elizondo et al., 2011). The geometry of the molecule is characterized by a dimensionless parameter P, which indicatively determines the preferred type of supramolecular arrangement:

$$P = \frac{v}{a \times l_c} \qquad 1$$

where v – volume of the hydrophobic part of the molecule, a – the polar surface of the molecule and l_c – the maximum chain length in the liquid-crystalline phase (Uhríková, 2015; Israelachvili, 2011; Meister et al., 2014). The preferred arrangement and influence of the geometry of the molecule on the curvature are schematically shown in the Figure 3.

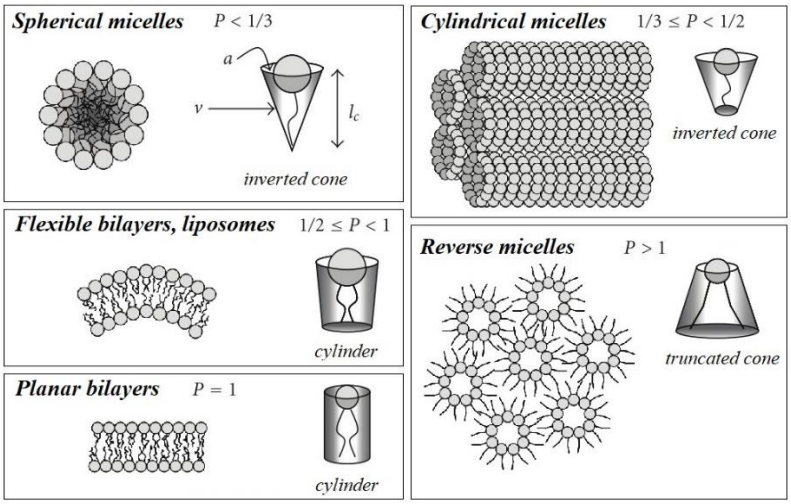

Figure 3: Parameter P of different lipid molecules and their preferred molecular arrangements.

Biological membranes are not only ordinary walls separating cells from their surroundings, there are many physiological and pathological processes occurring in the membranes. Membranes made only from lamellar lipids would be ideal insulators, but incompatible with cell function (Goni, 2014). The membranes may be positively or negatively curved, their deformability vary depending on the tension in the membrane. One way to modify curvature in membranes is by influencing the local composition, e.g. by changing the polar fragment, the FA chains of phospholipids, or by the presence of cholesterol. The shape of the individual different types of lipids present in the membrane gives it a spontaneous curvature. Membrane-bound proteins, whether asymmetrically nested hydrophobic protein domains, amphiphilic helical proteins, or various oligomeric protein structures also affect the curvature of the membrane. (Jarsch et al., 2016).

1.2.2 Lipid polymorphism

According to the liquid mosaic model, biological membranes are liquid-crystalline lipid bilayers with anchored proteins. However, in addition to bilayer-forming lipids, there are a large number of lipids, which after their isolation are more likely to acquire non-lamellar structures. Phases with different geometry and arrangement, called mesophases, are mutually related and are changing from one to another via ***phase transitions*** (Koynova and Tenchov, 2013). The ability of lipids to change their structural arrangement under the influence of changing external conditions is referred to as ***polymorphism***. The structural arrangement of lipids can be determined by optical methods (e.g. polarisation microscopy,

electron microscopy) or ^{31}P NMR spectroscopy. In case of symmetrical structures, a reliable method is small-angle diffraction and scattering of neutrons or X-rays (Uhríková, 2015).

Nomenclature proposed in the 1960s (Luzzati, 1968) is still used today. The lipid phases are generally characterised by:

a. ***lattice periodicity***: described by uppercase Latin letters – L = one-dimensional lamellar lattice; H = two-dimensional hexagonal lattice; P = two-dimensional oblique or rectangular lattice; T, R and Q = three-dimensional rectangular, rhombohedral and cubic lattice
b. ***arrangement of FAs chains***: the hydrocarbon chain conformation is described by the lower (Greek or Latin) index – α = liquid-crystalline (disordered), β = gel (ordered), β' = gel with tilted chains, C = crystalline (subgel)
c. ***type***: type of aggregate is denoted by Roman numerals: I = oil in water (normal type), II = water in oil (inverted type)

Structures, together with the names of the lipid phases that may arise in the lipid-water system due to various external conditions are depicted in the Figure 4.

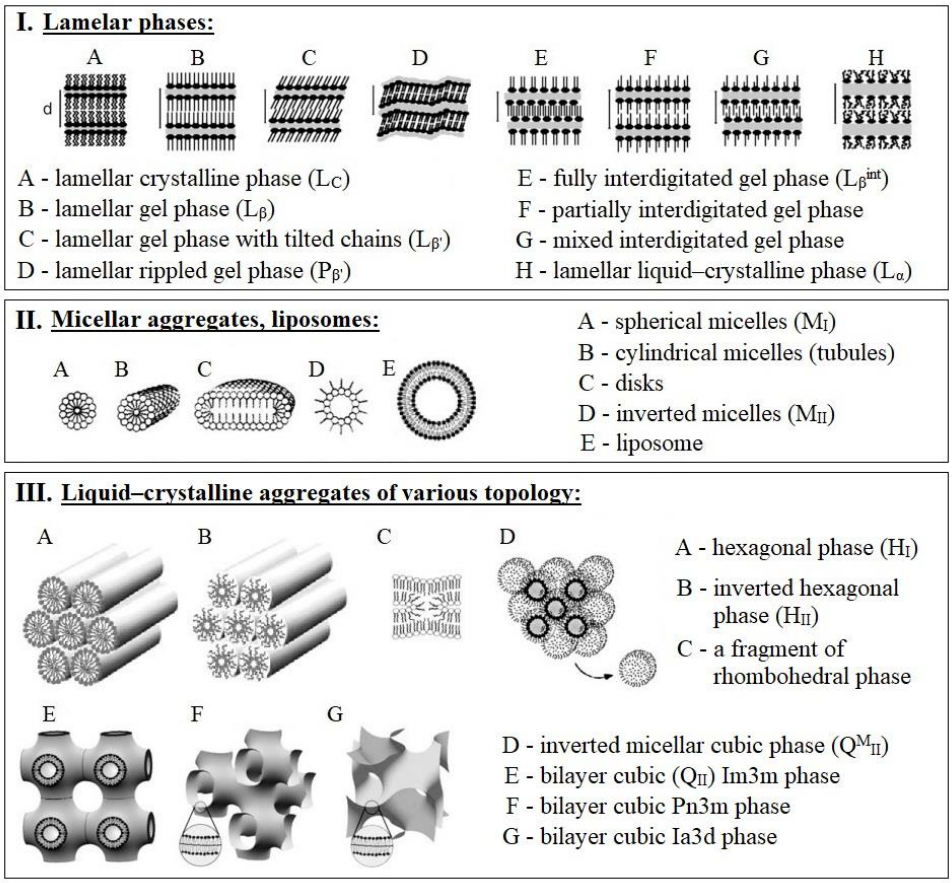

Figure 4: Examples of various lipid phases and aggregates. (Koynova and Tenchov, 2008) d – repeat spacing of the lattice

I. Lamellar phases:

The properties of lamellar phases are affected by several physico-chemical parameters such as temperature, pH, ionic strength or other factors (e.g. chemical structure of lipid component or a presence of cholesterol) (Eeman and Deleu, 2010).

Lamellar crystalline phase (L_C) is formed by lipids at low hydration and/or low temperature. It is characterised by the tight ordering of the hydrocarbon chains that are in the *all-trans* conformation (Kulkarni, 2012). By adding heat to the L_C phase, a phase transition into the ***lamellar gel phase (L_β)*** occurs. Hydrocarbon chains are still in *all-trans* conformation and high order restricts lateral diffusion of lipids (it is also called solid-ordered phase, S_o). Lamellar gel phase with tilted or interdigitated chains can also occur.

In ***liquid-crystalline phase (L_α)***, also known as liquid-disordered phase (L_d), *trans-gauche* isomerisation of the hydrocarbon chains allows less tight ordering of the bilayer. This facilitates both lateral and rotational diffusion of lipids. The transition between gel and liquid-crystalline phase occurs at the temperature of the ***main phase transition*** (T_m) (Eeman and Deleu, 2010). Because of the energy needed to expand the hydrocarbon area (to overcome the attractive van der Waals interactions) and to enlarge the surface of the bilayer (increasing the hydration of the polar fraction of the lipid molecules) is the main phase transition associated with a large enthalpy change and is the largest energy event occurring in a bilayer (Koynova and Tenchov, 2013).

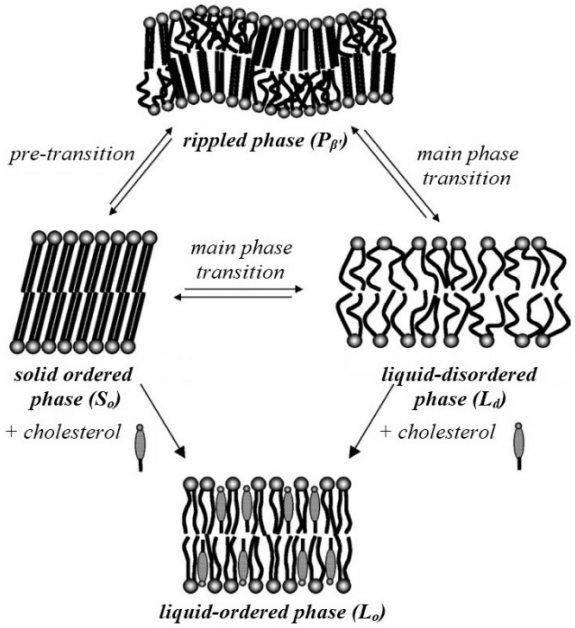

Figure 5: Schematic representation of various phases of lipid bilayer in aqueous environment. Adapted from (Eeman and Deleu, 2010)

For some membrane lipids, e.g. PCs or charged PGs, a ***pre-transition*** takes place a few degrees below the main phase transition. If the pre-transition is present, another phase can be observed, called ***rippled gel phase ($P_{\beta'}$)***. This phase is characterised by the rippled surface of the bilayer caused by its partial disorder. In the bilayer, ordered and disordered lipid domains alternate. In the presence of cholesterol, the lipid bilayer acquires a ***liquid-ordered phase (L_o)***, with less tight arrangement of the FA chains than in the gel phase, but higher order than liquid-crystalline phase (Eeman and Deleu, 2010).

II. Liposomes:

The lamellar lipid phase is considered to be the most relevant for biological functions, because it most closely resembles the structure of plasma membrane. Liposomes are vesicular structures consisting of one or more concentric spheres of lipid bilayers that enclose the aqueous medium. The size of the liposomes is directly related to the preparation method and can vary from 50 nm to several micrometres. They may be formulated as suspensions, aerosols or even in the form of gels and creams. Liposomes have low toxicity and are biocompatible and biodegradable. They have the ability to seal lipophilic and hydrophilic drugs. (Himanshi et al., 2015) An important characteristic of liposomes is their lamellarity, a term denoting the number of bilayers (separated from each other by the aqueous medium) that form it. One-layer liposomes are called unilamellar, while several concentrically arranged bilayers form multilamellar liposomes. Unilamellar liposomes are most similar to the cell membrane, both in terms of structure and function, and are therefore used in the study of membrane proteins, substances affecting stability or other properties of the membrane. Depending on the method used to prepare the liposomes, we can obtain liposomes of varying size and lamellarity: unilamellar liposomes (ULLs) – small unilamellar liposomes (SULs), large unilamellar liposomes (LULs), giant unilamellar liposomes (GULs); multilamellar liposomes (MLLs) or multivesicular liposomes (MVLs). (van Swaay and DeMello, 2013) These types of liposomes are depicted in Figure 6.

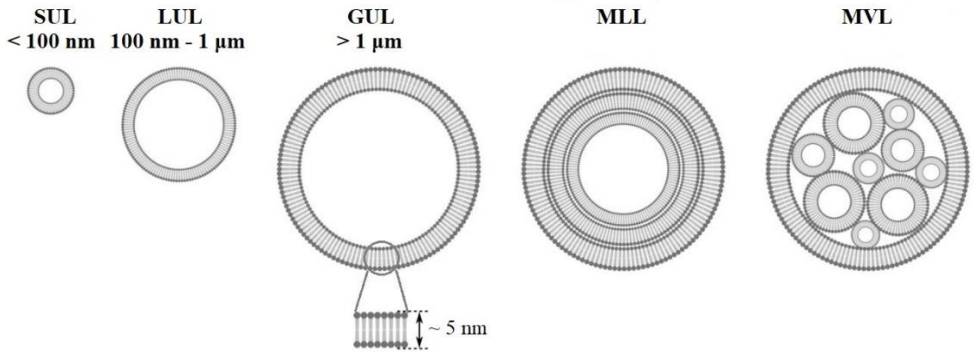

Figure 6: Liposomes of different size and lamellarity. (van Swaay and DeMello, 2013)

The use of liposomes has great potential in various fields of science, industry, but also in diagnostics and therapy. They can serve as carriers of hydrophilic or lipophilic drugs and genetic material. Usage was found, for example, in dermatology (therapeutic cosmetics) or in immunology (Garg and Goyal, 2014).

III. Non-lamellar phases:

Some membrane lipids are able to form non-lamellar lipid phases. Among the lipids constituting the predominantly lamellar phase we list PCs, PSs and SMs. The anionic phospholipids, such as PGs, PAs, PSs a CLs, form non-lamellar structures only under extreme conditions, e.g. high ionic strength, presence of divalent metal ions in high concentration or low pH. Therefore, it is assumed that these lipids will not form non-lamellar structures under physiological conditions, but on the contrary, they will help to stabilize lamellar structures. Lipids that prefer to form an inverse hexagonal phase include zwitterionic PEs, the most represented phospholipid in some bacterial membranes (Haney et al., 2010). Despite the high PEs content, bacterial cells are capable of regulating the FA chain composition of their inner membrane phospholipids to preserve its liquid-crystalline phase (Morein et al., 1996). Among the non-lamellar structures, we list the ***hexagonal phase (H_I)*** consisting of lipids arranged in the shape of cylinders or ***inverted hexagonal phase (H_{II})*** with water enclosed inside the cylinders and hydrocarbon chains oriented to the outside. In addition to these simpler architectures, more complex, but still well-organized lipid phases are to be found. The most common are cubic phases, which may be of two types: ***bicontinuous cubic phase (Q_{II}***: Ia3d, Pn3m and Im3m) formed by continuous lipid bilayer with a structure of mathematically minimal surface that separates two water channels. The second type is ***inverted micellar cubic phase (Q_{II}^M)*** consisting of discrete micelles arranged in a cubic lattice (Kulkarni, 2012). Some of the most common non-lamellar structures are depicted in the Figure 4.

At present, the liquid-crystalline phase and non-lamellar lipid phases are intensively studied as targeted drug carriers for their ability to encapsulate drugs. Non-lamellar phases are also able to protect peptides from enzymatic degradation. They may be applied topically to the skin, by injection (subcutaneously or intravenously) or by adhesion to the mucous membranes (Chang et al., 2015).

1.2.3 Membrane fluidity

Fluidity is probably the most obvious physical property of the membrane. FAs, an inseparable part of the phospholipid bilayer, significantly affect membrane fluidity and

interactions between lipids and proteins. Cholesterol is an important substance whose increasing concentration in the membrane regulates its structural and dynamic properties by affecting freedom of movement and hydrophobicity (Cócera et al., 2003). The conformational changes of FAs and the influence of cholesterol on phospholipid bilayer have already been discussed in Chapter 1.1.1 Lipids.

Lipid molecules are in the bilayer ***in motion***, continuously altering their intramolecular conformation, vibrating, even temporarily protruding from the bilayer. Depending on the type of movement, the length of the duration is also individual. ***Conformation changes*** (rotation around C – C bonds) usually take several picoseconds (10^{-12} s). The ***molecule rotates around its own axis*** within nanoseconds (10^{-9} s), while the ***movement in the lateral direction*** takes up to tens of nanoseconds. In the direction perpendicular to the membrane, the lipid molecule can protrude itself from the membrane in a few tens of picoseconds. The movement of the molecule from one layer to the other, so-called ***flip-flop movement***, may take several hours, maybe even days. Of course, all these movements are affected by factors such as the type of lipid molecule, the temperature and the phase in which it occurs. E.g. lateral diffusion in the gel phase is slowed by at least one hundred times compared to the liquid-crystalline phase. Not only single molecules or their parts (FA residues) can carry out the movement. Several molecules can also perform a variety of joint movements, e.g. bilayer waving, changes in the thickness of bilayer or collective diffusion of the entire cluster of molecules within the plane of the membrane (Mouritsen, 2005).

1.2.4 Lateral pressure

Structure of the cell membrane in the lateral direction is described weakly in the literature. This is due to the lack of direct methods for observing bilayers in the lateral direction, as well as dynamic changes occurring in bilayer (molecular motions) (Bagatolli et al., 2010). Changes in membrane composition can significantly modulate the activity of transmembrane proteins. Enzymes, ion and molecular transporters and ion channels are often sensitive to changes in the polar fragment and length of the FA chains, or to the concentration of cholesterol or some smaller molecules such as general anaesthetics (Cantor, 1997).

Lipids in the bilayer are maintained in place due to the hydrophobic effect. However, different attractive and repulsive forces also act between the individual parts of the lipid molecules. This property of the bilayer is referred to as lateral pressure. Unlike ***attractive forces*** on the lipid/water interface (induced by a hydrophobic effect), ***repulsive forces*** act

between polar lipid fragments. Hydrophobic hydrocarbon chains also repel each other (Mouritsen, 2005).

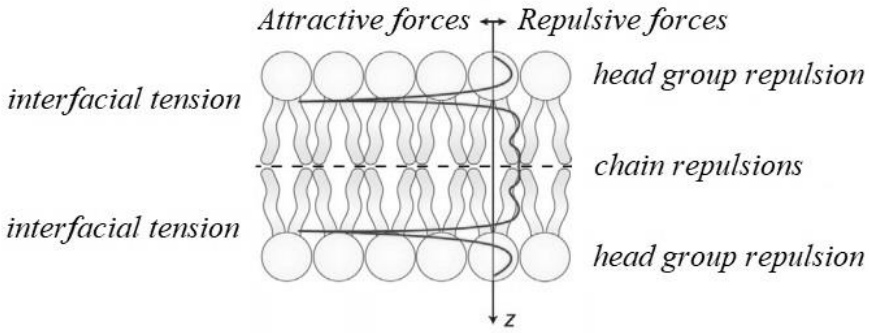

Figure 7: Schematic illustration of a lateral pressure profile on the cross section of a lipid bilayer.

1.3 Eukaryotic and prokaryotic cell membranes

The biomembranes are complex mixtures of lipids, proteins and other molecules. The lipid composition differs depending on the type of organism, tissue, cellular organelle, and to a certain extent, on the environmental and nutritional factors. In Table 1, we can see how big differences in lipid composition of the membrane are between the human erythrocytes (Lipowsky and Sackmann, 1995) and bacteria *Escherichia coli* (Lopes et al., 2010). Differences in the cell membrane construction of both types of cells will be discussed in the following chapters.

Table 1: Lipid composition (in weight %) of the membrane of human erythrocyte and Escherichia coli.

Membrane type	**PCs**	**PEs**	**PSs**	**PGs**	**PIs**	**CLs**	**SMs**	**GLs**	**CHOL**	**Other**
Erythrocyte	20	18	7	0	3	0	18	3	20	11
Escherichia coli	0	57	0	15	0	10	0	0	0	18

PCs – phosphatidylcholines, PEs – phosphatidylethanolamines, PSs – phosphatidylserines, PGs – phosphatidylglycerols, PIs – phosphatidylinositols, CLs – cardiolipins, GLs – glycolipids, CHOL – cholesterol

1.3.1 Eukaryotic cell membranes

The plasma membrane of mammalian cells is composed of lipids (phospholipids, glycolipids, cholesterol), proteins and carbohydrates. The molecular composition is highly dependent on the type of the cell, for example the weight ratio between proteins and lipids

varies from 1:5 to 5:1. Carbohydrates are present in the membranes in less than 10 % amount of the dry mass. (Mouritsen, 2005) The most prevalent lipids in mammalian plasma membranes are PCs, PEs, SMs and CHOL. Proteins can be peripheral (weakly bound to the membrane) or integral (bound more strongly to the membrane). (Dobrota, 2012) A liquid-mosaic model of mammalian (eukaryotic) plasma membrane is shown in the Figure 8.

Asymmetric distribution of lipids has been found in the plasma membranes. Lipid asymmetry is necessary for multiple cellular functions, such as cell fusion, coagulation cascade or apoptosis (death) of the cell. (Fadeel and Xue, 2009) The outer leaflet is mostly enriched in choline-containing phospholipids (PCs and SMs), while PEs, PSs and other minor phospholipids are oriented to the inside of the cell. Cholesterol is distributed equally between the two leaflets of the plasma membrane. (Daleke, 2008)

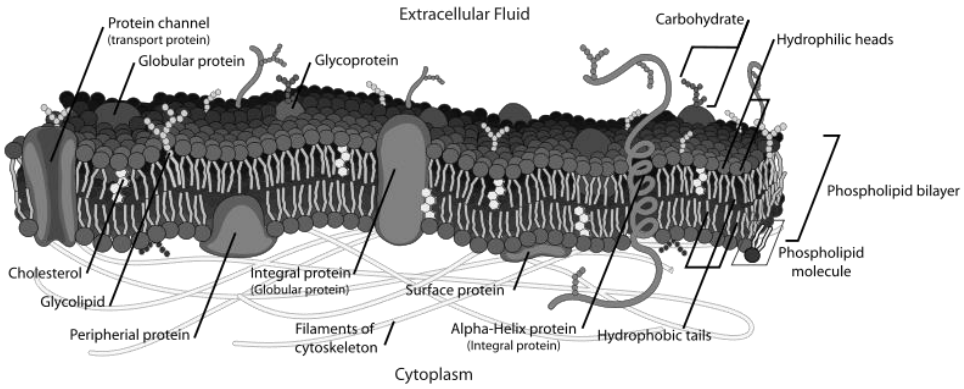

Figure 8: Liquid-mosaic model of eukaryotic cell membrane.

1.3.2 Prokaryotic cell membranes

The structure of prokaryotic cell is simpler at every level than eukaryotic cell, with the only exception – their cell membrane and additional cell wall are more complex. Based on the construction of the cell wall (Figure 9) we can distinguish two major groups of bacteria using Gram staining: gram-positive (G^+) and gram-negative (G^-) bacteria (Neidhardt, 2013).

The ***cell wall*** of both G^+ and G^- bacteria contains ***peptidoglycan***. The peptidoglycan structure consists of linear strands formed by alternating *N*-acetylglucosamine (Glc*N*Ac) and *N*-acetylmuramic acid (Mur*N*Ac) molecules (linked β-(1→4) glycosidic bonds) crosslinked with identical tetrapeptides. The tetrapeptide is attached to the carboxyl group of Mur*N*Ac and usually consists of L-alanine (L-Ala) in the first position, D-glutamic acid (D-Glu) in the second and D-alanine (D-Ala) in the fourth position. The amino acid in the third position is the most variable (Vollmer et al., 2008).

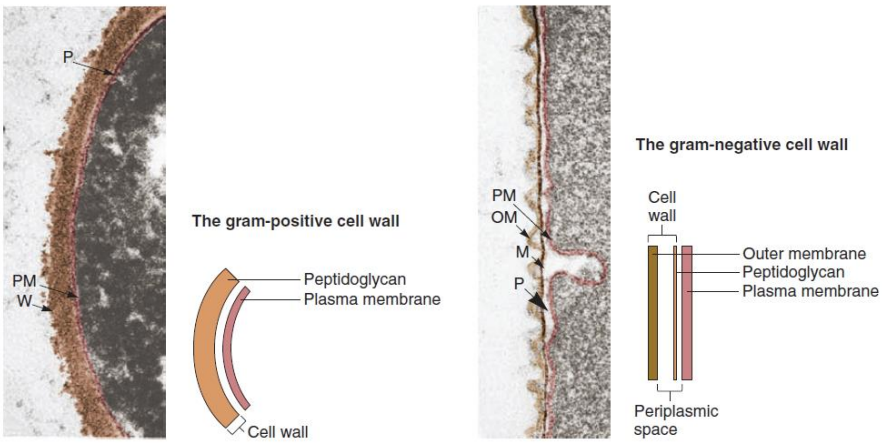

Figure 9: The cell walls of G^+ and G^- bacteria. PM – plasma membrane, M – murein (peptidoglycan), W – G^+ peptidoglycan wall, P – periplasmic space, OM – outer membrane. (Morse and Meitzner, 2013)

In ***G^+ bacteria***, the peptidoglycan is 30 – 100 nm thick and has many layers. Threading through the peptidoglycan layers are polymeric molecules called teichoic acids, which give the G^+ bacteria negatively charged surface (Silhavy et al., 2010). They consist predominantly of glycerol-phosphate, or ribitol-phosphate residues. The wall teichoic acids are covalently bound to the peptidoglycan. Teichoic acids covalently bound to membrane glycolipid are called lipoteichoic acids (Morse and Meitzner, 2013).

In ***G^- bacteria***, the cell wall consists of thin layer of peptidoglycan. For example, in *E. coli* more than 80% of peptidoglycan forms a monolayer and the thickness of its cell wall is smaller than 4 nm (Huang et al., 2008). Peptidoglycan is a part of the ***periplasmic space***, which accounts for approximately 20 – 40% of cell volume. It is a gel-like solution of proteins, for example binding proteins for specific substrates, hydrolytic enzymes or detoxifying enzymes (such as β-lactamase) for disabling certain antibiotics (Morse and Meitzner, 2013). The distinctive feature of G^- bacteria is the presence of an ***outer membrane*** that never occurs in the G^+ bacteria. The outer membrane of G^- bacteria contains phospholipids (20 – 25 w%), lipopolysaccharide (20 – 30 w%) and proteins (45 – 50%) (Kaufmann et al., 2012). The specificity of the outer membrane is that instead of it being formed by a bilayer of phospholipids, its inner leaflet resembles a composition of the plasma membrane whereas the outer leaflet contains molecules of ***lipopolysaccharide*** (LPS) (Kayser, 2005; Hogg, 2005). LPS is highly toxic for humans and other animals. It consists of lipid A, polysaccharide core and terminal series of repeat units called O-antigen. ***Lipid A***, responsible for the high toxicity, is formed by phosphorylated glucosamine disaccharide units with 6 – 7 long-chain FAs attached. LPS is called an endotoxin, because lipid A is released only after the lysis of the bacteria. Even at low concentration in the blood it causes fever, higher concentration leads to a septic shock (possibly deadly). The ***polysaccharide***

core of G^- bacteria consists of two characteristic sugars: ketodeoxyoctanoic acid and a heptose. The terminal repeat units are usually formed by either linear tri-saccharides or branched tetra- or penta-saccharides. They are called ***O-antigen*** because they are highly immunogenic. Negatively charged LPS molecules are non-covalently stabilized by divalent cations (Mg^{2+}, Ca^{2+}), thereby neutralizing the negative charge of the phosphate groups present in the molecule. The FA chains are saturated, allowing a tight alignment. This creates a very effective barrier for hydrophobic molecules. Selective permeability is provided by special proteins called ***porins*** along with other translocation systems. The porins are very abundant in the outer membrane, having approximately 250 000 copies per cell. (Kayser, 2005; Hogg, 2005; Morse and Meitzner, 2013; Neidhardt, 2013; Nikaido, 2003; Silhavy et al., 2010)

The plasma membrane of the bacteria is a phospholipid bilayer and over 200 different types of proteins. Proteins make up about 70% of the mass of the membrane, which is a higher proportion than that of mammalian cell membrane. Aerobic bacteria have the electron transport and oxidative phosphorylation system incorporated in the membrane, which is functionally analogous to eukaryotic mitochondria. The membrane also contains enzymes and other molecules necessary for biosynthesis of DNA, cell wall polymers and membrane lipids. Bacterial membranes do not contain sterols, with the exception of mycoplasmas, which incorporate sterols into the membrane when cholesterol is present in the medium in which they grow (Morse and Meitzner, 2013; Neidhardt, 2013).

There are considerable differences in the composition of the membrane between different types of bacteria. For most, zwitterionic PEs are dominant. G^- bacteria have a higher PEs content than G^+ bacteria. The predominant negative phospholipids in the bacterial membranes are PGs and CLs. All bacteria contain at least 15% of anionic phospholipids (from the total amount of phospholipids) (Epand and Epand, 2009).

1.4 Model membranes

1.4.1 Mammalian model membranes

One of the most studied mammalian plasma membranes is that of ***erythrocytes***. About 80 mol% of the FA chains in membrane phospholipids are 16 and 18 carbons long. Approximately 30 mol% is saturated, 43 mol% monounsaturated and 22 mol% polyunsaturated. (Luchini and Vitiello, 2021) ***PCs*** are the most common phospholipids in eukaryotic membranes. (van Meer et al., 2009) Therefore, PCs or mixtures containing PCs with another type of lipid are used as model membranes. This can be either from the group of PEs or PSs, but often it is ***cholesterol*** (CHOL), because of its effect on the arrangement

of PCs bilayers (described in Chapter 1.1.1 Lipids). The maximum solubility of CHOL in glycerophospholipid membrane is 50 – 66 mol% (depending on the prevalent lipid species). (Ohvo-Rekilä et al., 2002)

Because of all the above-mentioned information dioleoylphosphatidylcholine (DOPC), palmitoyloleoylphosphatidylcholine (POPC) and their mixtures with CHOL can serve as suitable model membranes to represent simplified mammalian plasma membrane. In our case the molar ratio of PC to CHOL was chosen to be 2:1 mol/mol. Figure 10 shows a phase diagram of POPC-PSM-CHOL mixtures (Simons and Vaz, 2004; de Almeida et al., 2003). Palmitoylsphingomyelin (PSM) is the major component of egg yolk sphingomyelin (EYSM) used in one of our experiments. As we can see from the phase diagram our mixture POPC-CHOL (X_{POPC} = 0.66; X_{CHOL} = 0.33) is formed by coexisting L_d and L_o phase. To compare POPC and DOPC, the latter has 2 unsaturated FA chains compared to only one present in POPC. This means the DOPC bilayer is more fluid compared to bilayer formed by POPC. The addition of CHOL into the DOPC bilayer would therefore consist of a uniform phase with properties between L_d and L_o phase or by coexisting L_d and L_o phase. (van Meer et al., 2009)

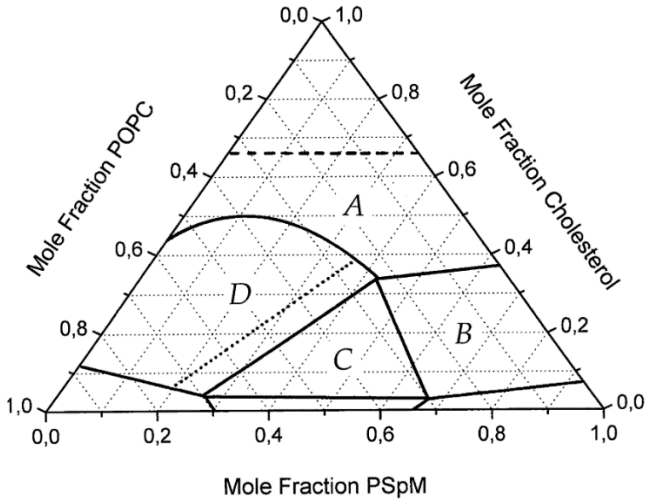

Figure 10: Phase diagram of POPC-PSM-CHOL mixtures. A – single L_o phase; B – S_o + L_o phase coexistence; C – L_d + L_o + S_o three-phase region; D – L_d + L_o phases coexistence. Dashed line represents approximate maximal solubility of CHOL. PSpM – palmitoylsphingomyelin. (Simons and Vaz, 2004)

1.4.2 Bacterial model membranes

For our experiments, G^- rod-shaped bacteria ***Escherichia coli*** (*E. coli*) were selected as model organisms. Membrane lipids of *E. coli* are a mixture of PEs (57 w%), PGs (15 w%), CLs (10 w%) and other lipids (18 w%) (such mixture of lipids is commercially

available as *E. coli* Total Lipid Extract). An extract of polar lipids of *E. coli* contains PEs (67%), PGs (23%) and CLs (10%). It is commercially prepared from *E. coli* Total Lipid Extract by precipitation with acetone and extraction with diethyl ether (*https://avantilipids.com/product-category/natural-lipids/extracts*, [12.4.2022]).

Frequently used models are ***two-component PEs and PGs mixtures*** (Lopes et al., 2010). The FAs found in *E. coli* are predominantly 16 – 18 carbons long, with a considerable part of them being unsaturated (Meister et al., 2014). Therefore, a mixture of palmitoyloleoylphosphatidylethanolamine (POPE) and palmitoyloleoylphosphatidyl-glycerol (POPG), in a molar ratio of POPE/POPG = 0.6/0.4 mol/mol was studied as bacterial model system in this thesis. More complex system containing CLs (in our case tetraoleoylcardiolipin, TOCL), POPE/POPG/TOCL in a molar ratio 0.67:0.23:0.1 mol/mol/mol was also used in this thesis. It was proven that the phase transitions of POPE/POPG/CL ***three-component mixture*** in this molar ratio shows the highest similarity to those of *E. coli* extracts (Lopes et al., 2010).

PEs are zwitterionic phospholipids. Polar headgroup of PEs is smaller in diameter compared to the hydrocarbon chain area, giving them molecular shape of a truncated cone. Therefore, they prefer to form structures with negative curvature, at higher temperatures they tend to form non-lamellar phases. (Lopes et al., 2012) In water solutions they form MLLs. PGs with a pKa value ~ 3 are negatively charged at physiological pH. Thanks to their cylindrical molecular shape, they prefer to create flat bilayers even at high temperatures. Because of the charge, in water solution they form ULLs. (Pozo Navas et al., 2005) At physiological pH, the PEs headgroup can act as a donor (NH_3^+) and acceptor (PO_2^-) for intermolecular hydrogen bonds. The polar fragment of PGs may be a hydrogen bond acceptor (PO_2^-), but can also serve as a weaker hydrogen bond donor (hydroxyl groups of glycerol). Differences in the hydrogen bonding capabilities and PGs additional hydroxyl groups cause that PGs headgroups are much more hydrated than those of PEs. PGs headgroups therefore occupy larger volume, which causes their FA chains being tilted ($L_{\beta'}$ phase) as opposed to the non-tilted (L_β) phase formed by PEs. This probably results in the ability of PGs to increase the hydration of PEs in the bilayer by breaking the tight packing of PE molecules. This effect is of greater importance in the gel phase. In the liquid-crystalline phase, polar fragments of the phospholipid molecules are generally more hydrated due to lateral expansion of the bilayer. (Garidel and Blume, 2000) Molecular dynamics simulation of POPE/POPG bilayer showed stronger interaction between PE-PG molecules than between PE-PE molecules (Murzyn et al., 2005).

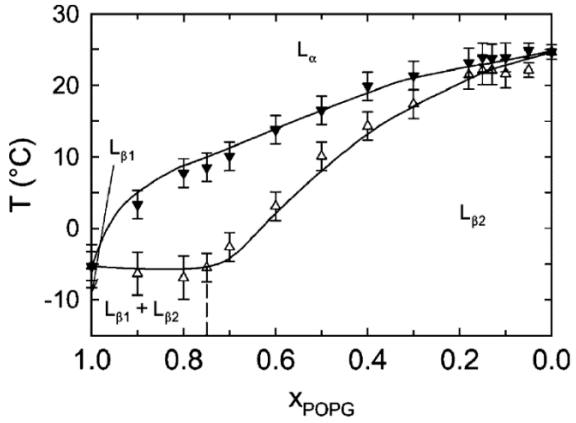

Figure 11: Phase diagram of POPE-POPG mixtures. (Pozo Navas et al., 2005) The empty symbols – beginning of the phase transition, full symbols – end of the phase transition. $L_{\beta 1}$ – gel phase of pure POPG, $L_{\beta 2}$ – gel phase of pure POPE, L_{α} – liquid-crystalline phase.

Figure 11 shows a phase diagram of POPE-POPG mixtures ($X_{POPG} = 0 – 1$). Because of its asymmetric shape, we assume non-ideal mixing in both liquid-crystalline and gel phase. At $X_{POPG} \geq 0.75$, lateral phase segregation occurs. Mixtures of POPE and POPG form oligolamellar liposomes (OLLs) with few bilayers (3 – 5). The main phase transition of the mixture POPE-POPG in a molar ratio 0.6:0.4 mol/mol was determined to be 19.4° (Pozo Navas et al., 2005). This matches the results in other works: from the measurements of steady-state anisotropy – 19.8 ± 0.6° C a 20.1 ± 0.7° C (using 2 different fluorescence probes), and dynamic light scattering – 19.6 ± 1.0° C (Lopes et al., 2010).

CLs are the third major component of the bacterial membrane. CLs are anionic lipids with two negative charges and have four FA residues in their molecule. It is a relatively rigid lipid (regarding the mobility of the molecule) of cylindrical shape. (Lopes et al., 2012) Despite CLs having 4 FAs in their molecules, the dominant types of cardiolipin usually contain only one or two kinds of FAs. It was found that the FA composition is relatively resistant to dietary manipulations, suggesting a specific composition is needed for its biological functions. (Schlame et al., 2005) TOCL has a gel to liquid-crystalline phase transition at approximately -15°C. (Chen, 2012) Therefore, we can assume that our ternary mixture (POPE-POPG-TOCL) is in liquid-crystalline phase at laboratory temperature (25°C).

The existence of ***lipid domains in bacterial membranes*** (lateral heterogeneities in the composition of the bilayer) has been demonstrated and is believed to be important for certain regulatory functions of the cell. Study with pyrene-labelled phospholipids (2-pyrene-decanoyl-PE and 2-pyrene-decanoyl-PG), which were introduced into living model organisms (G^- *E. coli* a G^+ *Bacillus subtilis*) revealed, that these phospholipids are segregated into domains. These domains differ in composition, protein-lipid interactions and

degree of order. It has been shown that a protein-rich domains are enriched with PE molecules. (Vanounou et al., 2003) During the bacterial cell division, the membrane septum between the two daughter cells is also rich in PEs. Thanks to the CLs-specific fluorescent dye, 10-nonyl acridine orange, CLs-enriched domains were also observed in the septal region of plasma membrane of *E. coli*. (Epand and Epand, 2009) Lipids like PEs and CLs may be used to accommodate membrane proteins and modulate their activities. (van Meer et al., 2009)

1.5 *N*-alkylamine-*N*-oxides

N-alkylamine-*N*-oxides are amphiphilic, at physiological pH non-ionic surfactants. The negative part of the molecule forms a monovalent (and thus negatively charged) oxygen covalently bound to a positively charged tetravalent nitrogen. This bond is strongly polar, with high electron density on the oxygen atom. *N*-alkylamine-*N*-oxides are crystalline substances with strong hygroscopic properties and are very well dissolved in water. They are considered weak bases, which in the acidic environment form *N,N,N*-trisubstituted hydroxylammonium salts (Devínsky, 1985; Devínsky et al., 2013).

Structure – effect relationship

The *N*-alkylamine-*N*-oxides, often used in pharmaceutical and cosmetic formulations and as surfactants in cleaning products, are those which contain two methyl groups and a hydrocarbon chain with variable length. Various biological activities of *N,N*-dimethyl-alkylamine-*N*-oxides (shortly C_nNO, subscript n specifies the length of the hydrocarbon chain) have been observed: antimicrobial and haemolytic activity (Devínsky et al., 1990), immunomodulatory effect (Bukovský et al., 1996; Kacáni et al., 1996), phytotoxic effect (Šeršeň et al., 1992) and antiphotosynthetic activity (Murín et al., 1990). The activity of C_nNO is non-linearly dependent on the length of the hydrocarbon chain. In a homologous series of C_nNO, the activity increases to a certain critical point at which the activity starts to decrease. Such behaviour is called ***cut-off effect*** (Balgavý and Devínsky, 1996). The authors suggested a free volume hypothesis to explain such structure – effect relationship. Due to the amphiphilic character of C_nNO, they intercalate into the phospholipid bilayer. Their polar fragment (N-O bond) is localised near the polar fragments of phospholipids, while the hydrophobic chains of C_nNO orient themselves parallel to the hydrocarbon chains of phospholipids. The partition coefficient of amphiphiles should increase exponentially with the increase of the chain length. On the other hand, the longer the chain length, the less will be the arrangement of the bilayer disturbed by the presence of the amphiphile. Amphiphiles

with shorter chain lengths will create a void (free volume) in the bilayer, because their chains are shorter than the chains of phospholipids. The void enables the change of the properties of the membrane (increased *trans-gauche* isomerisation of hydrocarbon chains, their bending or interdigitation – all resulting in the change of thickness of the bilayer). (Balgavý and Devínsky, 1996) Changes in the thickness of mammalian model bilayers were observed in studies of (Dubničková et al., 1997; Uhríková et al., 2001; Karlovská et al., 2004a). Changes in the properties of the bilayer might be the reason for the observed biological effects. (Balgavý and Devínsky, 1996)

The highest antimicrobial activity against *E. coli* was observed with a 12-carbon chain homologue, ***N,N-dimethyl-1-dodecanamine-N-oxide*** (hereinafter referred to as DDAO, also referenced in literature as $C_{12}NO$). (Balgavý and Devínsky, 1996) For this reason, DDAO was chosen for our experiments with mammalian and bacterial model membranes. DDAO is a water-soluble, commercially available surfactant with pKa ~ 5. Apart from its presence in cleaning products of everyday use, it has been used as a micellar catalyst of some chemical reactions and in biological studies as a mild surfactant for solubilisation of membranes and for reconstitution and crystallisation of membrane proteins. (Goracci et al., 2007; le Maire et al., 2000) At pH ≥ 7, all DDAO molecules are uncharged, at pH ≤ 3 all DDAO molecules are positively charged, while in the range of pH 3 – 7, there is a mixture of the uncharged and the charged form. (Lorenz et al., 2011) The pH sensitivity can play an important role while designing lipid based drug or DNA delivery systems. (Hubčík et al., 2015; Liskayová et al., 2017) The critical micellar concentration of DDAO at 27° C is 2.1 mmol/dm^3 and 1 micelle is composed of approximately 76 monomers (Herrmann, 1962).

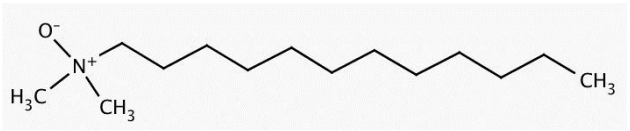

Figure 12: Structure of N,N-dimethyl-1-dodecanamine-N-oxide

1.5.1 Interactions of surfactants with model membranes (solubilisation)

Because of the complexity of construction and molecular diversity of biological membranes, studies of interactions with biologically active compounds are preferably performed on model systems, especially lipid bilayers in the form of liposomes. Based on the characteristic types of the lipid-surfactant aggregates, the interaction of lipid-formed liposomes with a surfactant can be divided into three stages (Helenius and Simons, 1975).

In the ***first stage*** (Figure 13, I), the surfactant molecules partition between the lipid bilayers and the water phase (according to the partition coefficient). As was described in the previous Chapter (1.5 *N-alkylamine-N-oxides*), the molecules of DDAO intercalate into the phospholipid bilayer, affecting its properties and creating defects and pores. Pore formation, typical during the first stage of solubilisation, can be observed by the method described in a later chapter (3.2 Fluorescence spectroscopy, Fluorescent probe leakage method).

In the ***second stage*** (Figure 13, II), the bilayers are saturated by the surfactant and begin to transform into lipid-surfactant mixed micelles.

In the ***third stage*** (Figure 13, III), the concentration of the surfactant is higher than necessary to convert all bilayers to mixed micelles and further addition of surfactant results only in a decrease in the size of mixed micelles. (Helenius and Simons, 1975; Ahyayauch et al., 2010; Lichtenberg et al., 2013a; Lichtenberg et al., 2013b; Heerklotz and Blume, 2012)

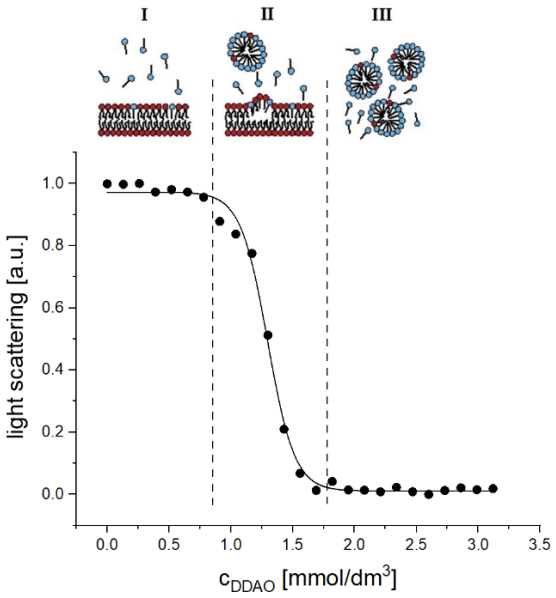

Figure 13: Interpretation of a three-stage model of surfactant interaction with ULLs observed by static light scattering.

Solubilisation is defined as a spontaneous process leading to a thermodynamically stable solution of a substance that is normally insoluble or very poorly soluble in the solvent by the addition of one or more amphiphilic substances (surfactants). Even though the term solubilisation itself refers, more precisely, to the second stage of the process described earlier (Lichtenberg et al., 2013b), it is often used to describe the whole complex process that can be observed in model membranes interacting with a surfactant in a wide range of surfactant concentration. The term solubilisation will be used in this thesis to describe the whole three-stage process.

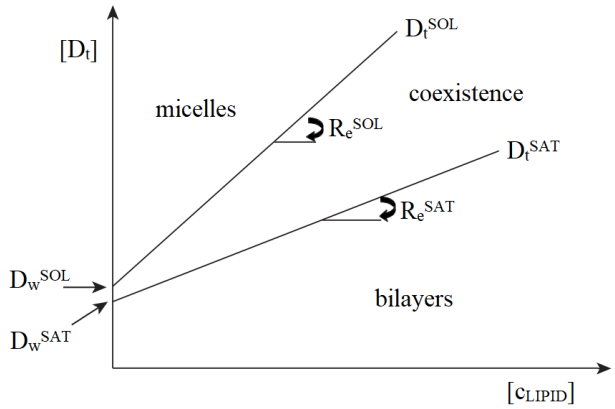

Figure 14: Characterisation of the lipid-surfactant aggregates using the dependence of D_t^{SAT} and D_t^{SOL} on concentration of lipid. The lines of the dependence distinguish the change between the three solubilisation stages with different lipid-surfactant aggregates.

Solubilisation and its critical steps can be characterised by several parameters. The total concentrations of surfactant (D_t) required for the initiation of the liposome-micelle transformation (D_t^{SAT}) and its completion (D_t^{SOL}) are linearly dependent on the lipid concentration of the mixture (Figure 14). D_t^{SAT} is the surfactant concentration at which the bilayer is completely saturated by the surfactant and the D_t^{SOL} denotes the total concentration of the surfactant causing complete solubilization of the bilayers to mixed micelles. Linear dependences of D_t^{SAT}, D_t^{SOL} on the lipid concentration in the Figure 14 define 3 regions with different composition. Prior to the saturation, the solution contains liposomes and surfactant molecules partitioned between the liposomes and the water phase. After saturation of the bilayers, there is a transition region of coexistence of surfactant-saturated bilayers and already formed mixed micelles. In the last region the mixed micelles are present together with the abundant surfactant in the form of monomers or micelles. Concentrations of surfactant in water at the onset of the second stage of solubilisation (D_w^{SAT}) and after its completion (D_w^{SOL}) can be obtained by extrapolating the dependences of D_t^{SAT} and D_t^{SOL} on the lipid concentration to zero lipid concentration. The slopes of these dependences, R_e^{SAT} and R_e^{SOL}, are the effective surfactant-lipid molar ratios causing the onset and completion of the second stage. (Lichtenberg et al., 2013a) With this dependence, it is also possible to determine the partition coefficient of the surfactant between lipid and water phase. This method will be discussed in a later chapter (3.4 Partition coefficient calculations).

Several mechanisms have been proposed for the process of solubilization and the way it proceeds. Based on the time it takes to achieve the liposome-micelle transition we distinguish slow and fast solubilisation. The ***fast solubilisation*** occurs via saturation of the bilayer by a surfactant capable of rapid flip-flop movement into the inner leaflet of the

liposome. This is also called ***transbilayer mechanism***. The amount of surfactant in the bilayer subsequently creates defects in the membrane and disruption of the bilayer because of high curvature stress. In some cases, solubilisation may start in a surfactant-rich region following a surfactant segregation for instance due to poor miscibility with the lipid. DDAO and Triton X-100 (TX-100), another surfactant often used in scientific research, are examples of such fast solubilising surfactants. On the other hand, ***slow solubilisation*** happens in the case of surfactants incapable of rapid flip-flop movement, such as anionic SDS (sodium dodecyl-sulphate) or surfactants with bulky molecules (bile salt, Tween-20). The so-called ***micellar solubilisation*** assumes the surfactant micelles extract the bilayer lipid components directly from the liposomes. The problem is that the slow solubilisation takes place at surfactant concentration below their critical micellar concentration (CMC). This was explained by the probability that the surfactants might be able to form unstable and short-lived small micelles even bellow their CMC, which can be stabilised by incorporating the lipid molecules. The completion of the micellar solubilisation process might take hours or even days to reach equilibrium. (Heerklotz and Blume, 2012; Lichtenberg et al., 2013b; le Maire et al., 2000)

Solubilisation of mammalian model membranes by surfactants have been studied by several experimental methods. The most commonly used are spectroscopic techniques, static and dynamic light scattering or fluorescence spectroscopy. The most commonly used, and hence the best-studied, in solubilisation literature is non-ionic surfactant ***TX-100*** (de la Maza and Parra, 1994; Sot et al., 2002; Ahyayauch et al., 2010; Mattei et al., 2017). In the works of (Schnitzer et al., 2005; Mattei et al., 2015), the authors observed the effect of added cholesterol on the solubilisation induced by the TX-100. As Ahyayauch (Ahyayauch et al., 2010) pointed out in his work, each surfactant exhibits unique behaviour when interacting with the membrane and therefore it is difficult to compare the effect of two different surfactants.

Our group (Department of Physical Chemistry of Drugs) studied the interaction of ***DDAO with mammalian model membranes*** using various methods. Densitometry study (Belička et al., 2014a) of DOPC proved ideal mixing of DOPC and DDAO within the studied range (0 – 30 wt.% of DDAO). Small-angle neutron scattering (SANS) study of ULLs of DOPC using the external H_2O/D_2O contrast variation technique showed that increasing the molar ratio n_{DDAO}:n_{DOPC} caused narrowing of the hydrocarbon region in DOPC bilayers (Belička et al., 2014b). Pore formation in DOPC and DOPC-CHOL model membranes by DDAO was detected by leakage of fluorescent probe calcein (Huláková et al., 2013; 2015). The effect of DDAO on Ca^{2+}-ATPase activity of a sarcoplasmic reticulum incorporated into a membrane composed of PCs with different chain lengths was studied in (Karlovská et al.,

2006). Complexes composed of DDAO, dioleoylphosphatidylethanolamine (DOPE) and DNA have been investigated as potential carriers of DNA in gene therapy in the works of (Hubčík et al., 2015; Liskayová et al., 2017). Destabilisation of DOPC-containing ULLs by DDAO and solubilisation it into mixed DOPC-DDAO micelles was studied in (Uhríková et al. 2001). Solubilisation of egg-yolk phosphatidylcholine (EYPC) ULLs by DDAO was studied in (Hrubšová et al., 2003). Solubilisation of EYPC MLLs was studied in (Karlovská et al., 2004b).

The study of ***solubilisation of bacterial model membranes*** is a novelty in our department. The effect of DDAO on bacterial membrane models in scientific literature is not documented and is therefore the subject of this study.

1.6 Antimicrobial peptides

Living organisms use different water-membrane soluble proteins and peptide toxins as defensive mechanisms. A large group of such substances includes antimicrobial peptides that serve as a ***non-specific defence system*** complementing pathogen-specific cell-mediated immune response. Shortly after a bacterial infection, these peptides are mobilized to have rapid effect against a broad spectrum of microorganisms. Rapid response is necessary because the highly specific cell-mediated immune response is relatively slow compared to the high reproductive potential of microorganisms. (Shai, 2002; Cisse et al., 2021)

Peptide antibiotics used in therapeutic practice

Polypeptide antibiotics belong to the most effective antimicrobial agents. A relatively large number of polypeptides have been isolated, but their practical use is limited by a number of undesirable effects, nephrotoxicity in particular. These polypeptide antibiotics are charged drugs with strong basic character, therefore are not absorbed by the gastrointestinal system. Against systemic infections, a parenteral (intravenous) application is necessary. An example is bacitracin, a cyclic decapeptide isolated from *Bacillus subtilis* or polymyxins isolated from *Bacillus polymyxa*. Their systemic use is limited only for bacteria resistant to less toxic antibiotics. Polymyxin E (colistin) is administered parenterally in a modified form, colistimethate sodium, while polymyxin B is used only topically. Tyrothricin (isolated from *Bacillus brevis*) is a mixture of two polypeptide antibiotics, gramicidin and tyrocidine. For severe side effects (nephrotoxicity and hepatotoxicity), only local use is allowed. ***Glycopeptide antibiotics*** are formed by a polypeptide chain with different carbohydrates linked via glycoside bonds. We include the ototoxic and nephrotoxic

vancomycin (from *Streptomyces orientalis*) and structurally similar teicoplanin (from *Actinoplanes teichomyceticus*). (Hartl et al., 2012)

In addition to these polypeptide and glycopeptide antibiotics that are already in use, a large number of antimicrobial peptides of various structural types have been discovered. Most multicellular organisms produce a mixture of multiple peptides of different structure. Even in related species, the diversity of produced antimicrobial peptides is very high. It is believed that the diversity reflects the adaptation of individual species to the unique microbial environment in which the organism was evolving.

Because of the great diversity of the antimicrobial peptides, it is difficult to categorise them, but it can be broadly done, based on their common structural properties:

I. ***Amphiphilic and hydrophobic α-helical peptides*** (e.g. alamethicin, gramicidin A, magainin, dermaseptin, cecropin, melittin, pleurocidin, LL37).
II. ***β-sheet peptides*** (e.g. tachyplesins, protegrins, lactoferricin, gramicidin S, polymyxin B, tyrocidine).
III. ***Peptides enriched in specific amino acids (AAs)*** (e.g. histatins, PR-39, prophenin, tritrpticin, indolicidin).
IV. ***Peptides with thioether rings*** (e.g. lantibiotics – nisin, cinnamycin).
V. ***Peptaibols*** (e.g. trichogin).
VI. ***Macrocyclic cystine-knot peptides*** (e.g. circulins A and B).

(Brogden, 2005; Epand and Vogel, 1999; Zasloff, 2002)

Structure – effect relationship

Antimicrobial peptides are a diverse group of substances produced by tissues and cell types of various plant and animal species. There are some characteristic structural properties that affect the antimicrobial activity. These include the size and the charge, primary and secondary structure and their amphiphilic character.

a. ***size***: The size of antimicrobial peptides ranges from 6 AAs for anionic peptides to more than 59 AAs (e.g. cationic Bac7 peptide). Dipeptides and tripeptides exhibiting antimicrobial activity have been recorded as well.
b. ***charge***: Negatively charged antimicrobial peptides complexed with zinc or highly positively charged peptides are usually more active than neutral peptides or peptides with lower charge. Aspartic and glutamic acids give peptides anionic character, while cationic peptides are enriched in arginine and lysine instead.
c. ***primary structure***: Antimicrobial peptides frequently consist of basic AAs (lysine or arginine), hydrophobic AAs (alanine, leucine, phenylalanine or tryptophan) and others

AAs (such as isoleucine, tyrosine, valine). In some peptides, the AAs sequences can be repeated. The ratio of hydrophobic and charged AAs can range from 1:1 to 2:1.

d. ***secondary structure***: Antimicrobial peptides can adopt various secondary structures including α-helixes, relaxed coils or antiparallel β-sheets. Amphiphilic (explained in the next point) α-helical peptides are usually more potent than peptides with a less defined secondary structure.
e. ***amphiphilicity***: For α-helical peptides, we often observe the arrangement of AAs with hydrophilic AAs at one side of the helix and hydrophobic AAs at the other side of the helix. For peptides with a different secondary structure, such spatial separation of hydrophilic and hydrophobic AAs is more difficult to qualify. Peptides with a strong amphiphilic structure exhibit haemolytic activity, while less amphiphilic peptides have stronger antimicrobial activity. The ability to fold into an amphiphilic structure is often induced by membrane interaction. Hydrophobic part of the peptide allows the incorporation into the membrane. (Lohner and Blondelle, 2005; Brogden, 2005; Powers and Hancock, 2003)

1.6.1 Interaction of antimicrobial peptides with model membranes

It is unlikely for such a diverse group of peptides to have the same mechanism of action, but the interaction of antimicrobial peptides with membranes is essential for most, if not all. This is supported by their broad spectrum of activity and quick mode of action (in vitro usually in minutes). (Epand and Vogel, 1999) Antimicrobial peptides containing D-forms (instead of the natural L-forms) of AAs showed the same activity as the natural peptides, which also supports the interaction with the membrane lipids mode of action rather than some stereospecific protein receptors. The bacterial membranes contain negatively charged lipids in higher amounts and despite the high diversity, the vast majority of antimicrobial peptides is positively charged. Therefore, we assume that the electrostatic interaction may play an important role in differentiation between eukaryotic and prokaryotic cells. (Huang, 2000) We believe that most of the antimicrobial peptides act by influencing membrane permeability (insertion and subsequent pore formation), but other mechanisms of action were also observed.

I. Carpet model and pore formation

Antimicrobial peptides cause damage to the membranes by disintegration or pore formation. The pores allow increased transport of water and ions across the membrane. The collapse of the transmembrane electrochemical gradient means the loss of energy source, because bacteria have the respiratory chain enzymes present in the plasma membrane.

Therefore, the formation of pores in the plasma membrane is ultimately lethal for bacteria. (Shai, 2002; Bechinger and Lohner, 2006) Several models describe the interaction of antimicrobial peptides with the membranes. The mechanism of membrane disruption depends both on the properties of the peptide and the composition of the membrane. Biophysical studies showed complex behaviour with regard to membrane disruption, which can vary from pore formation to micellization (carpet model). Formation of peptide-rich domains was observed as well, which can promote formation of cubic structures, affecting the membrane function and integrity. (Lohner, 2009)

A typical feature of the so-called ***carpet model*** is the adsorption of the antimicrobial peptide to the surface of the membrane and its coverage. Adsorption continues until a certain breakpoint concentration at which the peptide begins to insert into the hydrophobic core of the membrane resulting in its permeation and disruption. The explicit mechanism of this process is less determined, possibly disintegration in a similar way as in case of surfactants or creation of pores/channels. (Lohner, 2009) Some antimicrobial peptides are able to form oligomers with different behaviour than that of monomers. (Bechinger and Lohner, 2006) Whether it is monomers or oligomers, the antimicrobial peptides coat the surface of the membrane as indicated by the name of this model (like a carpet). At low peptide to lipid ratio (P/L), the antimicrobial peptides position their hydrophobic part of their secondary structure to the surface of the membrane and the hydrophilic parts towards the aqueous environment. Upon reaching the threshold peptide to lipid ratio (P/L*), the antimicrobial peptides permeate/disintegrate the membranes by distorting their curvature, with antimicrobial peptides stabilising (covering) any openings in the membrane, similarly as surfactants do. Therefore, this mechanism is also called in literature as “surfactant-like” model. The carpet mechanism was described for the interaction of dermaseptin S with the bacterial membrane and also for many other antimicrobial peptides, among the more known, e.g. cecropins and antimicrobial peptide produced by humans, LL-37. (Shai, 2002; Huang, 2000; Nicolas and Ladram, 2013; Marx et al., 2021)

Another possibility is the insertion of the antimicrobial peptides into the membrane and creation of pores. Two types of pores have been documented. In the case of ***barrel-stave model***, the α-helical peptides act like staves that form a barrel-like pore traversing the membrane. An example of such peptide is alamethicin, whose pores are formed by approximately eight monomers. When it comes to the ***toroidal-pore model***, the antimicrobial peptides insert into the membrane and cause the lipid monolayers to bend at the edges of the pore connecting the two leaflets. The lipid headgroups at the bend serve as a part of the pore. Toroidal pores are created by melittin, magainins and protegrins. (Brogden, 2005)

II. Some antimicrobial peptides also show ***intracellular targets*** (e.g. mersacidin, buforin II, pleurocidin and PR-39***)*** or ***receptor-mediated killing*** (e.g. nisin Z and mesentericin Y). (Shai, 2002)

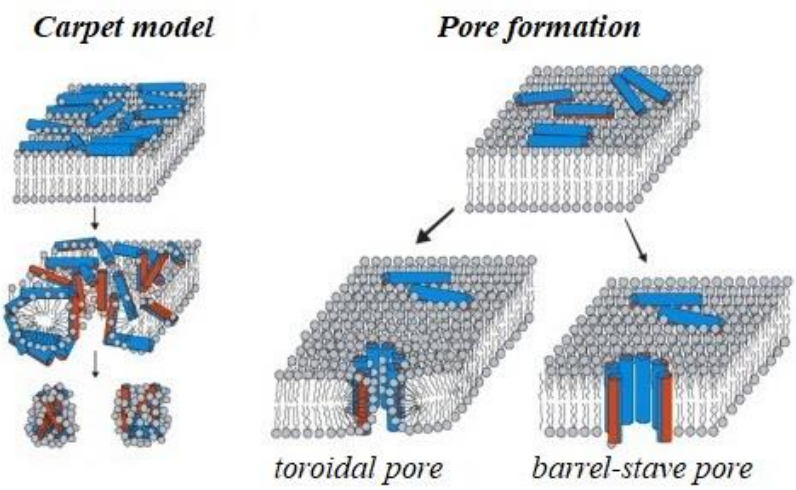

Figure 15: Models of the interaction of antimicrobial peptides with lipid bilayers. Blue represents the hydrophilic side of the peptide, red is the hydrophobic part. Fig. adapted from (Salditt et al., 2006).

1.6.2 Dermaseptin S1

Dermaseptins are a large group of cationic peptides exhibiting membrane damaging effects. Their antimicrobial activity have been already detected at micromolar concentrations against a wide spectrum of microorganisms: G^+, G^- bacteria, mycoplasma, fungi, protozoa, yeasts and enveloped viruses. The individual peptides of this group exhibit variability of effect on different organisms. (Nicolas and Ladram, 2013; Bartels et al., 2019) The dermaseptins consist of a 28 – 34 AAs long chain, with a typical incidence of 3 – 6 lysine residues and tryptophan in the third position (from the N-terminus). In addition to their antimicrobial effects, the spermicidal activity of dermaseptins against human spermatozoa was demonstrated. Dermaseptins have low to no detectable haemolytic activity. (Savoia et al., 2008)

Dermaseptin S1 (DS1) was extracted from dried skin of the frog *Phyllomedusa sauvagii*. It has 34 AAs (5 positively charged and 1 negatively charged AAs) and exhibits lytic activity against G^+, G^- bacteria, yeasts and protozoa. (Nicolas and Ladram, 2013) Dermaseptins S1 – S5 showed antiviral activity against Herpes simplex (type 1) and HIV-1. It has been shown that DS1 promotes the microbicidal activity of polymorphonuclear leukocytes by stimulating stimulating the production of reactive oxygen molecules and releasing myeloperoxidase already at concentrations 10 – 100 nmol/dm^3. (Nicolas and El

Amri, 2009) The minimum inhibitory concentration (MIC) of DS1 against *Staphylococcus aureus* and *Escherichia coli* is 12 μmol/dm^3. 50% haemolysis of human erythrocytes was observed at concentrations greater than 100 μmol/dm^3. DS1 exhibits the lowest haemolytic activity from natural dermaseptins. (Savoia et al., 2008) In comparison, DS4 stimulates 50% haemolysis at a concentration of 1.4 ± 0,2 μmol/dm^3, while the concentration required for 50% growth inhibition of *E. coli* was 40 ± 5 μmol/dm^3. (Feder et al., 2000) DS4 analogues have been recently examined as potential antiviral agents against Covid-19 infection (Sekar and Rajasekaran, 2021).

For DS1 to take effect on the plasma membrane of our model organism *E. coli*, it must first first overcome the outer membrane barrier. It is presumed that it happens via ***self-promoted uptake***. This hypothesis suggests that unfolded cationic peptides associate with the negatively charged surface of the outer membrane (created by LPS), neutralising the charge and creating an opening for the peptides to pass through. (Powers and Hancock, 2003; Shai, 2002)

Structure – effect relationship of DS1 and its analogues

The amino acid sequence of dermaseptin S1 ($C_{152}H_{257}N_{43}O_{44}S_2$) in its abbreviated form is ALWKTMLKKLGTMALHAGKAALGAAADTISQGTQ. (Nicolas and Ladram, 2013) Part of the DS1 molecule responsible for antimicrobial activity is the N-terminal α-helical fragment of AAs 1 – 18. An analogue shortened by 5 AAs, DS1(1-29)-NH_2 exhibits very high antimicrobial activity. This derivative showed high antiviral activity against human papillomavirus (associated with cervical cancer) when lysine was replaced by threonine in position 4 and threonine replaced with lysine in position 12.

The minimum of the bioactive sequence is DS1(1-15)-NH_2. Tryptophan in position 3 is essential for the antimicrobial activity but it may be replaced by a synthetic AA with a side chain containing a naphthyl residue, e.g. 3-(1-naphthyl)alanine. This exchange resulted in increased efficacy against *Candida albicans* (yeast causing skin and vaginal mycoses) but decreased the effect against *Trichomonas vaginalis* (causes a sexually transmitted disease trichomoniasis). High antiviral activity against herpes simplex virus was also observed. A decrease in activity was observed if the tryptophan was replaced by AA with 1H-imidazole, *p*-hydroxyphenyl or isobutyl side chain. Tryptophan is likely to be important in terms of anchoring the peptide on the surface of the membrane. Adding lysine to the N-terminus of DS1(1-15)-NH_2 increased efficacy against *E. coli*, probably due to the positive charge of lysine. (Savoia et al., 2008; 2010; Mor and Nicolas, 1994; Mor et al., 1994)

2 GOALS

This dissertation aims to examine and compare the interactions of two types of model membranes – mammalian and bacterial types – with compounds that exert antimicrobial activity – surfactant *N*,*N*-dimethyl-1-dodecanamine-*N*-oxide (DDAO) and antimicrobial peptide dermaseptin S1 (DS1) using a variety of methods.

Study of DDAO interactions with model membranes:

1. **Static light scattering:**
   a) To study and compare the interaction of mammalian and bacterial model membrane in the form of ULLs with DDAO.
   b) To determine concentrations of DDAO needed to reach certain stages of the solubilisation process.

2. **Fluorescence spectroscopy:**
   a) To study the leakage of an encapsulated fluorescent probe calcein from the ULLs after the addition of DDAO.

3. **Vibrational densitometry:**
   a) To measure the density of bilayers formed by lipids or mixtures of lipids used in this study, in order to be able to calculate the partition coefficient of DDAO.
   b) To calculate the volumetric parameters of lipids used in this study, essential to evaluate the data obtained from small-angle neutron scattering and diffraction.

4. **Partition coefficients** calculation of DDAO between the model membranes (mammalian and bacterial) and the aqueous phase.

5. **Small-angle neutron scattering (SANS):**
   a) To study the changes in the bilayers caused by DDAO before the solubilisation of mammalian and bacterial model membrane.
   b) To determine the geometry of LIPID-DDAO mixed non-lamellar aggregates.

6. **Small-angle neutron diffraction (SAND):**
   a) To study the mammalian and bacterial model membranes using the swelling method and the contrast variation method.

b) To obtain the diffraction data from mammalian and bacterial model membrane samples mixed with DDAO in various molar ratios up to $n_{DDAO}:n_{LIPID} = 1$.
c) To evaluate the diffraction data, reconstruct the neutron scattering length density profiles and calculate the water distribution probability across the membranes.

Study of DS1 interaction with model membranes:

1. **Fluorescence spectroscopy:**
   a) To study the release of fluorescent probe calcein after the addition of DS1 to the bacterial model membrane ULLs and compare its effect with the effect of DDAO.

2. **Small-angle neutron diffraction (SAND):**
   a) To study the mammalian and bacterial model membrane samples mixed with DS1 in various molar ratios using the contrast variation technique.
   b) To evaluate the diffraction data, reconstruct the neutron scattering length density profiles and calculate the water distribution probability across the membranes.

3 ANALYSIS OF METHODOLOGICAL APPROACH

3.1 Static light scattering

A focused monochromatic beam of radiation (with a wavelength λ) is scattered in all directions by particles smaller than 3/2 λ. We recognise two basic types of scattering: an elastic scattering (the energy of the radiation does not change) and inelastic scattering (the energy changes) (Harvey, 2000). For our research, only the elastic type of scattering, the so-called Rayleigh scattering, is interesting. Rayleigh scattering is observed at a particle size of less than 5% of the wavelength of the radiation used. Scattered radiation is symmetrically distributed, and the intensity of scattered radiation is the reciprocal of the 4th power of the wavelength of radiation (λ^{-4}), as described by the equation:

$$\frac{I_\theta}{I_0} = \left(\frac{n'}{n} - 1\right)^2 \left(\frac{NV^2}{r^2\lambda^4}\right)(1 + \cos^2\theta) \qquad 2$$

where I_θ – the intensity of the scattered light at the angle θ, I_0 – the initial light intensity, n' – refractive index of the particles, n – refractive index of the solvent, N – number of particles with volume V, r – distance from sample to detector (Lawler, 2005).

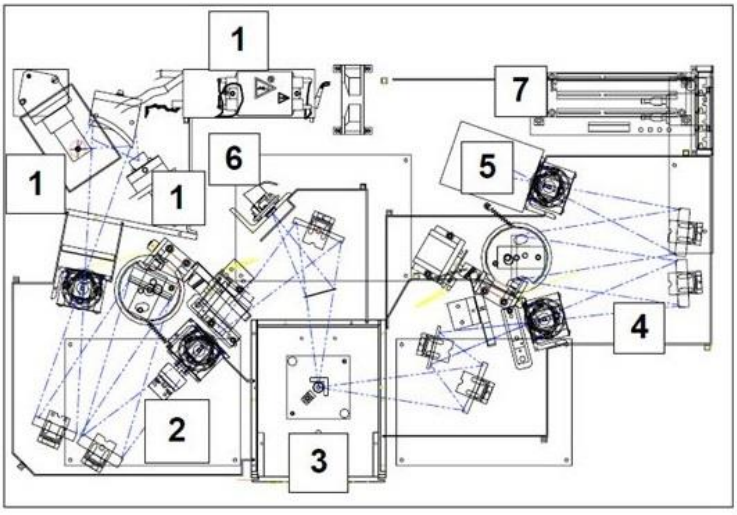

Figure 16: Scheme of a spectrofluorometer instrument. 1 – xenon lamp, xenon lamp power supply and flash lamp; 2 – excitation monochromator; 3 – sample compartment; 4 – emission monochromator; 5 – detector; 6 – reference detector; 7 – instrument controller (operation manual FluoroMax-4 Spectrofluorometer).

Both nephelometry and turbidimetry are methods based on the scattering of electromagnetic radiation by particles of the system under investigation. Turbidimetry measures the loss of radiation in the direction of the passing beam. In the case of

nephelometry, we measure true scattered radiation at 90° angle from the radiation source. Nephelometric measurements are most often carried out on a spectrofluorometer, with identical excitation and emission wavelengths (in the range of 400 – 700 nm). The spectrofluorometer scheme is shown in the Figure 16. The spectrofluorometer has a detector positioned at an angle of $\theta = 90°$. The method is very sensitive even at low sample concentrations. Higher sensitivity allows the use of higher wavelengths, which is advantageous in order for Rayleigh scattering conditions to be met. (Harvey, 2000; Goni and Alonso, 2000; Lawler, 2005; Brar and Verma, 2011)

3.1.1 Sample preparation (nephelometry)

3.1.1.1 Chemicals

1,2-dioleoyl-*sn*-glycero-3-phosphocholine (DOPC), 1-palmitoyl-2-oleoyl-*sn*-glycero-3-phosphocholine (POPC), cholesterol (plant derived) (CHOL), sphingomyelin (Egg, Chicken) (EYSM), 1-palmitoyl-2-oleoyl-*sn*-glycero-3-phosphoethanolamine (POPE), 1-palmitoyl-2-oleoyl-*sn*-glycero-3-phospho-(1'-rac-glycerol) (sodium salt) (POPG), 1',3'-bis[1,2-dioleoyl-*sn*-glycero-3-phospho]-glycerol (sodium salt) (also called tetraoleoylcardiolipin, TOCL) were purchased from Avanti Polar lipids (USA) and used without further purification. *N*,*N*-dimethyldodecylamine-*N*-oxide (DDAO) was obtained from Sigma-Aldrich (Germany). Buffer constituents monopotassium phosphate (KH_2PO_4), dipotassium phosphate (K_2HPO_4), sodium chloride (NaCl) and organic solvents chloroform ($CHCl_3$) and methanol (CH_3OH) were of analytical grade.

3.1.1.2 Phosphate-buffered saline (PBS)

PBS buffer consisting of 7.6 mmol/dm^3 KH_2PO_4, 42.4 mmol/dm^3 K_2HPO_4 and 150 mmol/dm^3 NaCl was prepared using redistilled water. pH ~ 7.5 was measured using pH meter MO 230 (Mettler Toledo, Switzerland) with combined glass electrode (4 mm InLab 422).

3.1.1.3 Liposome preparation

Various lipids/lipid compositions were studied using nephelometry: DOPC, POPC, POPC-CHOL (n_{POPC}:n_{CHOL} = 2:1 mol/mol), POPC-EYSM-CHOL (n_{POPC}:n_{EYSM}:n_{CHOL} = 0.375:0.375:0.25 mol/mol/mol), POPE-POPG (n_{POPE}:n_{POPG} = 0.6:0.4 mol/mol), POPE-

POPG-TOCL (n_{POPE}:n_{POPG}:n_{TOCL} = 0.67:0.23:0.1 mol/mol/mol). Weighted amounts of dry lipids in glass tubes were co-solubilised by dissolving in chloroform (or $CHCl_3$:CH_3OH 1:1 v/v mixture in case of POPC-EYSM-CHOL). Organic solvent was evaporated under a stream of gaseous nitrogen to dryness. Evacuation in a vacuum chamber using rotary oil pump for 8 h followed.

For nephelometric measurements, DOPC liposomes of various size and concentration were prepared to test the sensitivity of the method. Adequate amount of DOPC was hydrated with 1 ml of H_2O to obtain lipid concentration 50 mmol/ dm^3. 24 h long hydration allowed spontaneous formation of MLLs and a vortex mixer was used from time to time to obtain homogenous dispersion. ULLs with different sizes were prepared using filters with different size of pores (50, 100 and 200 nm pores) during the extrusion. MLLs dispersion was extruded (LiposoFast-Basic Extruder) 51 times through 50 nm, 100 nm or 200 nm polycarbonate filter (Olson et al., 1979; MacDonald et al., 1991). Extruded stock solution was used to create 10 samples with concentration ranging from 0.01 mmol/dm^3 to 0.1 mmol/dm^3.

For solubilisation experiments with DDAO, adequate amount of dry lipid film was hydrated with 1.3 ml of PBS buffer to obtain 10 mmol/dm^3 lipid concentration. Spontaneous formation of MLLs was accompanied by occasional mixing with a vortex mixer until a homogenous dispersion was obtained. MLLs dispersion was extruded through a 100 nm polycarbonate filter 51 times. Acquired dispersion was used to prepare a set of 25 samples with constant lipid concentration and increasing concentration of DDAO from 0 to 3.12 mmol/dm^3. POPC-CHOL, POPE-POPG and POPE-POPG-TOCL were prepared with lipid concentrations 0.02; 0.04; 0.06; 0.08 and 0.1 mmol/dm^3, while only 0.1 mmol/dm^3 samples were prepared in case of POPC and POPC-EYSM-CHOL.

3.1.1.4 DDAO stock solution preparation

Adequate volume of 1 mmol/dm^3 DDAO stock solution was prepared before each individual measurement. PBS with pH ~ 7.5 was used as a solvent.

3.1.2 Nephelometric measurements

Nephelometric experiments were carried out using Fluoromax 4 spectrofluorometer (Horiba Jobin Yvon, USA). Scattering of the light with 600 nm wavelength at a 90° angle was measured for 6 seconds every 0.1 second. The data were corrected for fluctuations caused by the light source (signal in CPS was divided by the lamp reference detector signal).

Average intensity of the scattered light was calculated. Samples were measured 3 hours after the DDAO was added to the ULLs dispersion at controlled temperature of 25°C.

3.1.3 Data treatment

The measured dependences of fluorescence intensity on the concentration of lipid (we will use the term "solubilisation curve" to describe these dependences) followed the three-stage process described in 1.5.1 Interactions of surfactants with model membranes. Surfactant concentration causing the turning points (signalising the progress to the next stage of the solubilisation process) in the course of the solubilisation curve will be referred to as "critical concentration" (D_t). Since there are three stages, two critical concentrations were sought. They were labelled D_t^{SAT} (progress from the first to the second stage) and D_t^{SOL} (from the second to the last stage). D_t^{SAT} is the total concentration of DDAO in the sample, which after partitioning between the liposomes and water phase saturates the bilayer sufficiently enough to start the transformation of liposomes into mixed micelles. D_t^{SOL} represents the total concentration of DDAO that causes complete transition of all present bilayers into mixed micelles.

Bilinear function was used to fit the solubilisation curve, specifically the transition from the first to the second stage:

$$y = (kx + q) \times 0.5 \times \left(1 - \frac{x - D_t}{|x - D_t|}\right) + (mx + D_t(k - m) + q) \times 0.5 \times \left(1 + \frac{x - D_t}{|x - D_t|}\right) \quad 3$$

where $y = kx + q$ and $y = mx + r$ are the equations for the straight lines, before and after the turning point (D_t), respectively. D_t is the x-coordinate of the turning point, in this case the fit was used to calculate D_t^{SAT}.

Because the signal in the third stage was not significantly changing, a modified bilinear function was used to fit the solubilisation curve to find the second turning point.

$$y = (mx + s - mD_t) \times 0.5 \times \left(1 - \frac{x - D_t}{|x - D_t|}\right) + s \times 0.5 \times \left(1 + \frac{x - D_t}{|x - D_t|}\right) \quad 4$$

where $y = mx + r$ is the equation for the straight line in the second stage of solubilisation and in the third stage the signal was considered constant (therefore, the straight line equation for the third stage is $y = s$).

Apart from the turning points, the solubilisation can also be characterized by a critical concentration labelled as D_t^{MID}. D_t^{MID} is total concentration of DDAO in the sample causing the turbidity from the first stage to diminish by a half. To determine its numerical value, we

have used ***reverse sigmoid function*** (also known as Boltzmann function) to fit the solubilisation curve:

$$A_T = A_{T,min} + \frac{A_{T,max} - A_{T,min}}{1 + \exp\left(-\frac{c_{DDAO} - D_t^{MID}}{dc_{DDAO}}\right)} \quad 5$$

where $A_{T,max}$ – the maximum turbidity, $A_{T,min}$ – the minimum turbidity and dc_{DDAO} is the width of the transition from liposomes to mixed micelles. D_t^{MID} is the x-coordinate of the midpoint of the sigmoid.

3.2 Fluorescence spectroscopy

The basis of fluorescence spectroscopy is a phenomenon called luminescence. Luminescence is the emission of light by a substance in an excited state. When the substance enters the excited state by absorbing the energy of light, we speak of photoluminescence. Depending on the nature of the excited state, we divide luminescence into 2 categories: ***fluorescence*** and ***phosphorescence***. The processes that take place between absorption and emission of light are described by Jablonski diagram (Figure 17) (Lakowicz, 2006).

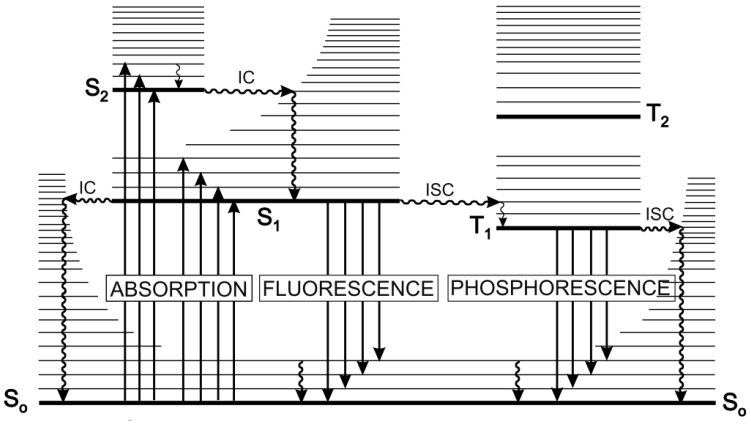

Figure 17: Jablonski diagram. IC – internal conversion, ISC – intersystem crossing, S_0, S_1, S_2 – singlet electronic states, T_1, T_2 – triplet electronic states. Horizontal lines represent different vibrational levels. (Valeur, 2002)

Under normal circumstances, most molecules occur at the lowest vibrational energy levels of the singlet ground electronic state (S_0). Electrons that make up an electron pair have a different spin in this state. After energy ***absorption***, the molecules are excited into the vibrational energy levels of the first or second singlet state (S_1, S_2). This means one of the valence electrons moves to the excited singlet state, keeping its original spin. Absorption is a very fast process (10^{-15} s). Relaxation, returning to a ground energy state, can happen

through several mechanisms. Excess energy can be released by radiationless deactivation or by releasing a photon with energy:

$$E = h\nu = \frac{hc}{\lambda} \qquad 6$$

where h – Planck's constant, ν – radiation frequency, c – speed of light in vacuum, λ – wavelength.

Fluorescence is the release of a photon when the electron passes from the singlet excited state to the ground state. The electron remains in the singlet excited state only for 10^{-5} – 10^{-8} s, thus fluorescence is a very fast process. If the spin of the electron changes in the excited state, we are talking about the triplet excited state (T_1). The transition from the lowest vibrational level of the excited state to the higher vibrational level of the electronic state with the lower energy with different spin is referred to as ***intersystem crossing*** ($S_1 \rightarrow T_1$). The transition of the electron from this state to the ground state is spin disabled, because both electrons have the same spin. Returning to the ground level is more challenging, resulting in a longer process – ***phosphorescence*** (10^{-4} – 10^{4} s).

There are several methods of ***radiationless deactivation***, e.g. vibrational relaxation, lasting less than 10^{-2} s. ***Vibrational relaxation*** means that the molecule loses energy by moving to lower vibrational levels of the same electronic state. For ***internal conversion***, an example of which is the transition $S_2 \rightarrow S_1$, the molecule from the lowest vibrational level of the excited state passes to a higher vibrational level of the excited state with lower energy but the same spin. ***External conversion*** means transferring excess energy to solvent molecules or other system components. The last way of radiationless deactivation is the already mentioned inter-system crossing. (Valeur, 2002; Harvey, 2000; Lakowicz, 2006)

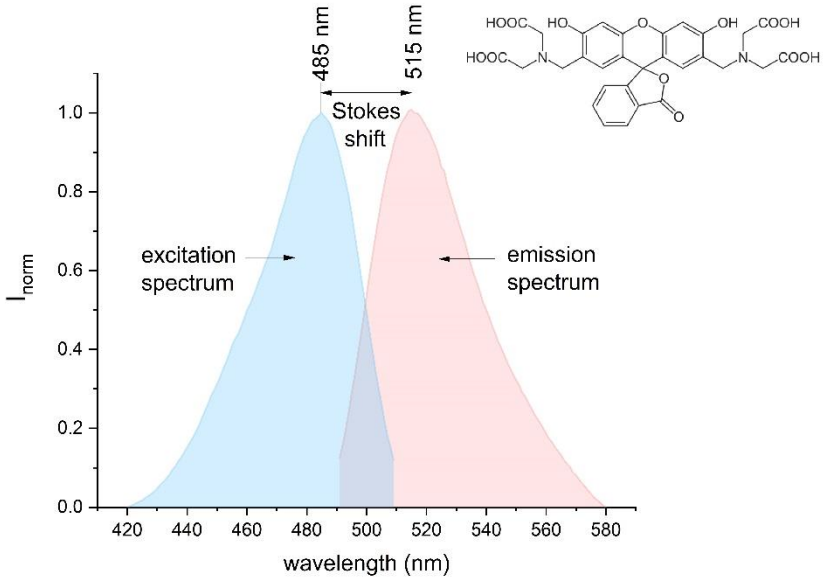

Figure 18: Excitation and emission spectra of fluorescent probe calcein and its chemical structure.

Figure 18 shows the excitation and emission spectra of our fluorescent probe calcein. The excitation spectrum shows a change in the fluorescence intensity measured at maximum emission wavelength (515 nm). The emission spectra were measured using the maximum excitation wavelength (485 nm). The excitation and emission spectra are similar, due to the vibrational levels of the ground and excited state being similar. This phenomenon is called ***mirror image rule***. The difference between the maxima of excitation and emission spectra is called the ***Stokes shift***. The energy of emission is typically smaller than that of excitation, therefore, it occurs at a longer wavelength. (Valeur, 2002; Harvey, 2000; Lakowicz, 2006)

Fluorescence efficiency (the fraction of excited state molecules returning to the ground state by fluorescence) is quantitatively expressed by the fluorescence quantum yield (Φ_F). Fluorescence does not occur if $\Phi_F = 0$, while each molecule in the excited state undergoes fluorescence if $\Phi_F = 1$. If the concentration of the solution is low ($\varepsilon cl < 0.01$), the ***fluorescence intensity*** (I_F) can be expressed by a relationship derived from the Lambert-Beer law as:

$$I_F = 2.303 k \Phi_F I_0 \varepsilon cl \qquad 7$$

where k – instrument constant (the efficiency of detecting the fluorescence emission), I_0 – intensity of the excitation source, ε – molar absorption coefficient, c – molar concentration, l – length of the optical path (Harvey, 2000).

The fluorescence intensity of certain fluorescent probes decreases at high concentrations. This process is known as ***self-quenching***. The mechanisms of self-quenching are not completely known. Because it happens at relatively high concentrations, it is likely caused by the formation of complexes lacking fluorescent properties (Hamann et al., 2002). The fluorescent probe calcein is an example of such self-quencher, which can be useful for fluorescent probe leakage experiments.

Surfactant-induced membrane leakage

Surfactants can cause leakage of liposomal internal contents by various mechanisms. In case of surfactants undergoing no spontaneous flip-flop (see 1.2.3 Membrane fluidity), the membrane may rupture because of the asymmetric lateral expansion of the outer layer. General mechanical failure of the membrane may occur as a result of thinning and disordering of the bilayer by the surfactant. The last mechanism of pore formation is that the surfactant stabilises the highly curved edges of the pores by creating surfactant-rich rims.

The formation of pores in the membrane due to the effect of surfactants or some antimicrobial peptides can be observed by fluorescent probe leakage method. The principle of this method is the entrapment of a fluorescent probe inside the ULLs at a self-quenching concentration. The non-encapsulated probe is removed from the dispersion by gel

chromatography. The pore formation in the bilayer of ULLs is observed by the release of the probe into the extra-liposomal space due to the addition of pore-forming compounds. The fluorescent probe that is released from the ULLs is diluted to such an extent that an increase in fluorescence intensity can be observed. Enclosure of fluorescent probes of different molecular weights can be an indicator of the size of the pores. (Heerklotz, 2008; Patel et al., 2009; Lichtenberg et al., 2013b; Ahyayauch et al., 2010)

3.2.1 Sample preparation (fluorescence spectroscopy)

3.2.1.1 Chemicals

POPC, CHOL, POPE, POPG were purchased from Avanti Polar lipids (USA) and used without further purification. DDAO was obtained from Sigma-Aldrich (Germany). Buffer constituents (KH_2PO_4, K_2HPO_4, NaCl) were of analytical grade.

3.2.1.2 Phosphate buffered saline (PBS)

PBS buffer was prepared according to 3.1.1 Sample preparation (nephelometry).

3.2.1.3 Calcein solution preparation

Calcein (Acros Organics, USA), also known as bis[*N*,*N*-bis(carboxymethyl)amino-methyl]-fluorescein or fluorescein (chemical structure shown in Figure 18), was used as a fluorescent probe in our fluorescent probe leakage experiments. Calcein solution was prepared by dissolving adequate amount of crystalline calcein in minimum effective amount (~ 150 μl) of 1 mol/dm^3 NaOH solution, which was followed by heavy stirring using a vortex mixer and subsequent diluting with PBS to required concentration 10 mmol/dm^3 (pH of the final solution was ~ 7.46).

3.2.1.4 Preparation of liposomes with encapsulated calcein

Adequate amount of dry lipid film was hydrated with 2 ml of 10 mmol/dm^3 calcein solution and vortexed resulting in formation of MLLs, which were then extruded 51 times through 100 nm polycarbonate filter. The liposomes containing calcein were separated from the untrapped calcein in the extra-liposomal space by column chromatography using Sephadex G-50 fine gel swollen in PBS (Benachir and Lafleur, 1995; Memoli et al., 1999a). After the chromatography, the dispersion of liposomes with encapsulated calcein was diluted

to a required concentration, which was subsequently used to prepare a set of samples with a constant lipid concentration. Model membranes with different lipid compositions were prepared: POPC (c_{POPC} = 0.3 mmol/dm^3), POPC-CHOL (n_{POPC}:n_{CHOL} = 2:1 mol/mol, $c_{POPC+CHOL}$ = 0.1, 0.2, 0.3, 0.4 mmol/dm^3) and POPE-POPG (n_{POPE}:n_{POPG} = 3:2 mol/mol, $c_{POPE+POPG}$ =, 0.1, 0.2, 0.3, 0.4 mmol/dm^3). POPE-POPG with encapsulated calcein at lower lipid concentration (0.01 mmol/dm^3) was prepared for the experiment with dermaseptin S1 and similarly with DDAO (for comparison).

3.2.1.5 DDAO stock solution preparation

Adequate volume of 1 mmol/dm^3 DDAO stock solution was prepared before each individual measurement. PBS with pH ~ 7.5 was used as a solvent.

3.2.1.6 Dermaseptin S1 (DS1) stock solution preparation

2 ml of DS1 stock solution was prepared with concentration of 0.579 mmol/dm^3. The stock solution was further appropriately diluted before being added into the samples.

3.2.2 Fluorescence measurements

Pore formation was observed using the fluorescent probe leakage technique. Fluorescence measurements were carried out using Fluoromax 4 spectrofluorometer (Horiba Jobin Yvon, USA). The excitation and emission spectra of calcein are shown in Figure 18. Using the excitation wavelength of 485 nm, emission spectra in the wavelength interval 490 – 580 nm were recorded. The data were corrected for fluctuations caused by the light source (signal in CPS was divided by the lamp reference detector signal). The fluorescence intensity was evaluated at maximum of calcein emission. For a solution of calcein, the maximum of emission spectrum is 515 nm (Figure 18). For other samples containing lipids, the maximum of fluorescence emission spectra slightly varied within the range 513 – 520 nm. The results were not significantly different if the data were evaluated at 515 nm or at the maximum of fluorescence emission. Therefore, we decided to use the fluorescence intensity results obtained at the wavelength with maximum fluorescence. Calcein leakage experiments were performed on a set of samples (usually 25 samples per set) with constant lipid concentration and increasing concentration of added DDAO (0 – 3 mmol/dm^3, depending on the lipid composition). The samples containing mammalian lipid liposomes gave similar results when measured right after the DDAO addition to those measured 3 and 24 hours later. The samples

containing bacterial lipid liposomes became unstable if measured 3 hours after the addition of DDAO. Therefore, all the samples (both mammalian and bacterial models) were measured right after adding DDAO.

The experiment with dermaseptin DS1 consisted of 18 samples with a constant concentration of lipid (0.01 mmol/dm^3) and increasing concentration of DS1 up to 0.01 mmol/dm^3, expressed in the molar ratios n_{DS1}:n_{LIPID} from 1:500 up to 1:1. The samples were measured right after the addition of DS1 and 3 hours afterwards. The experiment with 0.01 mmol/ dm^3 lipid was carried out with DDAO as well.

3.2.3 Data treatment

The leakage of the fluorescent probe calcein can be divided into three stages. In the first stage, a gentle rise in fluorescence intensity can be observed, because transient pores are created at low concentration of the surfactant. Upon further increase in surfactant concentration, causing the stabilisation of the pores leads to the second stage, where massive release of the fluorescent probe is detected. Critical DDAO concentration causing the onset of the massive leak of the encapsulated calcein from the liposomes will be labelled as D_t^{PERT}. The concentration of DDAO at which the fluorescence intensity reaches a stable value, that cannot be influenced by further DDAO addition will be marked as D_t^{RLS}. These two critical concentrations were evaluated similarly as in case of the solubilisation curves. The first two stages were fitted with bilinear function (Equation 3) to obtain D_t^{PERT}. Because the fluorescence intensity in the third stage stays approximately the same, the transition from second to the last stage was fitted with the modified bilinear function (Equation 4) to get the value of D_t^{RLS}.

3.3 Vibrational densitometry

The density (ρ) of a sample can be calculated as mass (m) divided by its volume (V):

$$\rho = \frac{m}{V} \ [g/cm^3] \qquad 8$$

In case of vibrational densitometry, the sample is measured inside a borosilicate glass U-shaped tube that vibrates at a characteristic frequency. This frequency changes depending on the density of sample inside the tube. The density is calculated from a quotient of the period of oscillations of the U-shaped tube and a reference oscillator by the densitometer. (Anton Paar, 2009)

3.3.1 Sample preparation

Adequate amount of lipid or lipid mixtures were (co-)dissolved in a small amount of chloroform in glass vials. The solvent was evaporated to dryness using a stream of gaseous nitrogen, followed by stay in a vacuum chamber for 8 hours. The dry lipid film was hydrated by deionised water 4 hours before the measurement to obtain the final lipid concentration ~ 2 w%. The amounts of lipid in the vial after chloroform evaporation and the amount of water added to the sample were gravimetrically controlled. The samples were degassed under a low pressure to prevent formation of bubbles in the U-shaped tube of the densitometer. The weight losses after the chloroform evaporation and degassing were negligible for all samples. The samples containing POPC, POPC-CHOL (n_{POPC}:n_{CHOL} = 2:1 mol/mol), POPG, POPE-POPG (n_{POPE}:n_{POPG} = 3:2 mol/mol) and POPE-POPG-TOCL (n_{POPE}:n_{POPG}:n_{TOCL} = 0.67:0.23:0.1 mol/mol/mol) were measured, as well as pure deionised water.

3.3.2 Densitometry measurements

Vibrational densitometer DMA 4500M (Anton Paar, Austria) was used for densitometric experiments. Samples were measured in a temperature range 12 – 40° C with a step of 1° C. The precision of density measurement was ± 0.00005 g/cm^3 and the precision of temperature control was ± 0.03 °C.

3.3.3 Data treatment

For the evaluation of densitometric data, we have used procedures used previously in (Gallová et al., 2017; Klacsová et al., 2010; Murugova and Balgavý, 2014).

Reciprocal value of the density of sample (ρ_S) is the ***specific volume of the sample*** (ν_S). If we assume that the specific volume of water (ν_W) in our sample is identical to that of pure water, the ***apparent specific volume of the lipid*** (ν_L) can be calculated as

$$\nu_L = \frac{\nu_S - (1 - w_L) \times \nu_W}{w_L} \qquad 9$$

where w_L is the mass fraction of lipid in the sample calculated from the mass of the lipid (m_L) and mass of the water (m_W) in the sample:

$$w_L = \frac{m_L}{m_L + m_W} \qquad 10$$

The ***apparent specific volume of a mixture of lipids*** (L1 and L2) can be calculated similarly:

$$\nu_{L1+L2} = \frac{\nu_S - (1 - w_{L1+L2}) \times \nu_W}{w_{L1+L2}} \quad 11$$

where

$$w_{L1+L2} = \frac{m_{L1} + m_{L2}}{m_{L1} + m_{L2} + m_W} \quad 12$$

If we further suppose that the specific volume of a lipid in the mixture does not depend on the presence of the other lipid, we can calculate the apparent specific volume of that lipid from the specific volume of the mixture:

$$\nu_{L2} = \frac{\nu_{L1+L2} - (1 - w_{L2}) \times \nu_{L1}}{w_{L2}} \quad 13$$

where

$$w_{L2} = \frac{m_{L2}}{m_{L1} + m_{L2}} \quad 14$$

This was used to calculate the apparent specific volumes of CHOL (from POPC-CHOL mixture) and POPE (from POPE-POPG mixture).

The density of the bilayer (ρ_b) can be calculated using the apparent specific volume of the lipid:

$$\rho_b = \frac{1}{\nu_L} \quad 15$$

where ν_L is the apparent specific volume of lipid or lipids in case of a mixed bilayer.

The apparent specific volume of a lipid can be used to calculate the ***apparent molecular volume of a lipid*** (V_L):

$$V_L = \frac{\nu_L \times M_L}{N_A} \quad 16$$

where M_L is the molar mass of the lipid and N_A is Avogadro's constant. (Gallová et al., 2017; Klacsová et al., 2010; Murugova and Balgavý, 2014)

3.4 Partition coefficient calculations

Molar partition coefficient (K_p) of surfactant molecule, in equilibrium state, is defined as the ratio of molar concentration of surfactant in the lipid phase (D_b, subscript b signifies bilayer) to its molar concentration in the water phase (D_w, subscript w represents water or water-based buffer).

$$K_p = \frac{D_b}{D_w} \quad (17)$$

In this thesis we are calculating partition coefficient of surfactant DDAO between our lipid bilayers and PBS buffer following previously described procedure (Hrubšová et al., 2003). After substituting the concentration in Equation 17 with the amount of DDAO in a specific case (specified by the subscript b and w) divided by the volume (V) of that phase ($D_b = n_b/V_b$; $D_w = n_w/V_w$), we can express it as

$$K_p = \frac{n_b \times V_w}{n_w \times V_b} \quad (18)$$

Total amount of DDAO in the sample (n_t) is

$$n_t = n_b + n_w \quad (19)$$

where n_b is the membrane-bound amount of DDAO and n_w is the amount of DDAO in the water phase. Because the volume of the bilayer (V_b) is much smaller than the volume of the water phase (V_w), we can assign the total volume of the sample (V_t) is approximately equal to V_w. The use of a low lipid concentration (ordinarily 10^{-4} mol/dm^3) in our experiments ensures that this assumption is maintained. Using this approximation and Equation 19 in the Equation 18, the concentration of DDAO in the bilayer can be rewritten as

$$\frac{n_b}{V_b} = \frac{n_t}{V_t} \times \frac{K_p}{1 + K_p \times \frac{V_b}{V_t}} \quad (20)$$

The volume of the bilayer (V_b) can be expressed

$$V_b = \frac{m_L}{\rho_b} = \frac{n_L \times M_L}{\rho_b} \quad (21)$$

using total amount of lipid (n_L), molar mass of a lipid (M_L) and density of the bilayer (ρ_b). In case of a mixed bilayer, its molar mass (M_L) was calculated using mole fractions of lipids (X_L) constituting the bilayer. For example,

$$M_{POPC+CHOL} = X_{POPC} \times M_{POPC} + X_{CHOL} \times M_{CHOL} \quad (22)$$

Total concentration of DDAO (D_t) in the sample is

$$D_t = \frac{n_t}{V_t} \quad (23)$$

After substituting Equation 21 and 23 into Equation 20

$$\frac{n_b}{n_L} \times \frac{\rho_b}{M_L} = D_t \times \frac{K_p}{1 + K_p \times \frac{n_L \times M_L}{V_t \times \rho_b}} \quad (24)$$

Using substitutions $R_e = n_b/n_L$ (R_e is the effective molar ratio) and $c_L = n_L/V_t$ (c_L is the concentration of lipid) in the Equation 24, it can be modified to obtain a linear dependence of total DDAO concentration (D_t) on the concentration of lipid

$$D_t = R_e \times \frac{\rho_B}{M_L} \times \frac{1}{K_p} + R_e \times c_L \qquad 25$$

The slope of the dependence (Equation 25) is the effective molar ratio (R_e) of the amount of DDAO integrated into the bilayer (n_b) to the amount of lipid (n_L) under equilibrium conditions. R_e is constant for specific surfactant-lipid mixture and it is not dependent on the concentration of lipid.

All experimentally acquired linear dependences of critical DDAO concentrations (D_t) on the concentration of lipid were fitted simultaneously with a global function (Equation 25), with the Multi-Data Fit Mode in Origin software (Version 2019b, OriginLab Corporation, Northampton, MA, USA). The constant ratio of ρ_b/M_L was denoted as a fixed parameter. The density of bilayer (ρ_b) was measured following the procedure described in 3.3 Vibrational densitometry. The global fit fitted the individual linear dependences and their slopes (R_e) and calculated one shared partition coefficient for all used dependences. Concentration of DDAO in the water phase (D_w) for the particular steps in the solubilisation process were obtained by extrapolation of the global function to zero lipid concentrations. Their value is the y-coordinate of the intersection points of the global function with thy y-axis.

3.5 Small-angle neutron scattering

Neutrons are ***sub-atomic particles*** found in all atomic nuclei (except for ^1H). Free neutrons are unstable with mean lifetime of 885.9 s (~ 15 min.) and decay into a proton, electron and antineutrino (Katsaras et al., 2006; Jackson, 2008). Neutrons have null electric charge and because of that they do not interact with the electron shells of atoms which grants them their high penetration ability into different materials. Depending on their state of motion, neutrons also display wave behaviour. Properties of the ***neutron wave*** are characterised by the wavelength (λ) given by the neutron mass (m_n), its velocity (ν) and Planck's constant (h), known as de Broglie relationship:

$$\lambda = \frac{h}{m_n \times \nu} \qquad 26$$

The energy (E) of a neutron is predominantly kinetic and is often expressed using thermodynamic temperature (T):

$$E = k_B \times T \qquad 27$$

where k_B is the Boltzmann's constant. (Belička et al., 2014c; Willis and Carlile, 2009)

Different neutron sources can provide neutrons with different energies, as show in Table 2. (Willis and Carlile, 2009)

Table 2: Energy and wavelength classification of neutrons.

	E [meV]	**λ [nm]**
Cold (20 K)	0.1 – 10	0.3 – 3
Thermal (300 K)	5 – 80	0.1 – 0.4
Hot (2000 K)	80 – 500	0.04 – 0.1

Different types of mutual interactions take place when neutrons interact with atomic nuclei. In case of small-angle neutron scattering (SANS) and small-angle neutron diffraction (SAND), elastic scattering occurs. There is no energy transfer between the neutron and the scattering particle and the size of their momentum is preserved.

The wave vector ($\vec{k}$) is used to describe the neutron wave

$$\vec{k} = \frac{2\pi}{\lambda} \times \overrightarrow{n_o} \qquad 28$$

where $\overrightarrow{n_o}$ is a unit vector with the same direction and orientation as the neutron momentum. (Beličkа et al., 2014c) The schematic illustration of neutron scattering on a single atomic nucleus is showed in the Figure 19.

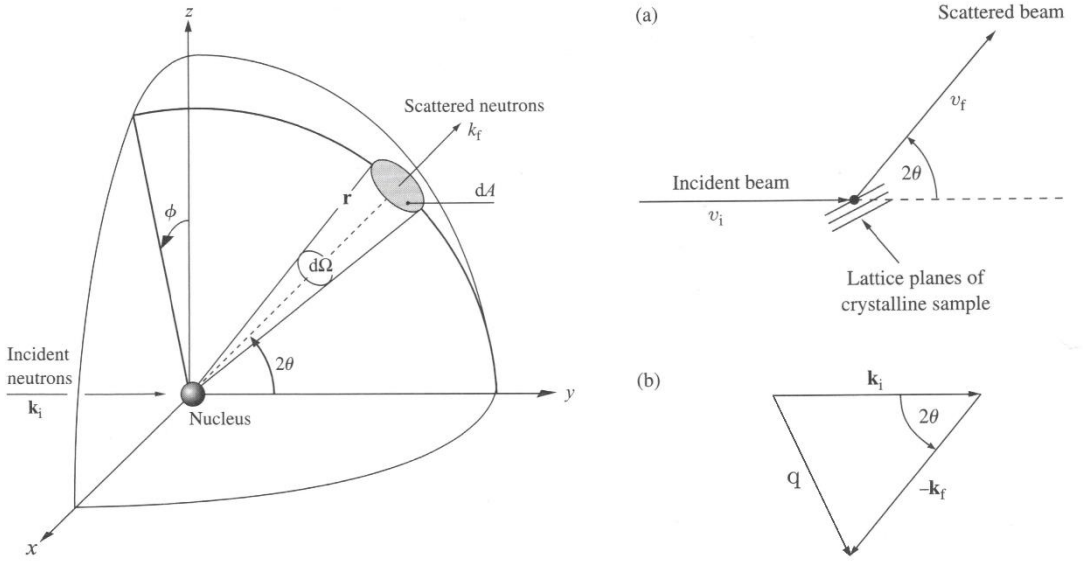

Figure 19: Schematic illustration of neutron scattering experiment (on the left). The incident neutron beam (wave vector k_i) is scattered on a nucleus in a specific direction characterised by angles 2θ-ϕ (to a point r). k_f characterises the scattered neutron beam wave vector, dΩ is a solid angle, dA represents the surface area collected by the detector. On the right:(a) Scattering of a neutron in real space. v_i and v_f are the initial and final velocities of the neutron. (b) Scattering in the reciprocal space displays the scattering vector q. (Willis and Carlile, 2009)

The incident neutron beam, specified by its wave vector $\overrightarrow{k_i}$, is scattered to a point r, with the scattering defined by angles 2θ and ϕ. Scattering occurs in an elementary cone of solid angle $d\Omega$. The scattered neutron wave vector is labelled $\overrightarrow{k_f}$.

Change in the wave vector is characterised by the ***scattering vector*** (momentum transfer vector):

$$\vec{q} = \overrightarrow{k_i} - \overrightarrow{k_f} \qquad 29$$

In case of ***elastic scattering*** of neutrons on a nucleus, $k_i = k_f$, the size of the scattering vector q is:

$$q = \frac{4\pi}{\lambda} \times \sin(\theta) \qquad 30$$

where 2θ is the scattering angle. We call the space containing all position vectors r the real space, and the space which contains the scattering vectors q the reciprocal space. The detection of scattered neutrons leads to the determination of the neutron scattering cross-section.

The ***total scattering cross-section*** **(σ)** is defined by the number of neutrons scattered in all directions per second divided by the incident flux (I_0). The incident flux is the number of neutrons hitting unit area of the sample, where the area is considered perpendicular to the incident neutron beam. The unit of cross-section is 1 barn = 10^{-28} m^2.

The ***differential scattering cross-section*** **($d\sigma/d\Omega$)** is given by

$$\frac{d\sigma}{d\Omega} = \frac{\text{number of neutrons scattered per second into a solid angle } d\Omega}{I_0 d\Omega} \qquad 31$$

and is measured by a *neutron diffractometer*, which records the scattered intensity as a function of the scattering vector q, without reference to any changes in energy. The units are barns/steradian. (Willis and Carlile, 2009)

Each atomic nucleus has a characteristic scattering ability, specified by the ***scattering length (b)***. The value is given by the negative ratio of the scattered and incident wave amplitudes. Since the scattering length value is dependent on the actual composition of the atomic nucleus (and in case of nuclei with non-zero spin also on the mutual neutron/nucleus spin configuration), it differs for isotopes of the same element. The scattering lengths values of individual isotopes have been experimentally determined and are compiled into tables. (Bellička et al., 2014c) This is very convenient for the studies of the biomolecules, since the scattering lengths of hydrogen (H) and deuterium (D) are very different, -3.74×10^{-15} m and 6.67×10^{-15} m, respectively. Hydrogen is ubiquitous in most biomolecules and solvents, therefore interchanging the two either in biomolecules or the solvent may serve as a useful tool in biological studies. Variation of the H_2O/D_2O ratio of the solvent is often used to change the contrast. This technique is called ***contrast variation technique***. (Poon and Andelman, 2006)

Since the studied samples contain a lot of particles, we use a quantity called ***scattering length density*** **(SLD, ρ)**, which is the summation of all atoms with scattering lengths (b_i) that are present in the volume ΔV:

$$\rho = \frac{1}{\Delta V}\sum_i b_i \qquad 32$$

Figure 20 shows scattering length density of various types of molecules plotted as a function of H/D ratio of the water in which they are immersed. The value of SLD in the Figure 20 is shown as $m/Å^3$, where angstrom (Å) is a unit of length Å = 10^{-10} m, often used instead of nm (nm = 10^{-9} m) in scattering and diffraction literature.

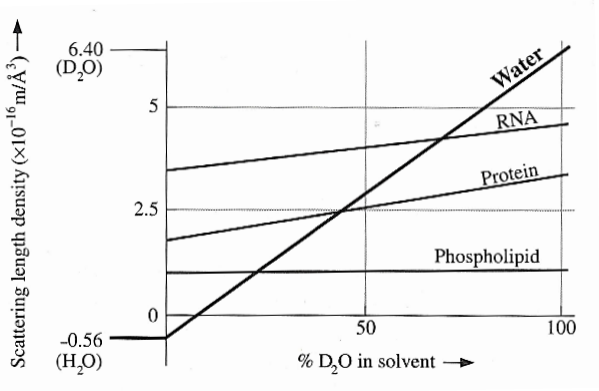

Figure 20: Scattering length density of various molecular components plotted as a function of the percentage of "heavy" D_2O water used as the solvent.(Willis and Carlile, 2009)

The ***scattering intensity*** **($I(q)$)** is measured as a function of the momentum transfer (q) and depends on the contrast factor between the particles and the solvent $\Delta\rho = (\rho_p - \rho_s)$, the form factor ($F(q)$), the structure factor ($S(q)$), the number (N_p) and volume (V_p) of particles: (Fragneto et al., 2018)

$$I(q) = \Delta\rho^2 F(q) S(q) N_p {V_p}^2 \qquad 33$$

The form factor ($F(q)$) describes the influence of the shape of the scattering particle on the observed intensity. Many possible shapes (sphere, ellipsoid, rod etc.) have known theoretical expressions of form factor. (Willis and Carlile, 2009) The structure factor ($S(q)$) contains information about the correlation between different particles. For very dilute systems without interaction between the particles, $S(q) = 1$. (Willis and Carlile, 2009; Pedersen, 1997) The neutron scattering data in low q region are sensitive to larger scales, such as the size of the particles. In the mid and high q region we can find the information about the bilayer structure. (Kučerka et al., 2007)

3.5.1 Sample preparation (SANS)

3.5.1.1 Chemicals

DOPC, CHOL, POPE and POPG were purchased from Avanti Polar lipids (USA) and used without further purification. DDAO was obtained from Sigma-Aldrich (Germany). Buffer constituents (KH_2PO_4, K_2HPO_4, NaCl) were of analytical grade.

3.5.1.2 Phosphate-buffered saline in D_2O (D_2O-PBS)

75 ml of PBS buffer with the same composition (7.6 mmol/dm^3 KH_2PO_4, 42.4 mmol/dm^3 K_2HPO_4, 150 mmol/dm^3 NaCl) as used for all other experiments was prepared using D_2O water instead of H_2O. pH of this buffer was 7.581. According to (Rubinson, 2017), no correction of measured pH is needed for 100% D_2O content within the range of measured pH 4 – 8.

3.5.1.3 Liposome preparation

DOPC, DOPC-CHOL (n_{DOPC}:n_{CHOL} = 2:1 mol/mol) and POPE-POPG (n_{POPE}:n_{POPG} = 0.6:0.4 mol/mol) model membranes were prepared. Weighed amounts of dry lipids were co-solubilised in glass vials using chloroform. Chloroform was then evaporated with gaseous nitrogen until dry and the vials were placed in a vacuum chamber for 8 hours to ensure complete evaporation of the chloroform. Lipid films were hydrated with D_2O-PBS buffer for 24 hours to obtain lipid dispersions with concentration of lipid 40 mmol/dm^3 for all three model membranes. Dispersions of MLLs were extruded 51 times through 100 nm and subsequently 51 times through 50 nm polycarbonate filter. Extruded liposomes were then used to prepare samples with constant concentration of lipid (8.9 mmol/dm^3), diluted by D_2O-PBS and appropriate amount of stock solution of DDAO in D_2O-PBS. The volume of each sample was 1 ml and the molar ratio of n_{DDAO}:n_{LIPID} in the sample was in the range 0 – 5 mol/mol, with 15 samples being prepared for each model membrane. For POPE-POPG, an additional sample was measured with the molar ratio 6 mol/mol. The LIPID+DDAO concentration, expressed in weight percentage (w%), increased from 0.64 w% in the first sample without DDAO to 1.56 w% in the last sample (n_{DDAO}:n_{DOPC} = 5). Similar weight percentages were present in the DOPC-CHOL and POPE-POPG samples.

Samples of DOPC (1 w%) without DDAO were also prepared using different aqueous phase: 1. 100% D_2O; 2. 150 mmol/dm^3 NaCl in D_2O; 3. 150 mmol/dm^3 NaCl in

D_2O-PBS. The DOPC dispersion in these samples was extruded 51 times through 50 nm filter.

3.5.1.4 DDAO stock solution preparation

10 ml of 174 mmol/dm^3 DDAO stock solution was prepared in D_2O-PBS. This stock solution was used to prepare all samples.

3.5.2 SANS measurements

Small-angle neutron scattering experiments were carried out at the small-angle neutron spectrometer YuMO at the IBR-2 fast pulsed reactor in Frank Laboratory of Neutron Physics, Joint Institute of Nuclear Research in Dubna, Russia. (Kuklin et al., 2017; Soloviev et al., 2017) The samples in quartz cells (Hellma, Müllheim, Germany) with a path length 2 mm were measured 24 hours after extrusion at 25.0 ± 0.1° C. The scattered intensity was normalised using vanadium standard and corrected for the background effect by the blank. The output of SANS experiment is a curve describing the dependence of the scattering intensity $I(q)$ as a function of the scattering vector q. These dependences will be referred to as "scattering curves" in further text.

3.5.3 Data treatment

SasView fitting software, version 4.1 (Doucet et al., 2017), was used for the analysis of scattering curves. The ideal model scattering curves were smeared by the instrumental resolution of approximately 10%. The scattering length density (ρ) for each sample was calculated using the known molar ratios of n_{DDAO}:n_{LIPID} and molecular volumes (calculated in Chapter 4.3 Densitometry) according to Equation 32.

Two model fitting functions were successfully used to fit the experimentally obtained scattering curves. In this Chapter, we will cover their theoretical background.

The ***paracrystal lamellar stack model*** calculates the scattering from a stack of repeating lamellar structures. The lamellar stacks (infinite in lateral dimension) are treated as a paracrystal to account for repeat spacing (d). The repeat spacing is the sum of the lamella (in our case lipid bilayer) thickness and the water layer thickness.

The scattering intensity is calculated as

$$I(q) = \frac{d\sigma(q)}{d\Omega} = 2\pi(\Delta\rho)^2\Gamma_m \frac{F(q)}{q^2} Z_N(q) \quad 34$$

where $\Delta\rho$ is the contrast between the SLD of particle and solvent; Γ_m is the scale factor (mass per area of the bilayer) and $Z_N(q)$ describes the interference effects of aggregates consisting of more than one bilayer. $Z_N(q)$ can be written as a function of the average number of layers of two clusters comprised of integer number of layers N, the fraction of which is x_N, and $N + 1$ layers, the fraction of which is $1 - x_N$:

$$N_L = x_N N + (1 - x_N)(N + 1) \quad 35$$

As an example, if N_L = 1.4, 60% of the mixture are ULLs (N_L= 1) and 40% are OLLs with 2 bilayers on average (N_L= 2) or interacting ULLs. This factor also includes the average repeat spacing (d).

The form factor $F(q)$ is separated into a contribution that accounts for the cross section of a planar bilayer with half the bilayer thickness (ξ) and a factor proportional to q^{-2}, which is typical for an infinitely large two-dimensional sheet.

$$F(q) = \left(\frac{\sin(q\xi)}{q\xi}\right)^2 \quad 36$$

In conclusion, this fitting model gives us back these parameters: scale factor (Γ_m), bilayer thickness ($2\xi = d_L$), number of layers (N_L) and repeat spacing (d). (Bergström et al., 1999; Silva et al., 2018)

The ***elliptical cylinder model*** calculates the scattering from cylinders with elliptical cross section. The cylinders are described by the length of the cylinder (L) and volume of the cylinder (V_{cyl}). Their cross-section is characterised by axial ratio (ν) of ellipse major radius (r_{major}) over minor radius (r_{minor}). Their position is characterised by angles θ (cylinder axis to beam angle), ϕ (rotation around the beam) and ψ (rotation around the axis of the cylinder). α is the angle between the axis of the cylinder and scattering vector q. The scattering intensity is calculated as

$$I(q) = \frac{1}{V_{cyl}} \int d\psi \int d\phi \int p(\theta, \phi, \psi)\, F^2(q, \alpha, \psi) \sin(\alpha)\, d\alpha \quad 37$$

The form factor can be expressed as

$$F(q, \alpha, \psi) = \frac{2J_1(r_{minor}) \sin(r_{major})}{r_{minor} \cdot r_{major}} \quad 38$$

where $J_1(r_{minor})$ is the first order Bessel function and the radii are given by $r_{minor} = qr' \sin(\alpha)$ and $r_{major} = q \cos(\alpha)\, L/2$ with r' being defined as

$$r' = \frac{r_{minor}}{\sqrt{2}} \sqrt{(1 + \nu^2) + (1 - \nu^2)\cos(\psi)} \quad 39$$

For 1D scattering without preferred orientation, the form factor is averaged over all possible orientations and normalised by the particle volume: $F(q) = \Gamma_m \langle F^2 \rangle / V_{cyl}$. (Feigin and Svergun, 1987; Pedersen, 1997)

To conclude, the fitted parameters are scale factor (Γ_m), minor radius of the ellipse (r_{minor}), axial ratio of the ellipse (ν) and the length of the cylinder (L). For more detailed description of the fitting functions, see the SasView User Documentation (*https://www.sasview.org/docs/user/qtgui/Perspectives/Fitting/models/index.html*, [12.4.2022])

3.6 Small-angle neutron diffraction

Diffraction (sometimes called Bragg scattering) is an elastic scattering process that can be observed on a set of scattering planes (Figure 21) in ordered (crystal) structure. Diffraction can be observed when the waves scattered from adjacent scattering planes remain in phase, resulting in the constructive interference.

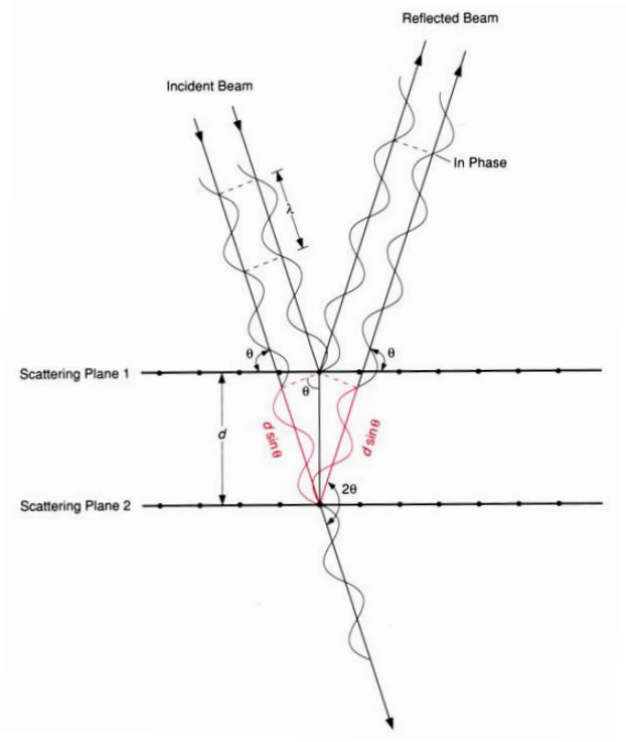

Figure 21: Scattering geometry and the derivation of Bragg's law. λ is the wavelength of the neutron wave, d is the distance between 2 scattering planes and θ is the angle between the incident neutron beam and the scattering plane. (Pynn, 2009)

For the diffraction to occur, the scattering vector must be perpendicular to a set of atomic planes. Figure 21 shows scattering on two adjacent planes, where we can see that wave scattered on the second scattering plane has to travel extra distance. For the

constructive interference to occur between the waves scattered from plane 1 and 2, the path length difference (calculated as $2d\sin(\theta)$ using trigonometry) must be integer multiple of the wavelength λ. This condition for diffraction is known as Bragg's law:

$$n\lambda = 2d\sin(\theta) \qquad 40$$

where n – diffraction order; λ – neutron wavelength (for D16 diffractometer λ = 0.4493 nm); d – repeat spacing (the distance between the two scattering planes) and θ – angle between an incident neutron beam and the scattering plane. (Pynn, 2009)

The SAND method enables us to obtain the scattering form factors from experimental diffraction data. Problem of assigning the scattering form factor phases can be solved by measuring the samples at either different relative humidities (swelling method) or by changing the H_2O/D_2O contrasts (contrast variation method). The Fourier transform of the scattering form factor with assigned phase then gives us information about the distribution of scattering length densities over the bilayer and the water layer, so-called neutron scattering length density (NSLD) profile.

3.6.1 Sample preparation (SAND)

3.6.1.1 Chemicals

POPC, CHOL, POPE, POPG and partially deuterated lipids – 1-palmitoyl-d31-2-oleoyl-*sn*-glycero-3-phosphocholine (16:0-d31-18:1 PC, dPOPC), 1-palmitoyl-d31-2-oleoyl-sn-glycero-3-phosphoethanolamine (16:0-d31-18:1 PE, dPOPE) and 1-palmitoyl-d31-2-oleoyl-sn-glycero-3-[phospho-rac-(1-glycerol)] (sodium salt) (16:0-d31-18:1 PG, dPOPG) were purchased from Avanti Polar lipids (USA) and used without further purification. DDAO was obtained from Sigma-Aldrich (Germany) and Dermaseptin S1 (DS1) was purchased from Bachem (Switzerland).

3.6.1.1 Preparation of oriented lipid bilayer stacks

Different model membranes were studied using SAND: models mimicking mammalian membrane: POPC, POPC-CHOL (n_{POPC}:n_{CHOL} = 2:1 mol/mol), and bacterial model membrane: POPE-POPG (n_{POPE}:n_{POPG} = 3:2 mol/mol).

Stock solution of lipid or a lipid mixture (in molar ratios specified earlier) in $CHCl_3$:CH_3OH = 1:1 v/v was prepared. All types of model membranes were prepared using the same procedures. Appropriate amount of the lipid stock solution was taken to create a final solution containing 5 mg of lipid/lipid mixture and volume 500 µl. The solutions were mixed thoroughly using a vortex mixer. The solutions were then deposited onto 25 x 50 mm

silicon wafers (covering the entire surface of the wafer) and gently rocked during evaporation of the solvent (the "rock and roll method", (Tristram-Nagle, 2007)). Samples were then placed under vacuum to remove the remaining traces of the solvent. The samples were put in an enclosed humid environment at a temperature 40° C for several hours before the measurement. This procedure is called annealing. Well-oriented bilayer stacks were confirmed by observation of up to 8 orders of Bragg diffraction.

Samples with DDAO: 1 ml of stock solution of DDAO in $CHCl_3$:CH_3OH = 1:1 v/v was prepared containing 30 mg of DDAO. Adequate amount of stock solution was added to the lipid mixture to form the 500 µl solution that was being deposited onto the wafer. Samples always contained 5 mg of lipid/lipid mixture and DDAO in molar ratios (n_{DDAO}:n_{LIPID} = 0.2:1, 0.5:1 and 1:1 mol/mol). 2 samples containing NaCl in a molar ratio n_{NaCl}:n_{LIPID} = 1:1 mol/mol without DDAO were also prepared.

Samples containing dermaseptin S1 (DS1) contained partially deuterated lipids: dPOPC, dPOPE and dPOPG. CHOL and DS1 were not deuterated. All sample components were dissolved in $CHCl_3$:CH_3OH = 1:1 v/v. All the lipid molar ratios were kept the same as with previous samples: dPOPC-CHOL (n_{dPOPC}:n_{CHOL} = 2:1 mol/mol) and dPOPE-dPOPG (n_{dPOPE}:n_{dPOPG} = 3:2 mol/mol). Samples with n_{DS1}:n_{LIPID} = 1:150, 1:100, 1:80, 1:50 mol/mol) were prepared by co-dissolving appropriate amounts of lipid and DS1 stock solutions to create 500 µl solution, which was then deposited onto silicon wafers, using the same procedure as described before.

3.5.1.2 Preparation of H_2O/D_2O contrasts

Different H_2O/D_2O contrasts were prepared for the measurements: 8%, 40%, 70% and 100% D_2O according to Table 3.

Table 3: H_2O/D_2O contrast preparation.

Contrast	V_{H_2O} [ml]	V_{D_2O} [ml]
8%	18.4	1.6
40%	12	8
70%	6	14
100%	0	20

3.5.2 SAND measurements

Small-angle neutron diffraction (SAND) data were measured at D16 cold-neutron diffractometer (Cristiglio et al., 2015) at the Institut Laue-Langevin (ILL) located in

Grenoble (France). The neutron beam with the wavelength of 0.4493 nm was achieved by a focussing pyrolytic graphite monochromator. The beam then passed through a set of slits with dimensions set to 150 x 6 mm^2 and 25 x 6 mm^2. Monochromator to sample distance is 2.8 m. The samples were measured in a BerILL humidity chambers (Gonthier et al., 2019). Silicon wafers with the samples were held in a vertical position on a goniometer. Lower part of the humidity chamber contains a temperature-controlled water bath (containing the contrast). The sample alignment was done optically using the goniometer and a laser before closing the chamber, which was followed by approximately 4 h equilibration. The inner and outer part of the chamber were separated by a vacuum during the equilibration and the whole measurement. The alignment of the sample in the beam (the "zero position") was corrected using the neutron beam before the measurement. The "zero position" refers to a position of the silicon wafer in the neutron beam where a minimum intensity is detected due to the enhanced absorption of the neutrons passing through a large amount of the sample on the wafer. The intensity of neutron scattering as a function of the scattering angle was detected by scanning the sample rotation (rocking scan) with two-dimensional ^{3}He detector at fixed position (the detector was fixed at Γ angles 12° and 28° to detect up to 8 diffraction orders). In the first Γ position, the sample was rotated in the incident neutron beam in the range from -1° to 12° (at 0.05° steps) to obtain first 4 orders of Bragg diffraction. In the second Γ position, Ω scan 8° – 20° was performed to detect higher diffraction orders.

3.6.2.1 Swelling experiments

POPC, POPC-CHOL (n_{POPC}:n_{CHOL} = 2:1 mol/mol) and POPE-POPG (n_{POPE}:n_{POPG} = 3:2 mol/mol) samples were prepared to test the possibility of using relative humidity technique to determine the phase of the scattering form factors needed for reconstruction of the one-dimensional neutron scattering length density profiles. Samples were placed vertically in the D16 chambers at 25°C. The chamber's bath reservoir was filled with 20 ml of 100% D_2O and the samples were hydrated from vapour using a setup for relative humidity (RH) control. The chamber was held under vacuum to ensure stable conditions throughout the whole measurement. The hydration of the samples from the D_2O vapour was controlled by changing the RH in the chamber – by varying the bath reservoir temperature.

Assuming ideal behaviour, the RH [%] at the reservoir is

$$\mathrm{RH}[\%] = \frac{\mathrm{P}}{\mathrm{P}_{\mathrm{H_2O}} \times \mathrm{T}} \times 100 \qquad 41$$

where P – partial pressure of water vapour in the chamber, P_{H_2O} – saturated water vapour

pressure in thermodynamic equilibrium with the condensed liquid, T – sample temperature (Gonthier et al., 2019)

According to the Clausius-Clapeyron equation for a liquid-gas equilibrium

$$\frac{d\ln(P)}{dT} \approx \frac{\Delta H_m}{RT^2} \qquad 42$$

where ΔH_m – enthalpy of vaporization of water, T – sample temperature

The equation can be rewritten as

$$\ln\left(1+\frac{\Delta P}{P}\right) \approx \frac{\Delta P}{P} \approx -\frac{\Delta H_m \Delta T}{RT^2} \qquad 43$$

where ΔT and ΔP are the temperature difference and the difference in partial pressure of water vapour between the sample and the reservoir, respectively. By controlling the temperature of the reservoir bath (T_r) and the temperature of the sample (T_s), we can control the temperature difference $\Delta T = T_r - T_s$. The distribution of water molecules in the water vapour rearranges according to the temperature gradient, which results in a change of relative humidity (Ma et al., 2015).

Table 4: Calculated values of bath reservoir temperature used in order to achieve the desired RH values.

RH [%]	**95**	**85**	**70**	**50**	**30**
T_s [°C]	25	25	25	25	25
T_r [°C]	24.14	22.3	19.15	13.86	6.23

3.6.2.2 Contrast variation experiments

Samples were placed vertically in the D16 humidity chambers at 25°C. The chamber's bath reservoir was filled with H_2O/D_2O mixture and the samples were hydrated from vapour. The chamber was held under vacuum to ensure stable conditions throughout the whole measurement. The samples were measured using at least three different contrasts (8%, 40%, 70% or 100% D_2O). This enabled us to determine the phase of the scattering form factors and reconstruct the one-dimensional neutron scattering length density profiles.

3.6.3 Data treatment

A computer code provided by (Hrubovčák et al., 2019) and a LAMP software (provided by ILL) were used for the analysis.

An example of 2D reciprocal space map in angular coordinates Ω and 2θ (measurements from both Γ positions of the detector) is shown in Figure 22. A series of reflections spaced periodically is caused by the regular lamellar ordering of the bilayer stack.

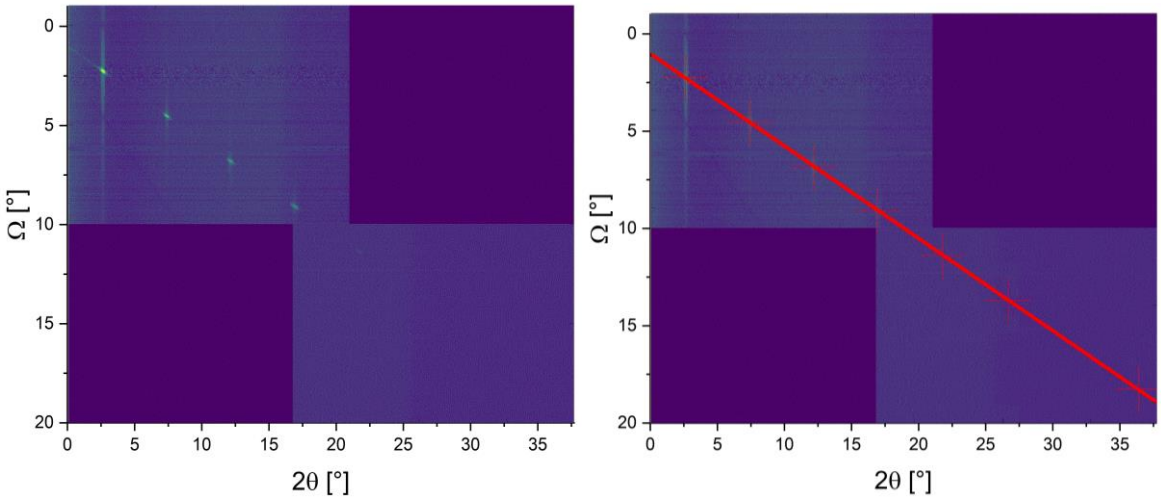

Figure 22: Reciprocal space map of sample POPC-CHOL measured with 8% D_2O as a contrast and at 97% relative humidity. The red line on the right shows the integration radius for acquiring the intensity dependence on 2θ. The red crosses signify the diffraction peaks.

From the reciprocal space maps, intensities were calculated by integrating along the line passing through all diffraction peaks (Figure 22, on the right). The result of the integration is shown in the Figure 23.

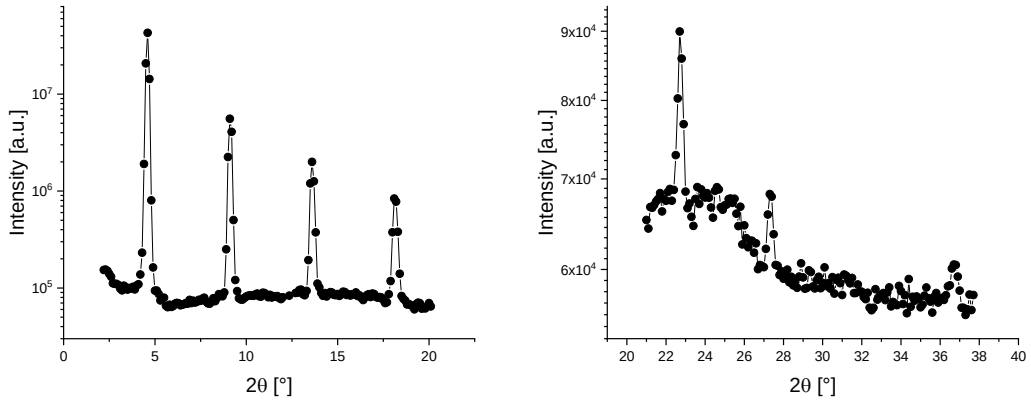

Figure 23: The intensity dependence on 2θ – example of diffraction data after the integration. Scans for Γ angles 12° (on the left) and 28° (on the right) of the detector. (POPC-CHOL, 8% D_2O)

The acquired Bragg peaks were analysed using a Gaussian function superimposed on a linear background:

$$y = y_0 + \frac{A}{w\sqrt{2\pi}} \exp\left(-\frac{1}{2} \cdot \frac{(x - x_n)^2}{w^2}\right) + kx \qquad 44$$

to obtain the parameters: A – area under the Gaussian; w – width of the Gaussian; x_n – 2θ position of the maxima; k and y_0 being the slope and intercept of the linear background, respectively. The area under the Gaussian peak (A) is the measured ***integrated intensity***

(**I**(**q**)). The maximum intensities of each diffraction peak ($x_n = 2\theta$) allow us to calculate the ***repeat spacing*** **(d)** (which is the sum of bilayer thickness and water layer thickness). Repeat spacing can be calculated from the Bragg's law:

$$d = \frac{n\lambda}{2\sin(\theta)} \qquad 45$$

In our case, the repeat spacing was calculated from the slope of the dependence of $2\sin(\theta)$ on the ***diffraction order*** **(n)**, using positions of maximum intensity of all fitted peaks (Figure 24).

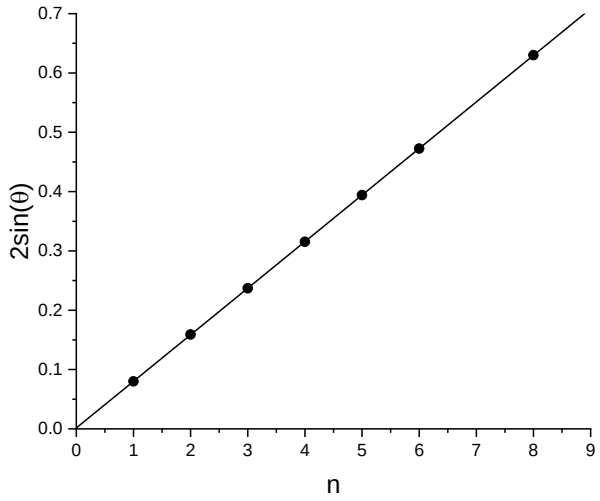

Figure 24: Plot of $2sin(\theta)$ vs. order of Bragg peak used to calculate the repeat spacing.

3.6.4 Neutron scattering length density profiles

The scattering length density distribution of the bilayer was calculated from the Fourier transform of the diffraction intensities. The intensity was corrected using the following corrections.

1. ***The flux correction:*** Varying neutron flux impinges on the sample caused by a Gaussian-shaped incident beam.

$$C_F = 1/\mathrm{erf}\left(\frac{w \times \sin(\theta)}{2s\sqrt{8}}\right) \qquad 46$$

where erf – error function; w – width of the sample and 2s – width of the beam.

2. ***The Lorentz correction:*** A geometric correction factor that accounts for different rate at which the sample rotates through the Bragg condition.

$$C_L = \sin(2\theta) \qquad 47$$

3. ***Correction for absorption:***

$$C_A = \frac{\alpha}{1 - e^{-\alpha}} \quad (48)$$

where

$$\alpha = \frac{2\mu t}{\sin(\theta)} \quad (49)$$

μ is the absorption coefficient, calculated by taking into account all atoms in the unit cell, and t is the thickness of the sample.

The amplitude of the ***Fourier coefficients*** $\mathbf{F_n}$ (will be referred to as "form factors" in the text) was determined as a square root of the integrated intensities and the correction factors:

$$|F_n| = \sqrt{I(q)_n \times C_F \times C_L \times C_A} \quad (50)$$

Another step in the analysis was the assignment of a phase.

4. ***Extinction effect correction:*** The diffraction planes first encountered by the beam reflect some of the incident radiation, so that the inner parts of the multilayer have less chance of contributing to the measured intensity. This is called extinction effect and it is prominent for the stronger Bragg reflections. A correction for this effect was made for the first Bragg peak intensities by multiplying the Fourier coefficient with a factor 1 – 1.2. This correction was done only if the sample was measured using the 70% or higher D_2O contrast (The linear dependence of the Fourier coefficients F_n on the % of D_2O was checked).

(Kučerka et al., 2009; Gawrisch et al., 2007; Harroun et al., 2008; Marquardt et al., 2018; Willis and Carlile, 2009)

Determination of scattering phases

The scattering form factor phases were determined thanks to the contrast variation. This method is based on the fact that the Fourier transform of a hydrated structure is a linear function of the isotopic composition of the water (D_2O content in the contrast). The phase can also be determined from swelling experiments, but in our case, the structure of the lipid bilayer was not constant throughout the swelling experiments. Therefore, a contrast variation method was applied.

In case of centrosymmetric structures (such as the bilayer), we only need to determine the sign (+/-) of the form factors. For the 1st diffraction order, the form factors were always assigned as negative to obtain a minimum on the NSLD profiles in the centre of the bilayer ($z = 0$). All other phases were assigned by making sure that the linearity of the dependence $F_n = f(\%D_2O)$ is preserved and by observing the shape of all 3 NSLD profiles.

Figure 25 shows the linear dependences of the scattering form factors on the varying contrast composition. Table 5 shows the calculated form factors (F_n) with above mentioned corrections and assigned phase sign for the sample POPC-CHOL. The form factors of peaks that were not detected were assigned the value 0.

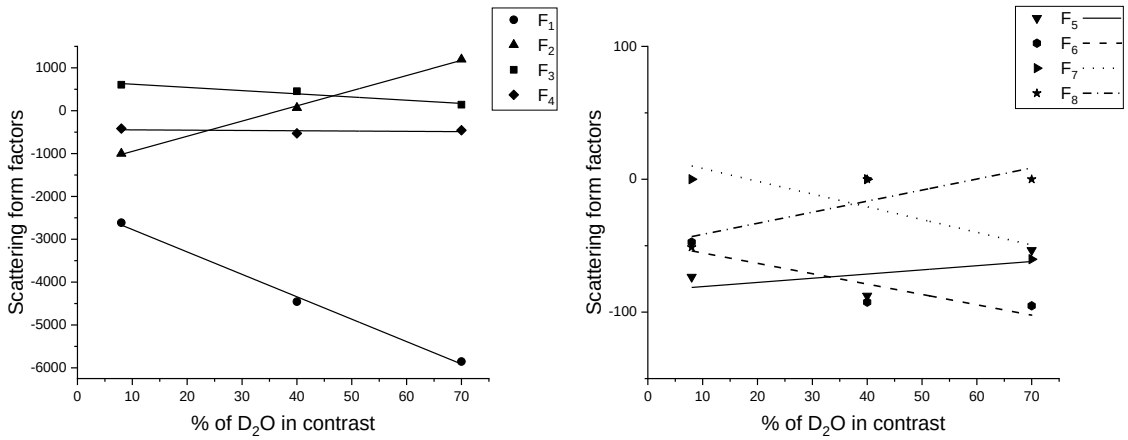

Figure 25: Linear dependence of the scattering form factors F_n as a function of D_2O content in the contrast. POPC-CHOL, diffraction orders F_1 – F_4 (on the left), F_5 – F_8 (on the right).

Table 5: Calculated repeat spacing d and corrected scattering form factors F_n with assigned phases for the POPC-CHOL sample measured at 3 different contrasts.

Sample	**% D_2O**	**d [nm]**	**Diffraction peak order**							
			F_1	**F_2**	**F_3**	**F_4**	**F_5**	**F_6**	**F_7**	**F_8**
POPC-CHOL	8	5.72 ± 0.003	-2613	-1000	+605	-416	-74	-47	0	-51
	40	5.72 ± 0.005	-4456	+69	+453	-529	-88	-93	0	0
	70	5.68 ± 0.005	-5852	+1197	+139	-457	-54	-95	-60	0

The ***neutron scattering length density profile*** **(NSLD, $\rho(z)$)** of the bilayer was determined from the Fourier coefficients according to the following equation:

$$\rho(z) = 2\sum_{n=1}^{n_{max}} F_n \cos(qz) \qquad 51$$

where z is the distance from the centre of the bilayer and $q = 4\pi\sin\theta/\lambda$.

The NSLD profile was then put on an absolute scale:

$$\rho(z)^{abs} = \rho_w + \frac{F_0}{d} + \frac{\left(\rho(0) - \rho_w - \frac{F_0}{d}\right)}{\rho(0) \times \rho(z)} \quad 52$$

where ρ_w is the scattering length density of the water contrast; $\rho(0)$ is the scattering length density in the centre of the bilayer and the parameter F_0 is the forward scattering intensity used to put the data on an absolute scale. F_0 cannot be measured and it is therefore estimated as:

$$F_0 = \frac{2(b_L - \rho_w \times V_L)}{A_L} \quad 53$$

where b_L is the scattering length of the unit cell; V_L is the volume of the unit cell and A_L is the area of the unit cell. These parameters are calculated based on the composition of the sample.

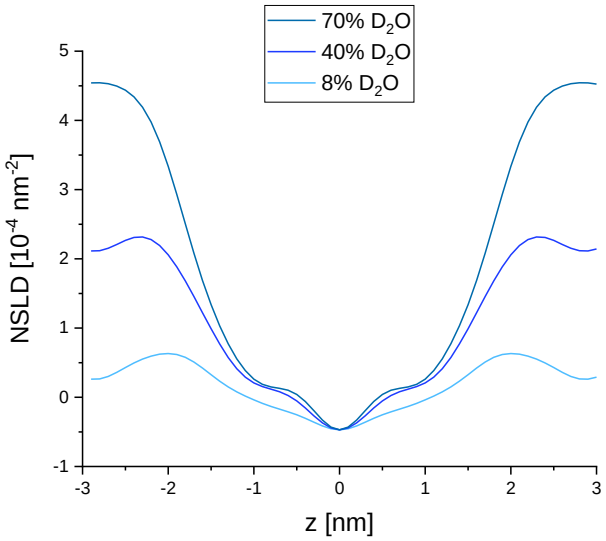

Figure 26: NSLD profiles of POPC-CHOL sample measured with 3 different H_2O/D_2O contrasts.

The ***water distribution*** was calculated by subtraction of NSLD profiles of contrast varied experimental data. The NSLD profiles are comprised of the contributions of the bilayer and water molecules.

$$\rho(z) = \rho_b P_b(z) + \rho_w P_w(z) \quad 54$$

Where ρ_b, ρ_w are the mean NSLDs of bilayer and water, respectively, and $P_b(z)$, $P_w(z)$ are the probabilities of occurrence at a distance from the centre of bilayer (z = 0).

The NSLD profile of the bilayer is not dependent on the changing contrast, whereas the NSLD of the water changes according to the ratio of H_2O/D_2O used as a contrast.

Therefore, by subtracting the NSLD profiles measured at different contrasts ($\rho_{w1}(z) - \rho_{w2}(z)$), we could calculate the probability of water occurrence along the profile of the membrane:

$$P_w(z) = \frac{\rho_{w1}(z) - \rho_{w2}(z)}{\rho_{w1} - \rho_{w2}} \qquad 55$$

where ρ_{w1} and ρ_{w2} are the calculated NSLDs of the contrast.
The water probability is between 0 and 1 if $\rho_{w1}(z)$ and $\rho_{w2}(z)$ are on an absolute scale.

The average of the water probability profiles was then fitted with the sum of two classical error functions placed at the bilayer/water interface:

$$\mathrm{erf}(z, z_0, \sigma) = \frac{2}{\sqrt{\pi}} \int_0^{\frac{z-z_0}{\sqrt{2}\sigma}} e^{-u^2} du \qquad 56$$

where σ is the width of the lipid/water interface and z_0 is the mean position at which the area under the curve from the centre of bilayer up to that point is equal to the area above the curve in the rest of the profile. The distance between $-z_0$ and z_0 gives us the bilayer thickness (d_b). Since repeat spacing d was defined earlier as the sum of a bilayer thickness (d_b) and water layer thickness (d_w), we can calculate the water layer thickness as well. This proved to be a suitable model for describing the profile of water distribution in (Klauda et al., 2006; Kučerka et al., 2009; Hrubovčák et al., 2019) and references therein.

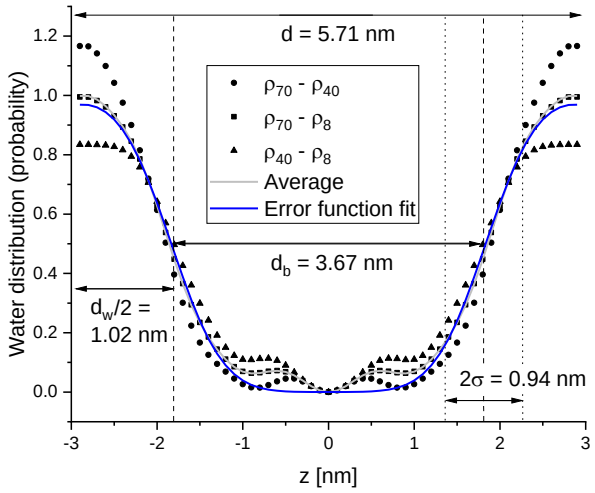

Figure 27: Water distribution probability obtained from subtraction of NSLD profiles of contrast varied experimental data. Averaged distribution was fitted with the error function to determine the thickness of the bilayer (d_b), water layer thickness (d_w) and the width of the lipid/water interface (σ). Sample is POPC-CHOL (97% RH).

4 RESULTS AND DISCUSSION

4.1 Static light scattering (nephelometry)

Turbidimetric method of studying the solubilisation process has been used many times in our Department of physical chemistry of drugs (e.g. Karlovská et al., 2004b; Karlovská et al., 2007; Huláková et al., 2013; 2015; Hrubšová et al., 2003; Bullová and Balgavý, 2005). However, using nephelometry proposed more advantages, such as higher sensitivity or lower lipid concentration needed in the samples. Initial experiments were performed to examine the sensitivity of the method. Pure DOPC liposomes dispersed in redistilled water were prepared using filters with three different sizes of pores during the extrusion: 50 nm, 100 nm and 200 nm filter. The dependence of the intensity of scattered light (with wavelength 600 nm) on the lipid concentration can be seen in Figure 28.

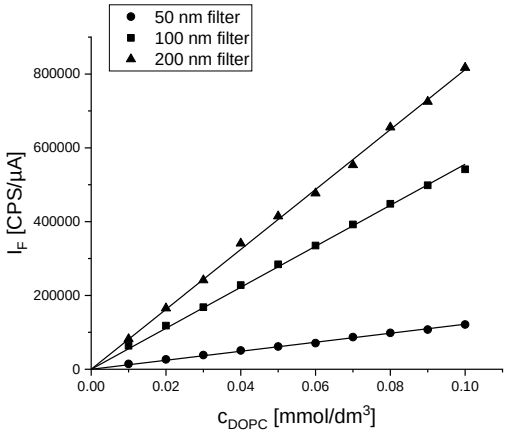

Figure 28: Dependence of intensity of scattered light on lipid concentration of 3 different sizes of liposomes.

Our experiments have shown that the intensity of the scattered light is sufficiently sensitive to the size of liposomes and the concentration of lipid. 100 nm size of the filter was chosen for subsequent solubilisation experiments. The results were not significantly different if PBS was used instead of redistilled water (the experiment was repeated using 100 nm filter and PBS as a solvent).

4.1.1 Solubilisation of mammalian model membranes by DDAO

Solubilisation of POPC-CHOL model membranes by non-ionic surfactant DDAO (at pH ~ 7.5) at various lipid concentrations was studied using nephelometry. Decrease in the

particle size is a typical indication of the solubilisation, as liposomes transform into the smaller mixed micelles during the process. Dependence of fluorescence intensity (I_F) on the concentration of DDAO (solubilisation curve) of POPC-CHOL model membrane at different lipid concentrations is shown in Figure 29. We can see the typical three-stage solubilisation process, which was described in Chapter 1.5.1 Interactions of surfactants with model membranes.

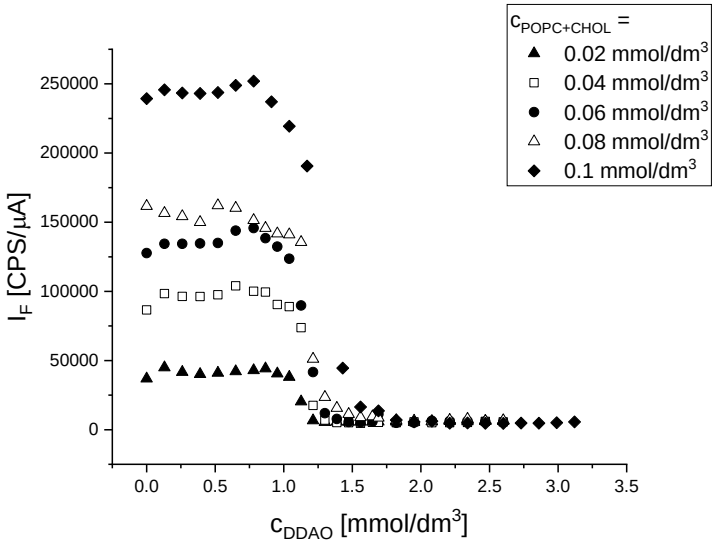

Figure 29: Dependences of fluorescence intensity (I_F) on the concentration of DDAO (solubilisation curves) of POPC-CHOL at different concentrations of lipid.

An example of solubilisation curve ($c_{POPC\text{-}CHOL}$ = 0.04 mmol/dm^3) fitting with the bilinear (Equations 3 and 4) and Boltzmann (Equation 5) functions, can be seen in Figure 30 and Figure 31, respectively. The equation of the straight line in the second stage is identical for both bilinear fits (one for D_t^{SAT} and the second one for D_t^{SOL}).

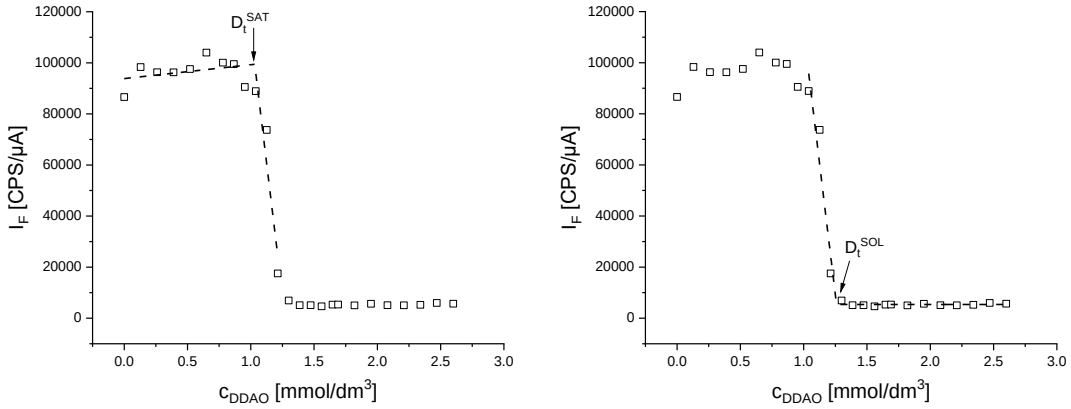

Figure 30: Fitting of the solubilisation curve of $c_{POPC\text{-}CHOL}$ = 0.04 mmol/dm^3 with bilinear functions. D_t^{SAT} and D_t^{SOL} are the x-coordinates of the turning points indicated by the arrows.

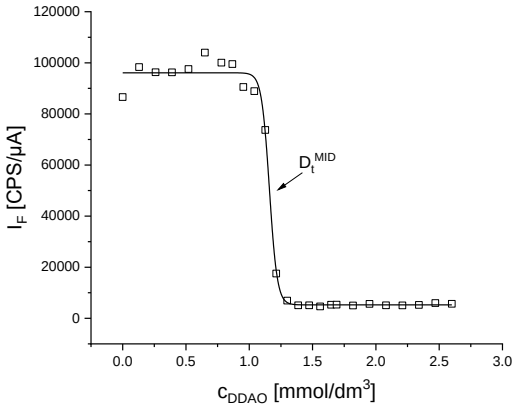

Figure 31: Boltzmann function fitting on the solubilisation curve of $c_{POPC\text{-}CHOL}$ = 0.04 mmol/dm³. D_t^{MID} is the x-coordinate of the midpoint of the sigmoid indicated by the arrow.

All acquired critical concentrations can be seen in the Table 6**.** All critical concentrations will be used to calculate the partition coefficient of DDAO (Chapter 4.4 Partition coefficients).

Table 6: Critical DDAO concentrations for POPC-CHOL model membranes.

POPC-CHOL			
$c_{POPC+CHOL}$ [mmol/dm³]	**D_t^{SAT} [mmol/dm³]**	**D_t^{MID} [mmol/dm³]**	**D_t^{SOL} [mmol/dm³]**
0.02	1.02 ± 0.02	1.114 ± 0.005	1.198 ± 0.003
0.04	1.03 ± 0.02	1.159 ± 0.005	1.232 ± 0.001
0.06	1.00 ± 0.01	1.158 ± 0.005	1.307 ± 0.005
0.08	1.12 ± 0.01	1.187 ± 0.005	1.26 ± 0.01
0.1	1.00 ± 0.05	1.224 ± 0.009	1.46 ± 0.03

Figure 32 shows comparison of solubilisation curves of three different mammalian model membranes, with the same lipid concentration. Intensity of fluorescence was normalised for better graphical comparison of the overall trend of the solubilisation curves:

$$I_{norm} = \frac{I - I_{min}}{I_{max} - I_{min}} \qquad 57$$

where I_{min} is the lowest detected fluorescence intensity and I_{max} is the highest detected intensity.

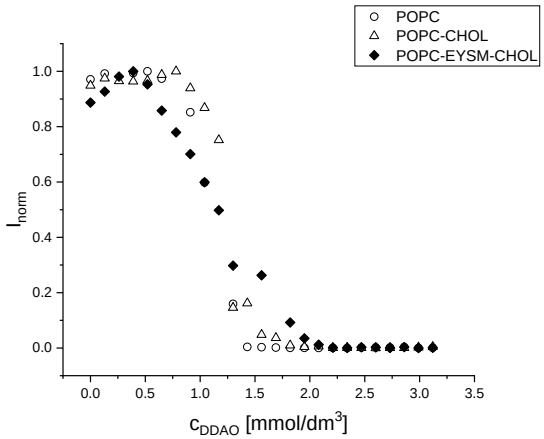

Figure 32: Comparison of solubilisation curves of different mammalian model membranes (POPC, POPC-CHOL and POPC-EYSM-CHOL), concentration of all compared lipids is 0.1 mmol/dm^3.

Both solubilisation curves of POPC and POPC-EYSM-CHOL were fitted with the bilinear (Equations 3 and 4) and Boltzmann (Equation 5) functions. The acquired critical concentrations of DDAO are shown in Table 7.

Table 7: Critical concentrations of POPC, POPC-CHOL and POPC-EYSM-CHOL model membranes at lipid concentration 0.1 mmol/dm^3.

	D_t^{SAT} [mmol/dm^3]	D_t^{MID} [mmol/dm^3]	D_t^{SOL} [mmol/dm^3]
POPC	0.83 ± 0.01	1.093 ± 0.006	1.387 ± 0.004
POPC-CHOL	1.00 ± 0.05	1.224 ± 0.009	1.46 ± 0.03
POPC-EYSM-CHOL	0.39 ± 0.07	1.17 ± 0.03	1.91 ± 0.04

As we can see from the results (Table 7 and Figure 32) the POPC membrane enriched by EYSM+CHOL reached the saturation concentration at lower DDAO concentration than it was for both POPC and POPC-CHOL. On the other hand, the concentration of DDAO needed for complete solubilisation was highest out of the three mammalian model membranes. The exchange of a part of POPC molecules by CHOL caused a slight increase in all 3 fitted parameters.

In (Ruiz et al., 1988) it was reported that the solubilisation of EYPC-CHOL (n_{EYPC}:n_{CHOL} = 3:1) liposomes induced by non-ionic surfactant Triton X-100 (TX-100) was similar as that observed for CHOL-free liposomes. The solubilisation was more difficult at equimolar EYPC-CHOL ratio. Study of Mattei et al. (2015) showed changes in the ability of TX-100 to solubilise POPC-CHOL and EYSM-CHOL liposomes with 30 mol% of CHOL. The liposomes became either partially (POPC-CHOL) or completely (EYSM-CHOL) insoluble by TX-100.

In this thesis, DDAO was able to achieve complete solubilisation of all of the studied membranes. Ahyayauch et al. (2010) concluded that all surfactants interact with the model membrane differently, therefore, it is difficult to compare them.

In our previous solubilisation study (Želinská et al., 2020) of DOPC and DOPC-CHOL (33 mol% of CHOL) induced by DDAO, we reported insignificant effect of the presence of CHOL on the critical concentrations (c_{DOPC} = 0.3 mmol/dm^3: D_t^{SAT} = 1.41 ± 0.05 mmol/dm^3, D_t^{SOL} = 2.38 ± 0.04 mmol/dm^3 and for $c_{DOPC+CHOL}$ = 0.3 mmol/dm^3: D_t^{SAT} = 1.43 ± 0.1 mmol/dm^3, D_t^{SOL} = 2.28 ± 0.07 mmol/dm^3).

4.1.2. Solubilisation of bacterial model membranes by DDAO

Solubilisation of two types of bacterial model membranes – POPE-POPG (n_{POPE}:n_{POPG} = 0.6:0.4 mol/mol) and more realistic POPE-POPG-TOCL (n_{POPE}:n_{POPG}:n_{TOCL} = 0.67:0.23:0.1 mol/mol/mol) by DDAO was studied at 5 different concentrations of lipid nephelometrically. Solubilisation curves (Figure 33) followed the typical three stage process described earlier.

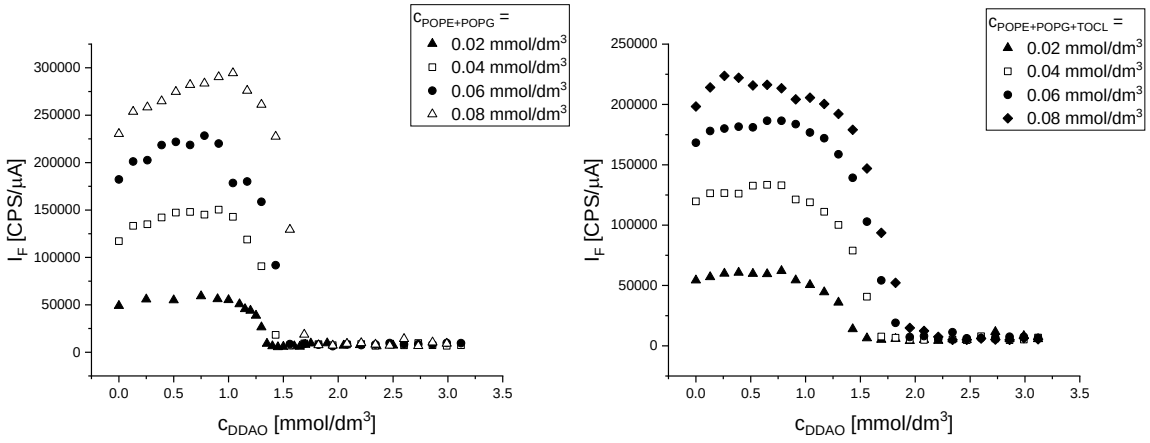

Figure 33: Solubilisation curves of POPE-POPG liposomes (on the left) and POPE-POPG-TOCL liposomes (on the right) at different concentrations of lipid.

All solubilisation curves were fitted with bilinear functions (Equations 3 and 4) and a Boltzmann function (Equation 5) to obtain the critical DDAO concentrations D_t^{SAT}, D_t^{MID} and D_t^{SOL}. All critical concentrations (Table 8) will be used to calculate the partition coefficient of DDAO (Chapter 4.4 Partition coefficients).

Table 8: Critical DDAO concentrations for POPE-POPG and POPE-POPG-TOCL model membranes.

POPE-POPG			
$c_{POPE+POPG}$ [mmol/dm^3]	**D_t^{SAT} [mmol/dm^3]**	**D_t^{MID} [mmol/dm^3]**	**D_t^{SOL} [mmol/dm^3]**
0.02	1.08 ± 0.03	1.27 ± 0.01	1.40 ± 0.02
0.04	1.03 ± 0.04	1.32 ± 0.01	1.51 ± 0.02
0.06	0.97 ± 0.06	1.39 ± 0.02	1.65 ± 0.05
0.08	1.27 ± 0.03	1.54 ± 0.01	1.73 ± 0.02
0.1	1.27 ± 0.04	1.62 ± 0.01	1.88 ± 0.03
POPE-POPG-TOCL			
$c_{POPE+POPG+TOCL}$ [mmol/dm^3]	**D_t^{SAT} [mmol/dm^3]**	**D_t^{MID} [mmol/dm^3]**	**D_t^{SOL} [mmol/dm^3]**
0.02	0.98 ± 0.05	1.29 ± 0.02	1.57 ± 0.03
0.04	1.14 ± 0.04	1.46 ± 0.01	1.73 ± 0.02
0.06	1.25 ± 0.03	1.57 ± 0.01	1.87 ± 0.02
0.08	1.37 ± 0.03	1.65 ± 0.01	1.97 ± 0.01
0.1	1.47 ± 0.03	1.81 ± 0.01	2.19 ± 0.01

Solubilisation of bacterial model membranes is not well documented in the literature. Most studies focus on the isolation of proteins from bacterial membranes rather than the solubilisation of the lipids that are present in it. In comparison with the mammalian model membrane POPC-CHOL studied in this thesis, both bacterial model membranes required more DDAO for complete solubilisation. A comparison between the solubilisation curve of POPC-CHOL and POPE-POPG can be seen in the Figure 34 (on the left). Figure 34 (on the right) shows a comparison of solubilisation curves of both types of bacterial model membrane at the same concentration of lipid 0.1 mmol/dm^3. The intensity of fluorescence was normalised (Equation 57) for better graphical comparison.

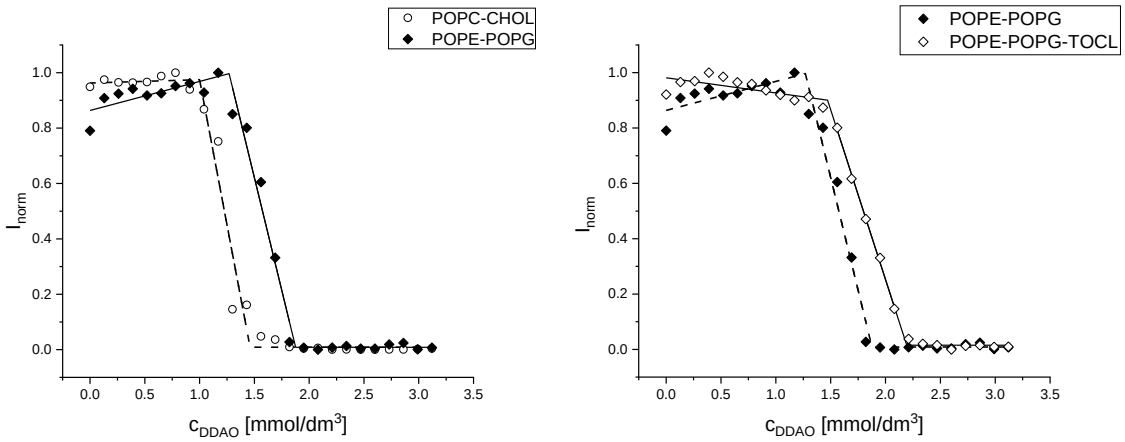

Figure 34: Comparison of solubilisation curves of mammalian model membrane POPC-CHOL and bacterial model membrane POPE-POPG (on the left) and both bacterial model membranes (on the right). Lipid concentration is 0.1 mmol/dm^3 for all shown solubilisation curves.

From the results in Table 8 and Figure 34, we can see that the cardiolipin containing model was more stable against the DDAO-induced solubilisation. This is important because many studies on bacterial model membranes tend to neglect the importance of the presence of cardiolipin in model membranes, because of its low occurrence in the bacterial membrane (only 10 w% in *E.coli*).

4.2 Fluorescence spectroscopy

4.2.1 Calibration curve of calcein

In the Figure 35, we can see a calibration curve of calcein – the dependence of the fluorescence intensity on the concentration of calcein. In the first part of the dependence, within 0 – 0.007 mmol/dm^3 (the full points), fluorescence intensity increases linearly with calcein concentration. The dependence reaches maximum at about 0.02 mmol/dm^3, beyond which it starts to decrease due to a phenomenon called self-quenching. The fluorescence intensity becomes negligible at the concentration higher than 0.1 mmol/dm^3. Similar results were observed by authors (Memoli et al., 1999b; Huláková et al., 2013). As proven by (Huláková et al., 2013), the spectral behaviour of calcein is not affected by the presence of DDAO.

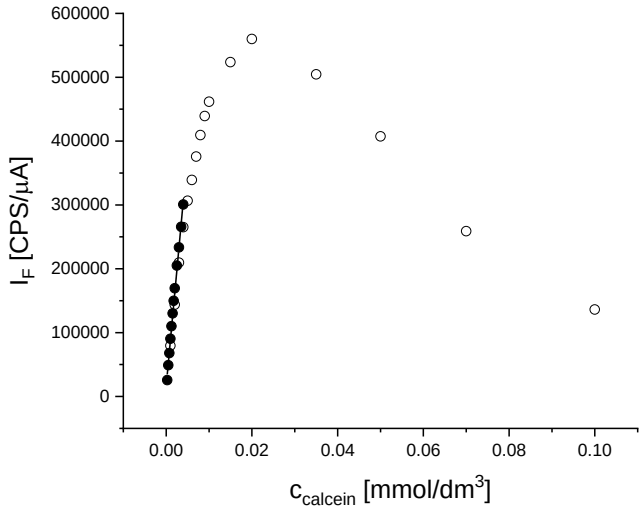

Figure 35: Dependence of fluorescence intensity on the concentration of calcein. Full circle points indicate the linear part of the dependence.

Prepared samples contained calcein encapsulated in liposomes at a concentration 10 mmol/dm^3, so its fluorescence was insignificant. After the surfactant was added, calcein leaked into extra-liposomal space, where it was diluted to the calcein concentration which is

in the linear range of the dependence. Since the probe no longer self-quenched, an increase in fluorescence was monitored as an indicator of pore formation in the liposomes.

4.2.2 Calcein leakage from mammalian model membranes

Calcein leakage experiments have been performed on mammalian model membranes containing lipids POPC and POPC-CHOL (n_{POPC}:n_{CHOL} = 2:1 mol/mol). Samples were measured immediately after the addition of DDAO. Dependences of the normalised fluorescence intensities (I_{norm}) on the concentration of DDAO measured with POPC-CHOL model membranes are shown in the Figure 36. The description of the process of calcein leakage was explained earlier in Chapter 3.2.3 Data treatment.

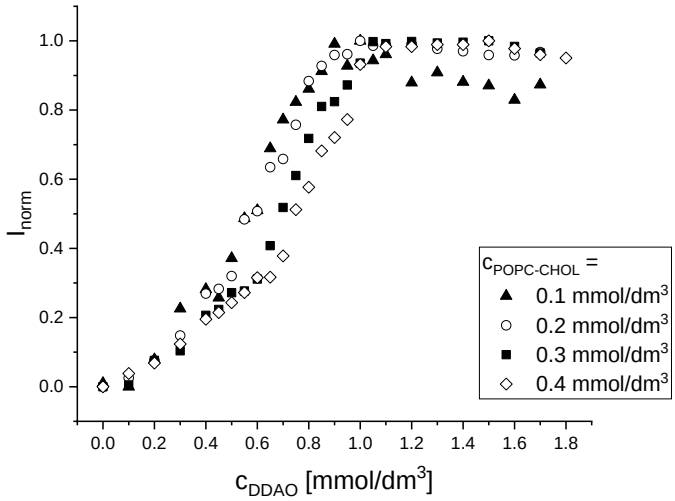

Figure 36: Calcein leakage experiments – dependence of normalised fluorescence intensity on concentration of DDAO using POPC-CHOL liposomes.

In Figure 37, we can see an example of the fluorescent probe leakage data and their fitting with bilinear functions, Equation 3 (on the left) to obtain D_t^{PERT} and Equation 4 (on the right) to get the value of D_t^{RLS}. The fit for the straight line in the second stage (described in 3.2.3 Data treatment) is identical for both fits.

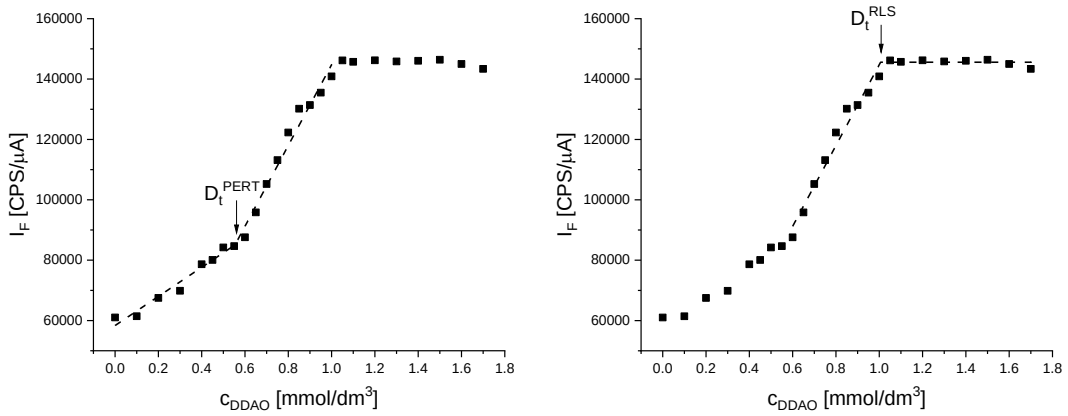

Figure 37: Example of the fitting with bilinear functions on the calcein leakage data ($c_{POPC+CHOL}$ = 0.3 mmol/dm^3).

The same procedure was used to fit all data from calcein leakage experiments. Figure 38 shows a comparison of experiments with POPC and POPC-CHOL using the same concentration of lipid (0.3 mmol/dm^3).

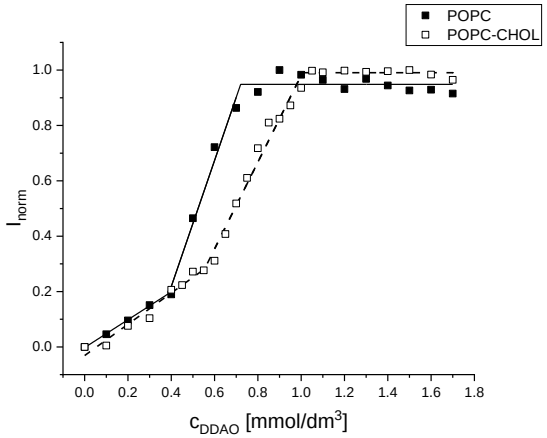

Figure 38: Comparison of calcein leakage experiment between POPC and POPC-CHOL at c_{LIPID} = 0.3 mmol/dm^3.

All critical concentrations acquired using the mammalian model membranes are shown in the Table 9. These results will be used to calculate the partition coefficient of DDAO in the Chapter 4.4 Partition coefficients, except for POPC, for which we have insufficient data.

Table 9: Critical DDAO concentrations of studied mammalian model membranes POPC and POPC-CHOL.

POPC+CHOL		
$c_{POPC+CHOL}$ **[mmol/dm³]**	D_t^{PERT} **[mmol/dm³]**	D_t^{RLS} **[mmol/dm³]**
0.1	0.46 ± 0.04	0.79 ± 0.02
0.2	0.44 ± 0.03	0.87 ± 0.01
0.3	0.55 ± 0.03	1.01 ± 0.01
0.4	0.65 ± 0.02	1.05 ± 0.01
POPC		
c_{POPC} **[mmol/dm³]**	D_t^{PERT} **[mmol/dm³]**	D_t^{RLS} **[mmol/dm³]**
0.3	0.39 ± 0.03	0.71 ± 0.01

As we can see from Table 9 and Figure 38, the POPC-CHOL model membrane was more resistant against DDAO-induced pore formation than the CHOL-lacking model. The effect of the presence of CHOL in POPC bilayers on the leakage of fluorescent probe 5,6-carboxyfluorescein from liposomes was investigated in (Apel-Paz et al., 2005). CHOL have linearly increased the resistance of liposomes against the surfactant sodium dodecylsulphate (SDS) until 30 mol% of CHOL was reached, the amount of CHOL higher than 30 mol% had "super-toughening effect" on the bilayer. (Nagawa and Regen, 1991) reported significantly reduced ability of 4 different membrane-disrupting surfactants to release the internal contents of EYPC and POPC liposomes that contained more than 33 mol% of CHOL. They also reported that the surfactant TX-100 was not sensitive to the presence of CHOL, when the leakage of 5,6-carboxyfluorescein was observed from POPC-CHOL liposomes (at molar ratios n_{POPC}:n_{CHOL} = 4:1, 2:1 and 1:1).

4.2.3 Calcein leakage from bacterial model membranes

Calcein leakage experiments have been performed on bacterial model membranes containing lipid mixture POPE-POPG (n_{POPE}:n_{POPG} = 0.6:0.4 mol/mol). Samples were measured immediately after the addition of DDAO. Two sets of samples with $c_{POPE+POPG}$ = 0.1 mmol/dm^3 were prepared identically, one of them was measured immediately after DDAO addition and the second one was measured 3 hours after the addition of DDAO. A comparison of the two experiments is seen in the Figure 39 (on the left). The samples measured 3 hours after the addition did not follow the typical three-stage process, which was probably caused by instability of the liposomes with the encapsulated fluorescent probe.

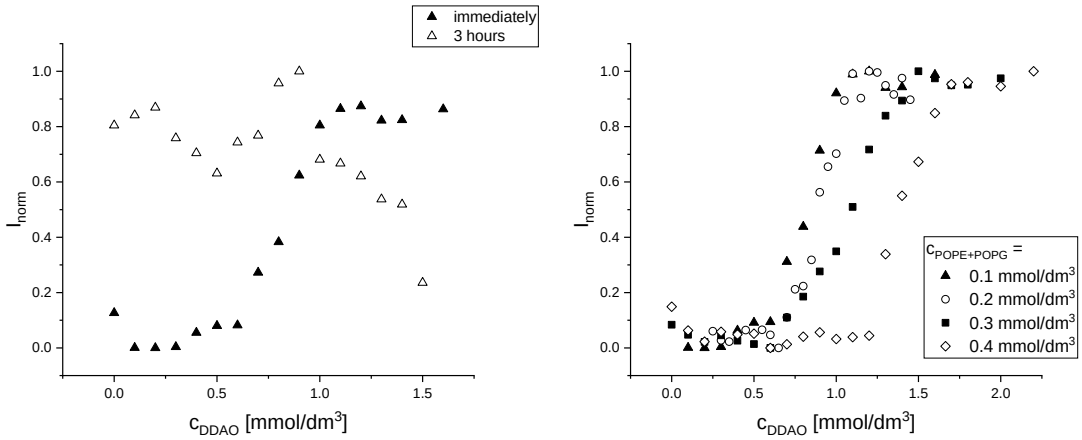

Figure 39: Comparison of the calcein leakage experiment from POPE-POPG liposomes ($c_{POPE+POPG}$ = 0.1 mmol/dm^3) measured immediately after the addition of DDAO and three hours later (on the left). Calcein leakage experiments with $c_{POPE+POPG}$ = 0.1 – 0.4 mmol/dm^3 (on the right).

All dependences of fluorescence intensity on the concentration of DDAO were fitted with bilinear functions to obtain the values of D_t^{PERT} and D_t^{RLS}. Results of this fitting are shown in the Table 10. These critical concentrations will be used to calculate the partition coefficient of DDAO (Chapter 4.4 Partition coefficients).

Table 10: Critical DDAO concentrations of studied bacterial model membrane POPE-POPG.

POPE-POPG		
$c_{POPE+POPG}$ [mmol/dm^3]	**D_t^{PERT} [mmol/dm^3]**	**D_t^{RLS} [mmol/dm^3]**
0.1	0.62 ± 0.02	1.03 ± 0.02
0.2	0.69 ± 0.02	1.09 ± 0.02
0.3	0.65 ± 0.03	1.45 ± 0.02
0.4	1.16 ± 0.02	1.64 ± 0.02

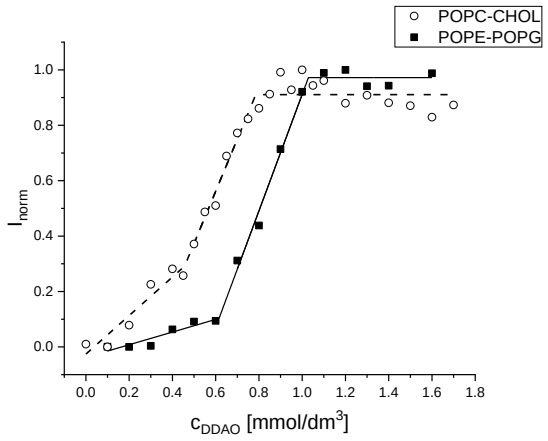

Figure 40: Comparison of calcein leakage experiment between POPC-CHOL and POPE-POPG at c_{LIPID} = 0.1 mmol/dm^3.

Figure 40 shows a comparison of the calcein leakage experiment of POPC-CHOL and POPE-POPG at the same concentration of lipid (c_{LIPID} = 0.1 mmol/dm^3).

As we can see from the critical concentrations obtained from these two types of model membrane (Table 9 and Table 10) and from the graphical comparison (Figure 40), the bacterial model membrane POPE-POPG was more resistant against the DDAO-induced leakage than the mammalian model (POPC-CHOL). Another noticeable difference when comparing the calcein release data of these two model membranes is the difference in the first stage of calcein release. In case of POPC-CHOL, the straight line in the first stage of calcein release had a positive slope, whereas for POPE-POPG, it was much closer to zero or it had even a slightly decreasing tendency. The dependence of the slope of the straight line in the first stage on the concentration of lipid is depicted in Figure 41. This suggests that the pore formation and their stabilisation requires higher amount of DDAO in case of POPE-POPG membrane.

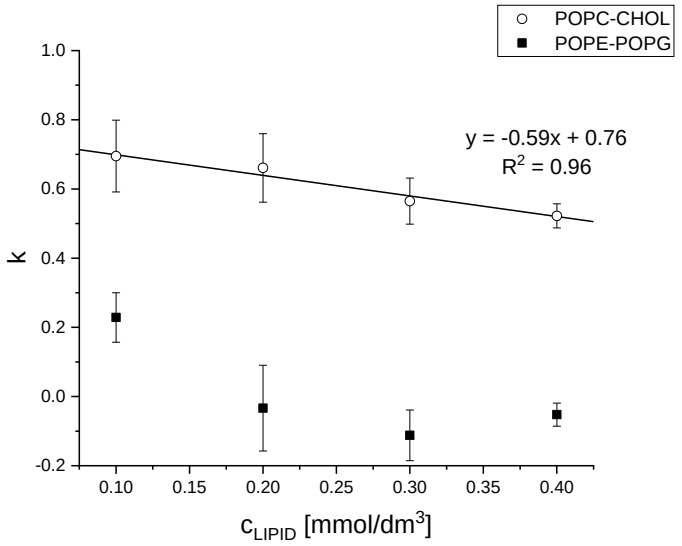

Figure 41: The dependence of the slope (k) of the linear fit in the first stage of calcein release on the concentration of lipid.

The difference may be caused by the different interactions between the lipid molecules and/or their ordering. The difference between the predominant phospholipids in our model membranes, PCs and PEs, is just that the choline group of the PCs polar fragment is replaced by the ammonium group in PEs. The polar fragment of PEs is therefore smaller in diameter than the polar part of the PCs molecule and binds smaller amount of water molecules. The ammonium group is able to form hydrogen bonds with phosphate and oxygen atoms of adjacent molecules. Molecular dynamics simulation of POPE-POPG (in the proportion 3:1) model membrane with Na^+ ions to neutralise the negative charge of

POPG was done by authors (Murzyn et al., 2005). In the study it was concluded that POPE molecules interact readily with POPG and other POPE molecules with hydrogen bonds and water bridges. These bonds strengthen the interlipid contact within the bilayer.

On the other hand, we have the mammalian model membrane POPC with 33 mol% of CHOL. CHOL incorporation into the phospholipid bilayer leads to higher ordering of the phospholipid hydrocarbon chains, but the bilayer maintains the relatively high rates of lateral and rotational diffusion (Ohvo-Rekilä et al., 2002). Because of the relatively large and rigid molecule, CHOL increases the separation between the polar fragments of phospholipids and reduces the possible interactions between them (Kučerka et al., 2007; Gallová et al., 2010a and references therein).

4.2.4 Dermaseptin S1 induced leakage

Calcein release from POPE-POPG liposomes ($c_{POPE+POPG}$ = 0.01 mmol/dm^3) induced by an antimicrobial peptide dermaseptin S1 (DS1) was observed. The dependence of I_{norm} on the concentration of DS1 is shown in the Figure 42. The results were similar if measured 3 hours after the addition of DS1. Complete calcein release was monitored by preparing a sample from the same stock solution of lipid and adding DDAO at a concentration c_{DDAO} = 1.5 mmol/dm^3, which is sufficient for a complete release of the probe (the highest concentration of DDAO added in Figure 43).

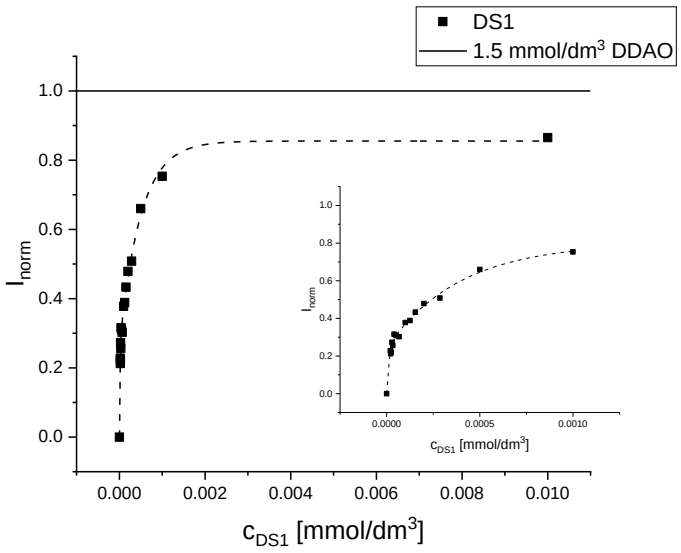

Figure 42: Normalised fluorescence intensity (I_{norm}) after the addition of DS1 to 0.01 mmol/dm^3 POPE-POPG liposomes with encapsulated calcein. Exponential decay function (dashed line) serves graphical purpose only. The horizontal line shows the I_{norm} after the addition of DDAO at a concentration causing maximum release of calcein (c_{DDAO} in the sample is 1.5 mmol/dm^3). The inset displays the same data in smaller range of c_{DS1}.

When compared with the sample containing redundant amount of DDAO, we can see that the DS1 was not able to fully release the probe. The ability to release the probe was decaying exponentially with concentration of DS1. Figure 43 shows a comparison of calcein release experiment induced by DS1 and DDAO (both with 0.01 mmol/dm^3 of POPE-POPG). Even though the DS1 was not able to completely release the probe, it was highly effective at low n_{DS1}:n_{LIPID} molar ratios – reaching approximately 75% release at n_{DS1}:$n_{POPE+POPG}$ = 0.1 (mol/mol). In comparison, n_{DDAO}:$n_{POPE+POPG}$ = 90 (mol/mol) was needed to achieve similar effect. The large difference might be explained by the fact that due to the small concentration of lipid in these samples, large amount of DDAO might not partition into the lipid phase (partitioning will be discussed in Chapter 4.4 Partition coefficients), while the antimicrobial peptide attaches to the liposomes much more effectively even at low lipid concentration.

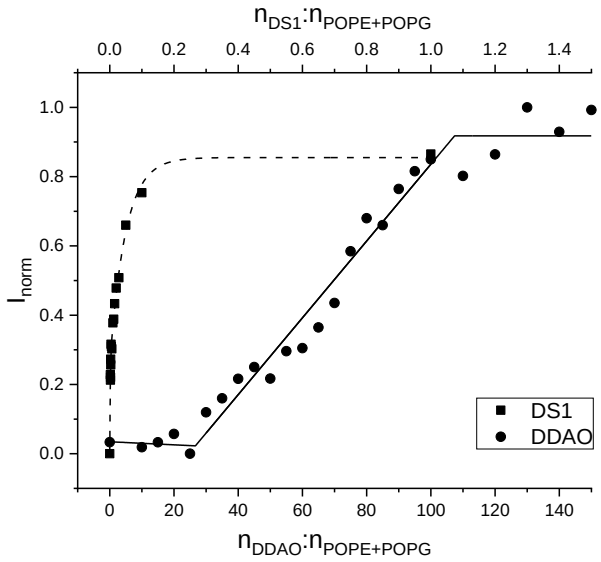

Figure 43: Calcein release from POPE-POPG ($c_{POPE+POPG}$ = 0.01 mmol/dm^3) liposomes induced by DS1 (squares) and DDAO (circles).

We compared our findings with a study of Pouny et al. (1992), who studied the interaction of dermaseptin S1 with model membranes consisting of EYPC, EYPC-PS (1:1 w/w ratio) and soybean PC, all mixed with 10 w% of CHOL. The comparison of calcein release is shown in Figure 44. In their study, the fluorescence recovery was calculated similarly as we did our normalised intensity (I_{norm}, Equation 57). As 100% fluorescence recovery, the authors have used the intensity of fluorescence after the addition of surfactant TX-100.

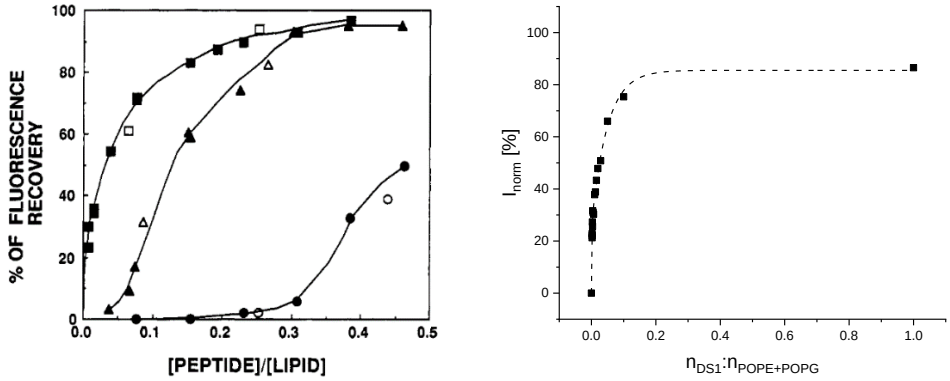

Figure 44: On the left: Calcein release induced by dermaseptin, reproduced from (Pouny et al., 1992). *Increasing amounts of dermaseptin S1 were added to 2.5 μmol/dm^3 of EYPC (circles), EYPC-PS (1:1 w/w) (triangles) and soybean (squares), all containing 10 w% of CHOL. The open symbols correspond to dermaseptin fluorescently modified with tetramethylrhodamine (Rh-dermaseptin). On the right: Our calcein release data from POPE-POPG model membrane by dermaseptin.*

As we can see in the Figure 44, DS1 was the least effective in releasing the calcein from the EYPC-CHOL liposomes. Dermaseptin has high activity in inducing calcein release from EYPC-PS-CHOL and soybean PC-CHOL mixtures as compared to EYPC-CHOL. For example, the peptide/lipid molar ratios causing 20% release were observed to be 0.005, 0.075 and 0.350 for soybean PC-CHOL, EYPC-PS-CHOL and EYPC-CHOL liposomes, respectively. In our case, 20% release from POPE-POPG liposomes was observed at even lower peptide/lipid ratio, 0.002 specifically. Pouny et al. (1992) reported strong binding and ability to permeate membranes composed of negatively charged phospholipids as opposed to zwitterionic phospholipids, such as EYPC.

Calcein leakage induced by melittin, antimicrobial peptide (26 AAs, 5 positive charges, α-helical structure) similar to DS1, was studied by authors Benachir and Lafleur (1995). The authors observed rapid binding of melittin to liposomes without subsequent interliposomal migration. They reported that adding negatively charged palmitic acid or POPG to POPC limited the release of encapsulated calcein. It was proposed to be caused by electrostatic anchorage of the peptide at the bilayer interface. Similar results have been reported for a positively charged lantibiotic nisin when interacting with DOPC liposomes containing anionic lipids. On the other hand, the opposite effect was observed for magainin – its lytic effect was increased by the addition of anionic lipids in EYPC (Benachir and Lafleur (1995) and references therein).

4.3 Densitometry

The densitometric and volumetric parameters acquired following the procedures described in 3.3 Vibrational densitometry are essential for our method of calculating the partition coefficient of DDAO, as well as to evaluate the data obtained from small-angle neutron scattering and diffraction.

Table 11 shows parameters calculated using procedures described in Chapter 3.3.3 Data treatment. The values of density of DOPC and DOPC-CHOL (2:1 mol/mol) mixed bilayer were taken from literature (Gallová et al., 2015) and will be needed for the evaluation of our SANS data. The apparent molecular volume and density of DDAO in a DOPC bilayer at 20° C were taken from literature as well (Belička et al., 2014a). We presume the values do not change significantly in model membranes with different composition.

Table 11: Calculated densitometric and volumetric parameters of used lipids and lipid mixtures and DDAO.

Lipid/lipid mixture	ρ_b [g/cm^3]	V_L [nm^3]
DOPC	1.0062[a]	1.2974[a]
DOPC-CHOL	1.0076[a]	1.0654[a]
POPC-CHOL	1.0151	1.0398
POPC	1.0079	1.2523
CHOL	1.0446	0.6146
POPE-POPG	1.0384	1.1821
POPE	1.0231	1.1654
POPG	1.0606	1.2071
POPE-POPG-TOCL	1.0360	1.2961
DDAO	0.9498[b]	0.4011[b]

[a] taken over from (Gallová et al., 2015) [b](Belička et al., 2014a)

4.4 Partition coefficients

Permeabilisation and solubilisation study of liposomes (Chapter 4.1 Static light scattering (nephelometry) and 4.2 Fluorescence spectroscopy) representing mammalian and bacterial model membranes at various lipid concentrations by surfactant DDAO enabled us to calculate the partition coefficient of DDAO between the model membrane and aqueous phase. The calculation process is described in Chapter 3.4 Partition coefficient calculations. The linear dependence of critical concentrations (from nephelometric and fluorescence spectroscopy experiments) on the concentration of lipid (Equation 25), was used to calculate the partition coefficient (K_p) of DDAO between our model membranes and water phase, the

effective molar ratio (R_e) of the amount of DDAO integrated into the bilayer to the amount of lipid and the molar concentration of DDAO in the water phase (D_w).

The constant parameters used for fitting are listed in Table 12. The density of the bilayers was taken from Table 11. Molar mass of mixed bilayers was calculated according to Equation 22 (p. 49).

Table 12: Constant fitting parameters used for partition coefficient calculations.

Membrane type	ρ_b [g/cm^3]	M_L [g/mol]	ρ_b/M_L [mmol/dm^3]
POPC-CHOL	1.0151	635.6	1597
POPE-POPG	1.0384	739.2	1405
POPE-POPG-TOCL	1.0360	808.6	1281

4.4.1 Mammalian model membrane

The critical concentrations of DDAO acquired from nephelometric experiments (D_t^{SAT}, D_t^{MID} and D_t^{SOL}, Table 6) and fluorescence spectroscopy experiments (D_t^{PERT} and D_t^{RLS}, Table 9) were plotted as a function of lipid ($c_{POPC+CHOL}$) concentration. The dependences can be seen in the Figure 45. The concentrations of DDAO in the water phase (D_w) for each critical step are indicated by the arrows.

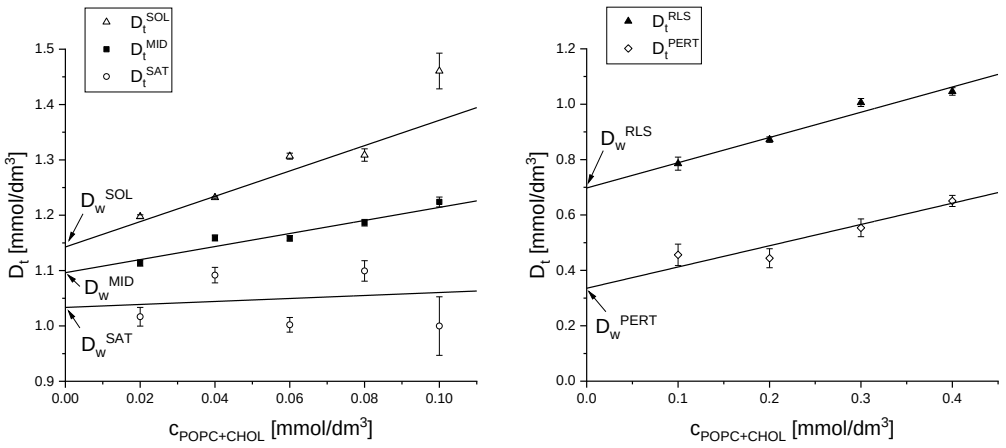

Figure 45: Linear dependences of critical DDAO concentration on the concentration of lipid ($c_{POPC+CHOL}$) obtained from nephelometric data (on the left) and fluorescence spectroscopy data (on the right). D_w values are indicated with arrows.

Figure 46 shows the global fit of all linear dependences from nephelometric and fluorescence spectroscopy experiments.

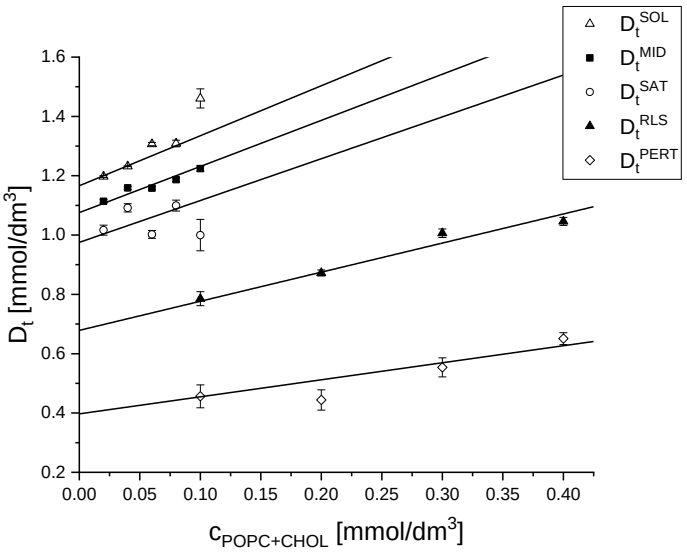

Figure 46: Global fit of the dependences of critical DDAO concentrations (D_t) on the concentration of lipid ($c_{POPC+CHOL}$).

Table 13 shows the effective molar ratio (R_e) and the concentration of DDAO in the water phase (D_w) for each particular step of the studied process. The partition coefficient of DDAO between POPC-CHOL model membrane and PBS buffer was calculated to be **2300 ± 300**.

Table 13: Effective ratio (R_e) of the amount of DDAO integrated into the bilayer to the amount of lipid ($n_{POPC+CHOL}$) and concentration of the monomeric surfactant in the water phase (D_w).

POPC-CHOL		
Critical concentration	**R_e**	**D_w [mmol/dm^3]**
D_t^{PERT}	0.57 ± 0.07	0.40 ± 0.10
D_t^{RLS}	0.98 ± 0.10	0.68 ± 0.17
D_t^{SAT}	1.41 ± 0.18	0.98 ± 0.27
D_t^{MID}	1.56 ± 0.20	1.08 ± 0.29
D_t^{SOL}	1.69 ± 0.22	1.17 ± 0.32

As can be seen from the values of R_e, the perturbation of the bilayer and complete release of the fluorescent probe happen before the bilayer is completely saturated by the surfactant. A graphical comparison of both methods (nephelometry and calcein release) can be seen in Figure 47 for identical lipid concentration of POPC-CHOL and POPE-POPG, 0.1 mmol/dm^3. Concentration of surfactant needed to create pores in the membrane is not sufficient enough to start the liposome–micelle transformation process. Further increase in the membrane bound DDAO concentration is needed to stabilise those pores and proceed into the next stage of the solubilisation.

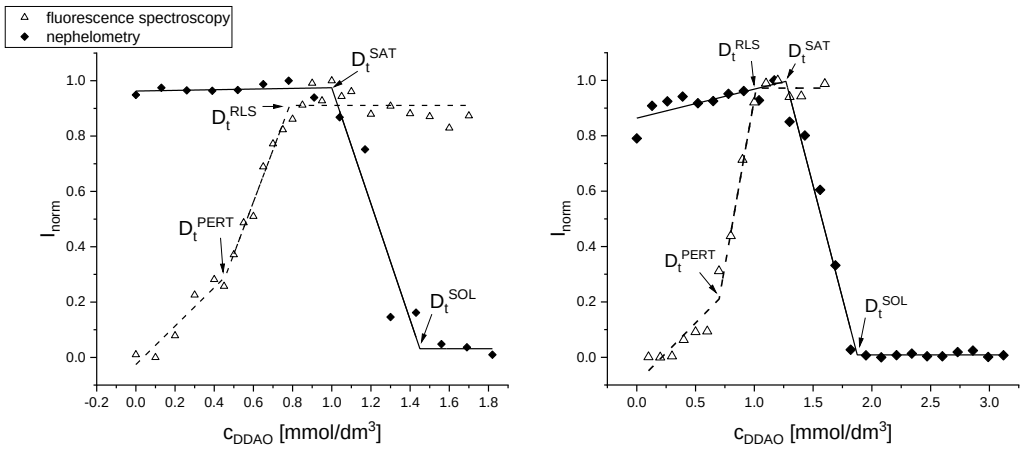

Figure 47: Dependence of the normalised fluorescence intensity (I_{norm}) on the concentration of DDAO (c_{DDAO}). Fluorescence spectroscopy data (fitted with bilinear functions – dashed line) and nephelometric experiment (fitted with bilinear functions – full line) with $c_{POPC\text{-}CHOL}$ = 0.1 mmol/dm^3 (on the left) and $c_{POPE\text{-}POPG}$ = 0.1 mmol/dm^3 (on the right).

In comparison with our previous study (Želinská et al., 2020), where we calculated the partition coefficient of DDAO in a system DOPC/PBS ($K_P = 2300 \pm 400$) and DOPC-CHOL/PBS ($K_P = 2100 \pm 600$), the partition coefficient calculated in this thesis for POPC-CHOL/PBS is very similar ($K_P = 2300 \pm 300$) suggesting that DDAO interacts similarly with these lipids/lipid mixtures. On the other hand, in the study of (Hrubšová et al., 2003), the partition coefficient of DDAO in the system EYPC/water was calculated to be smaller $K_P = 500 \pm 200$. Only the dependence of D_t^{MID} on the lipid concentration was used. The effective molar ratio R_e for the D_t^{MID} concentration was 0.60 ± 0.16, which is much lower than in our case for the system POPC-CHOL/PBS (1.56 ± 0.20). We suspect the difference is caused by a part of DDAO molecules being charged in the absence of the buffer. Similarly, Karlovská et al. (2004b) reported a partition coefficient of MLLs composed of EYPC dispersed in TRIS buffer to be 1200 ± 400. The author suggested that the different curvature of MLLs and ULLs might affect the partitioning, but with the samples being measured only 30 minutes after the preparation it is not guaranteed that the partitioning equilibrium has been reached in their multilamellar system. (Kragh-Hansen et al., 1998) reported the $K_p = 4000$ for DDAO in a dispersion of ULLs made of sarcoplasmic reticulum lipids in a buffered aqueous phase. From these different results, we can conclude that the partitioning is affected by the type and the composition of the model membrane, as well as the aqueous phase it is dispersed in.

The partition coefficients of DDAO stated in the previous paragraph were lower than for some other surfactants. For example, the partition coefficients of TX-100 and sodium dodecylbenzene sulfonate (SDBS) in a system of EYPC ULLs/HEPES buffer were calculated to be 6337 for TX-100 and 23800 for SDBS (Marcelino et al., 2007). The higher the K_p, the higher the predisposition to accumulate in the environment.

4.4.2 Bacterial model membranes

The critical concentrations of DDAO acquired from nephelometric experiments (D_t^{SAT}, D_t^{MID} and D_t^{SOL}, Table 8) and fluorescence spectroscopy experiments (D_t^{PERT} and D_t^{RLS}, Table 10) were plotted as a function of POPE-POPG concentration. Figure 48 shows the global fit of all linear dependences from nephelometric and fluorescence spectroscopy experiments. Table 14 shows the effective molar ratio (R_e) and the concentration of DDAO in the water phase (D_w) for each particular step of the studied process. The partition coefficient of DDAO between POPE-POPG model membrane and PBS buffer was calculated to be **4800 ± 500**.

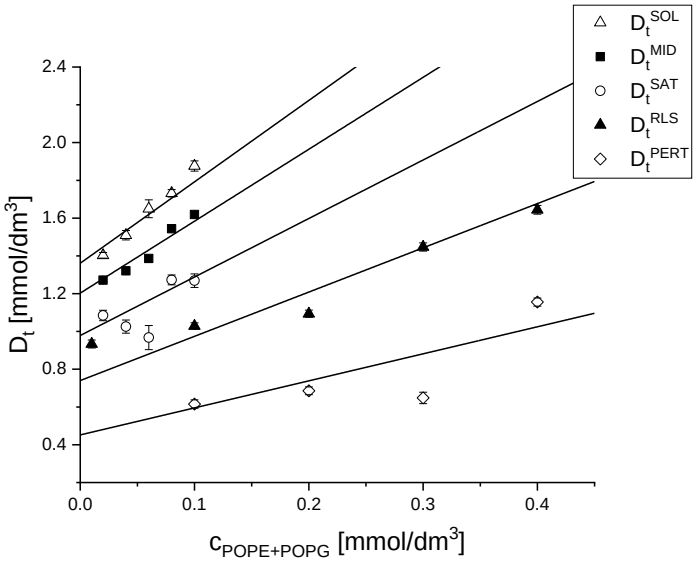

Figure 48: Global fit of the dependences of critical DDAO concentrations (D_t) on the concentration of lipid ($c_{POPE+POPG}$).

Table 14: Effective ratio (R_e) of the amount of DDAO integrated into the bilayer to the amount of lipid ($n_{POPE+POPG}$) and concentration of the monomeric surfactant in the water phase (D_w).

POPE-POPG		
Critical concentration	**R_e**	**D_w [mmol/dm^3]**
D_t^{PERT}	1.43 ± 0.13	0.45 ± 0.08
D_t^{RLS}	2.34 ± 0.19	0.74 ± 0.13
D_t^{SAT}	3.09 ± 0.36	0.98 ± 0.19
D_t^{MID}	3.81 ± 0.41	1.20 ± 0.23
D_t^{SOL}	4.31 ± 0.47	1.36 ± 0.26

Similar procedure was followed for POPE-POPG-TOCL mixed bilayers. The critical concentrations of DDAO acquired from nephelometric experiments (D_t^{SAT}, D_t^{MID} and D_t^{SOL},

Table 8) were plotted as a function of POPE-POPG-TOCL concentration. Only these three linear dependences were used for the calculation of K_p, R_e and D_w.

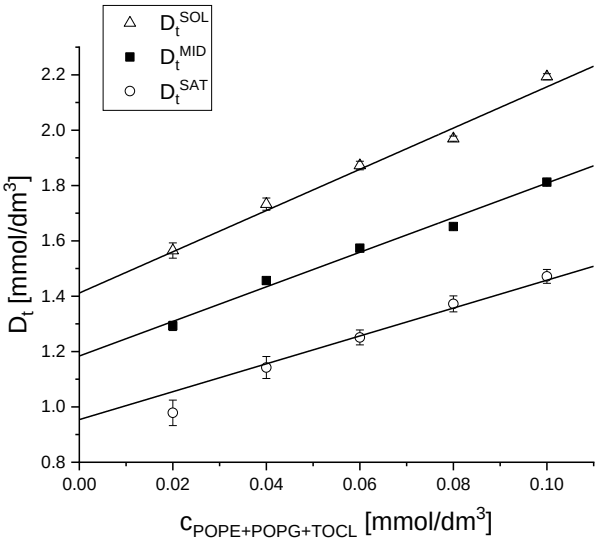

Figure 49: Global fit of the dependences of critical DDAO concentrations (D_t) on the concentration of lipid ($c_{POPE+POPG+TOCL}$).

Table 15 shows the effective molar ratio (R_e) and the concentration of DDAO in the water phase (D_w) for each particular step of the studied process. The partition coefficient of DDAO between POPE-POPG-TOCL model membrane and PBS buffer was calculated to be **6500 ± 500**.

Table 15: Effective ratio (R_e) of the amount of DDAO integrated into the bilayer to the amount of lipid ($n_{POPE+POPG+TOCL}$) and concentration of the monomeric surfactant in the water phase (D_w).

POPE-POPG-TOCL		
Critical concentration	**R_e**	**D_w [mmol/dm^3]**
D_t^{SAT}	5.04 ± 0.28	0.95 ± 0.12
D_t^{MID}	6.25 ± 0.33	1.18 ± 0.15
D_t^{SOL}	7.45 ± 0.37	1.41 ± 0.17

In conclusion, the solubilisation process induced by DDAO follows the same three-stage process for all model membranes studied in this thesis. When looked-upon closer, we can see some differences, mainly in the amount of DDAO needed to undergo the particular stages of the solubilisation process. We were able to calculate the partition coefficients of DDAO between the aqueous phase and lipid model membranes with various compositions. ***The partition coefficients calculated in this thesis were: 2300 ± 300 for POPC-CHOL, 4800 ± 500 for POPE-POPG and 6500 ± 500 for POPE-POPG-TOCL.*** In comparison with mammalian model membranes, the partition coefficients for the bacterial model membranes

are greater. On the other hand, the effective molar ratio (R_e) needed for complete solubilisation were 1.69 ± 0.22 for POPC-CHOL, 4.31 ± 0.47 for POPE-POPG and 7.45 ± 0.37 in case of POPE-POPG-TOCL. Our data show that the partitioning of DDAO is higher when interacting with bacterial model membranes and the bacterial model membranes need more incorporated surfactant to undergo solubilisation. This proves that DDAO destabilises the POPC-CHOL bilayer with more ease than POPE-POPG, with even more distinct difference when compared to POPE-POPG-TOCL. Multiple factors might cause such differences. As discussed earlier (in Chapter 4.2.3 Calcein leakage from bacterial model membranes), the ammonium group of PEs is able to form hydrogen bonds with adjacent molecules, thus strengthening the interlipid contacts, resulting in more resilient membrane. Presumably, the negative charge in the polar fragments of POPG and TOCL and their interaction with ions present in PBS buffer might also have an impact. Different geometry of the molecule might also be a contributing factor. PE molecules have a characteristic truncated cone shape because of their smaller polar fragment compared to the cross-section of their hydrocarbon chains. During the solubilisation of lipid bilayers by DDAO, aggregates with positive curvature are created, but PEs tend to form aggregates with negative curvature, due to their truncated cone shape. That being the case, more DDAO might be needed to disturb the POPE-POPG bilayer, compared to POPC-CHOL, to compensate for the curvature preference. The bacterial model membrane is also able to better compensate the mismatch in the length of the hydrocarbon chains of phospholipids and DDAO thanks to the *trans-gauche* isomerisation, which is suppressed in the case of the mammalian model membrane, due to the presence of cholesterol.

4.5 Small-angle neutron scattering

4.5.1 Mammalian model membranes

Using the small-angle neutron scattering (SANS), we studied the structure of DOPC-DDAO and DOPC-CHOL-DDAO aggregates in a D_2O-PBS. Despite the thorough extrusion of the MLLs dispersion (51 times through the 100 nm filter and 51 times through the 50 nm filter), all samples up to n_{DDAO}:n_{LIPID} = 1 show a noticeable correlation peak at q ~ 1 nm^{-1} (Figure 50).

The existence of the correlation peak indicates aggregation of ULLs or existence of oligolamellar structures. For this reason, a ***paracrystal lamellar stack model*** was chosen instead of a model of unilamellar liposomes. Detailed description of the model is in Chapter 3.5.3 Data treatment. This model determines the bilayer thickness (d_L), number of layers (N_L) and repeat spacing (d) from the scattering data. Example of the fitting is depicted in

Figure 50. The fitting model calculates from stack of lamellae infinite in the lateral dimension. Because our liposomes are not infinite in diameter, there is a small discrepancy between the fit and scattering data in the small q region.

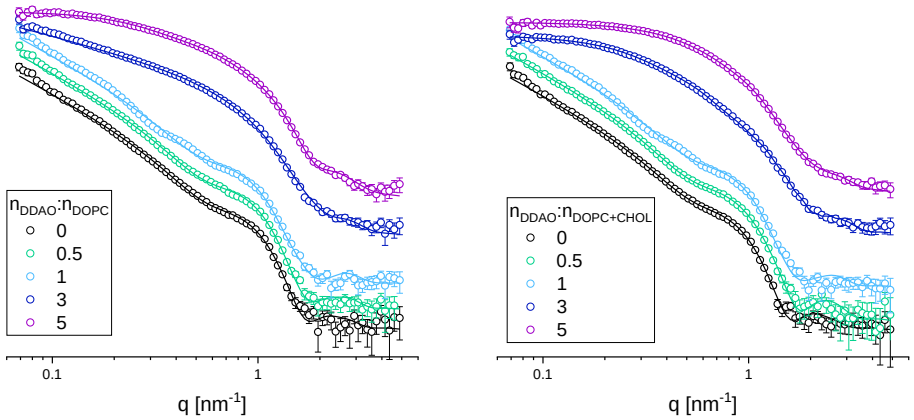

Figure 50: Scattering intensity I(q) as a function of the scattering vector q for samples containing DOPC (on the left) and DOPC-CHOL (on the right) and their mixtures with DDAO in various amounts (the legend depicts n_{DDAO}:n_{LIPID}). Fitting of scattering curves using the paracrystal lamellar stack model (n_{DDAO}:n_{LIPID} = 0, 0.5 and 1) and the model of elliptical cylinder (n_{DDAO}:n_{LIPID} = 3, 5). The scattering curves are shifted in vertical direction for better clarity.

The ***bilayer thickness*** was found to be d_L = 3.61 ± 0.02 nm for DOPC bilayer and d_L = 3.94 ± 0.02 nm for DOPC-CHOL bilayer. The increase in bilayer thickness after adding CHOL to DOPC bilayer is caused by increased acyl chain ordering. Similar increase was also observed by authors (Kučerka et al., 2007; Gallová et al., 2010b). Insertion of the DDAO molecules into the bilayer creates voids because of the mismatch of the chain lengths of DDAO and lipid molecules. This disturbs the chain packing and enables *trans-gauche* isomerisation of the hydrocarbon chains, resulting in a thinner membrane. We observed bilayer thickness decrease of 0.30 ± 0.04 for DOPC and 0.36 ± 0.04 for DOPC-CHOL at n_{DDAO}:n_{LIPID} = 1 for both types of phosphatidylcholine model membranes (Figure 51, on the left).

The ***repeat spacing*** was found to be d = 6.26 ± 0.03 nm for DOPC and d = 6.64 ± 0.03 nm for DOPC-CHOL. The higher value of repeat spacing of DOPC-CHOL is caused mainly by the higher bilayer thickness. Upon the addition of DDAO, we detected undistinguished changes in repeat spacing in samples n_{DDAO}:n_{LIPID} = 0 – 0.5, followed by an increase up to a value ~ 6.75 nm for n_{DDAO}:n_{LIPID} = 1 (Figure 51, on the right). Due to the small number of interacting bilayers, we do not consider this parameter to be sufficiently reliable.

Our results regarding the bilayer thickness and repeat spacing of DOPC coincide well with previous studies of (Nagle and Tristram-Nagle, 2000; Kučerka et al., 2005; Pullmannová et al., 2012), as well as the influence of DDAO on the DOPC bilayer thickness reported by (Bělička et al., 2014b).

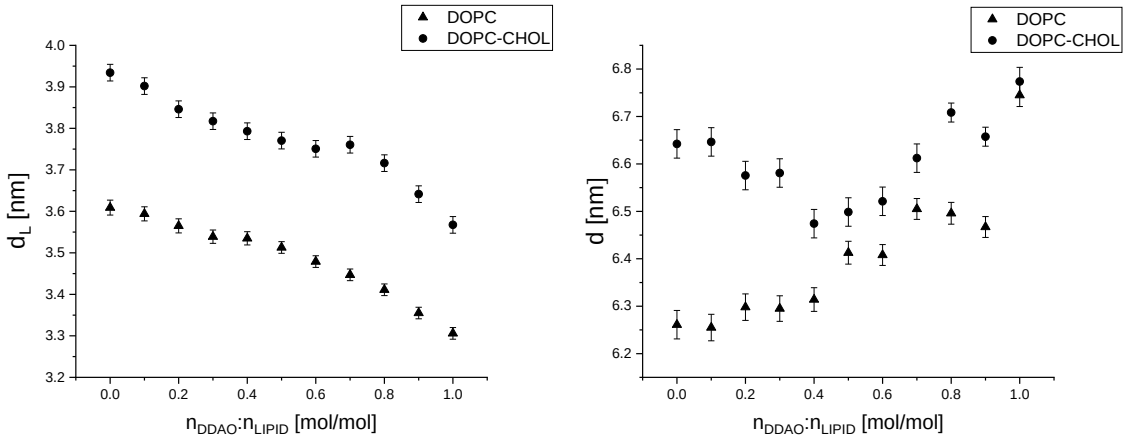

Figure 51: Bilayer thickness (d_L, on the left) and repeat spacing (d, on the right) of liposomes composed of DOPC and DOPC-CHOL as a function of the molar ratio n_{DDAO}:n_{LIPID}.

The ***correlation peak*** at q ~ 1 nm^{-1} (Figure 50) suggests the presence of aggregated ULLs or oligolamellar structures. N_L was around 1.4 for all DOPC and DOPC-CHOL samples up to molar ratio 0.9, and it decreased to approximately 1.35 for the last samples fitted with the paracrystal lamellar stack model (n_{DDAO}:n_{LIPID} = 1). According to the definition of this parameter (Equation 35), the value of 1.4 suggests that our sample consists of 60% unilamellar liposomes and 40% of oligolamellar liposomes with 2 bilayers on average.

We also studied samples of pure DOPC dispersed in ***different aqueous phase***: 1. 100% D_2O; 2. 150 $mmol/dm^3$ NaCl in D_2O; 3. 150 $mmol/dm^3$ NaCl in D_2O-PBS. The sample in D_2O showed a scattering curve typical for non-interacting ULLs 3 hours after the preparation, but showed an indication of interaction after 24 h with N_L being approximately 1.3. The samples prepared in 150 $mmol/dm^3$ NaCl in D_2O and D_2O-PBS both showed correlation peak at q ~ 1 nm^{-1} 3 h after preparation and the scattering curves did not change significantly after 24 h.

χ^2, representing the coincidence between the fit and the data was in the range 2–3 at low DDAO concentration. The agreement increased for samples n_{DDAO}:$n_{LIPID} \geq 0.7$ and the lamellar paracrystal model was no longer suitable for samples n_{DDAO}:$n_{LIPID} > 1$.

We were not able to fit the sample n_{DDAO}:n_{DOPC} and n_{DDAO}:$n_{DOPC+CHOL}$ = 2 by neither of the two fitting models and were not analysed further. This probably occurred because at

this molar ratio a liposome-micelle transition occurred, during which a complex mixture of mixed micelles are present, as well as remaining surfactant-saturated bilayers and surfactant monomers. Using the Equation 25 (p. 50), we can calculate the effective molar ratio (R_e) of DDAO in DOPC-CHOL bilayer in this sample. Sample composition is known – total DDAO concentration (D_t = 17.8 mmol/dm^3) and concentration of lipid (c_L = 8.9 mmol/dm^3) and the values of ρ_b/M_L = 1543 mmol/dm^3 and K_p = 2092 ± 594 were taken from (Želinská et al., 2020). The calculated R_e value for the sample n_{DDAO}:$n_{DOPC+CHOL}$ = 2 is 1.85 ± 0.04, which is very close to the effective molar ratio of DDAO at the midpoint of the solubilisation sigmoid fit (R_e^{MID} = 1.82 ± 0.31) as was reported in (Želinská et al., 2020). This corresponds well with our assumption.

Elliptical cylinder model was used to fit the scattering curves in the range n_{DDAO}:n_{LIPID} = 3–5. Detailed description of the model is in Chapter 3.5.3 Data treatment. This model determines the minor radius of the elliptical cross-section (r_{minor}), axial ratio of the ellipse ($\nu = r_{major}/r_{minor}$) and the length of the rigid cylinder (L) from the scattering data. An example of the fitting is depicted in Figure 50. The acquired parameters are presented in Table 16. Small values of χ^2 indicate high agreement of the fits and the scattering curves.

Table 16: Parameters of the cylindrical DOPC-DDAO and DOPC-CHOL-DDAO aggregates with elliptical cross section detected at high concentrations of DDAO.

	n_{DDAO}:n_{LIPID} [mol/mol]	r_{minor} [nm]	ν	L [nm]	χ^2
DOPC	3	1.76 ± 0.01	1.79 ± 0.02	521.33 ± 75.41	3.66
	4	1.67 ± 0.01	1.67 ± 0.02	34.38 ± 1.56	1.38
	5	1.67 ± 0.01	1.55 ± 0.02	18.76 ± 0.30	1.19
DOPC-CHOL	3	1.77 ± 0.01	2.87 ± 0.03	19.73 ± 0.30	1.94
	4	1.77 ± 0.01	2.04 ± 0.02	13.13 ± 0.14	1.65
	5	1.79 ± 0.01	1.70 ± 0.03	10.23 ± 0.10	0.63

r_{minor} – minor radius of the ellipse, ν – axial ratio of the ellipse, L – the length of the cylinder, χ^2 characterises the agreement of the fit with experimental data

The cross-sectional dimensions of the ***DOPC-DDAO*** elliptical cylinders with the lowest amount of DDAO (n_{DDAO}:n_{DOPC} = 3) were $2r_{minor}$ = 3.52 ± 0.02 nm and $2r_{major}$ = 6.30 ± 0.02 nm. The former dimension of the cross section is similar to the thickness of DOPC-DDAO bilayer, which suggests that the central part of the cylinder is formed by DOPC-DDAO mixed bilayer that is stabilised by a DDAO-rich rim, as illustrated in Figure 52.

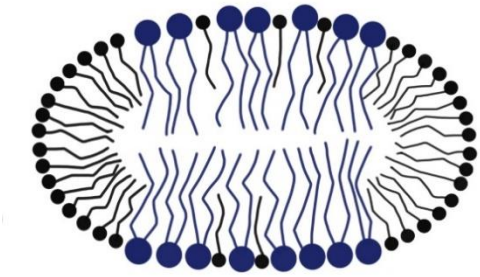

Figure 52: Schematic representation of the elliptical cross section of DOPC-DDAO cylinder. DOPC (two chains), DDAO (single chain)

Similar results were observed with the ***DOPC-CHOL-DDAO*** cylinders, with some of the geometrical parameters being different. The dimensions of the cross section of cylinders with lowest amount of DDAO (n_{DDAO}:$n_{DOPC+CHOL}$ = 3) were found to be 3.54 ± 0.02 nm and 10.16 ± 0.02 nm. The former value is similar to that of DOPC-DDAO, but the later value suggests the ellipse is more prolonged in the direction of the major axis. On the other hand, the DOPC-CHOL-DDAO cylinders were found to be shorter than the DOPC-DDAO ones.

As far as the ***length of the cylinders*** is concerned, it decreased with increasing amount of DDAO for both DOPC-DDAO and DOPC-CHOL-DDAO cylinders (Table 16). The ratio of elliptical radii also decreased with increasing DDAO concentration. If this decrease continued upon further addition of DDAO, this could eventually lead into the formation of round mixed micelles. These findings are in good agreement with the previous study of (Uhríková et al., 2001), where DOPC aggregates up to n_{DDAO}:n_{DOPC} = 1.5 were identified as bilayers/bilayer fragments, rod-like particles were observed within the molar ratios of n_{DDAO}:n_{DOPC} = 2.5–3.5, followed by transition into globular particles at n_{DDAO}:n_{DOPC} > 4. Lichtenberg et al. (2013b) claim that the largest mixed micelles forming during the liposome/micelle phase transition are long thread-like structures that are decreasing in length with increasing surfactant concentration. This is supported by our data, in case of our model systems we managed to identify these thread-like structures as cylinders with elliptical cross section. A theoretical analysis of Fattal et al. (1995) and Kozlov et al. (1997) also suggested that cylindrical micelles are the most probable aggregates arising from phospholipid bilayer interacting with micelle-forming surfactants. Edwards and Almgren (1991) observed cylindrical micelles coexisting with bilayer sheets in a system of EYPC and non-ionic surfactant $C_{12}E_8$. Cylindrical aggregates with elliptical cross-section were also theoretically predicted by Goltsov and Barsukov (2000) and later experimentally observed by Kiselev et al. (2008) in a mixture of dimyristoylphosphatidylcholine (DMPC) and surfactant sodium cholate.

4.5.2 Bacterial model membrane

Using the small-angle neutron scattering (SANS), we studied the structure of POPE-POPG-DDAO aggregates in a D_2O-PBS. All samples up to $n_{DDAO}:n_{POPE+POPG} = 1$ show a noticeable correlation peak at q ~ 1 nm^{-1} (Figure 53), just as it was observed with the mammalian model membranes.

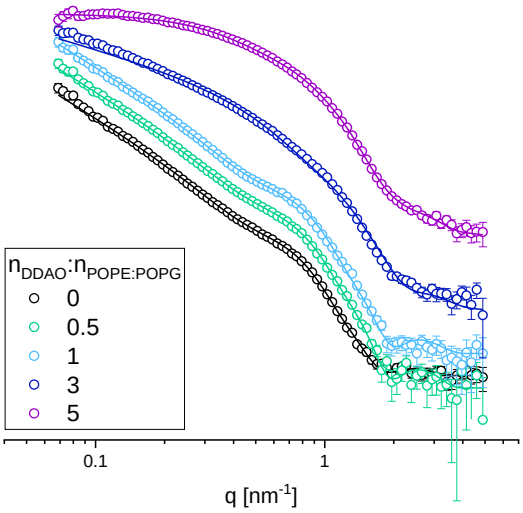

Figure 53: Scattering intensity I(q) as a function of the scattering vector q for samples containing POPE-POPG and its mixtures with DDAO in various amounts (the legend depicts $n_{DDAO}:n_{LIPID}$). Fitting of scattering curves using the paracrystal lamellar stack model ($n_{DDAO}:n_{LIPID}$ = 0, 0.5 and 1) and the model of elliptical cylinder ($n_{DDAO}:n_{LIPID}$ = 3, 5). The scattering curves are shifted in vertical direction for better clarity.

The samples with molar ratios up to $n_{DDAO}:n_{POPE+POPG} = 2$ were fitted with the ***paracrystal lamellar stack model***. The agreement between the fits and the scattering curves, expressed as χ^2, was approximately 1 for all the fits, confirming the suitability of the model for our samples.

The ***bilayer thickness*** was found to be 3.47 ± 0.02 nm for pure POPE-POPG membrane and it decreased to a value of 3.27 ± 0.02 nm at $n_{DDAO}:n_{POPE+POPG} = 1$. The decrease in bilayer thickness, 0.21 ± 0.04 nm, was lower than that observed for both of the mammalian models (0.30 ± 0.04 for DOPC and 0.36 ± 0.04 for DOPC-CHOL) The change in the bilayer thickness correlates with the magnitude of the defect that DDAO causes in the bilayer. This defect being larger in the mammalian model membrane than the bacterial one corresponds well with the findings from the solubilisation and fluorescent probe leakage experiments.

The ***repeat spacing*** has reached 8.18 ± 0.05 nm for neat POPE-POPG bilayer. Higher value of repeat spacing was probably influenced by the negative charge of POPG molecules, resulting in repulsive forces between the individual liposomes. Due to the small number of interacting bilayers, we do not consider this parameter to be sufficiently reliable.

The electrostatic repulsion probably also influenced the lower value of N_L, which was stable for samples up to $n_{DDAO}:n_{POPE+POPG} = 1$, with the value being ~ 1.2. This means, only approximately 20% of the liposomes were oligolamellar with 2 bilayers on the average. For the last sample fitted with the model ($n_{DDAO}:n_{POPE+POPG} = 2$), the value of N_L dropped to 1.0.

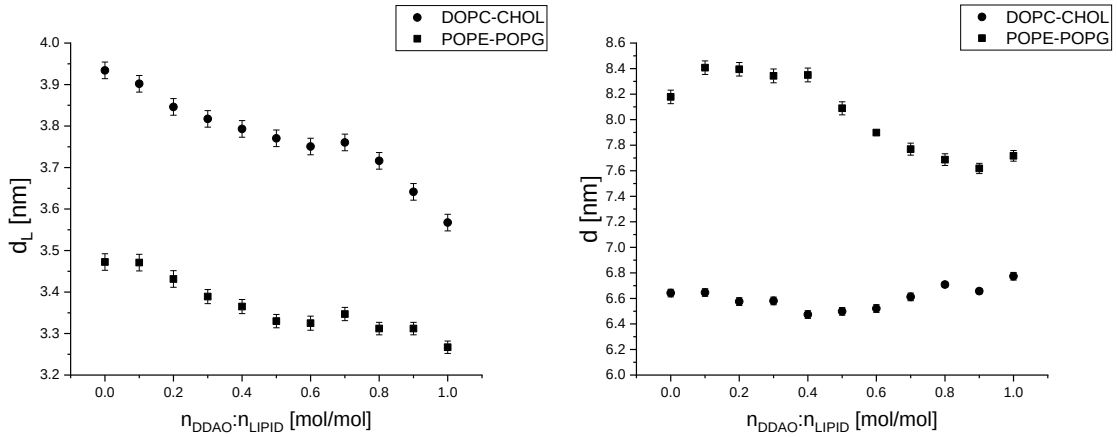

Figure 54: Comparison of the changes in bilayer thickness (d_L, on the left) and repeat spacing (d, on the right) of liposomes composed of DOPC-CHOL and POPE-POPG plotted as a function of increasing molar ratio $n_{DDAO}:n_{LIPID}$.

Elliptical cylinder model was used to fit the scattering curves in the range $n_{DDAO}:n_{POPE+POPG} = 3–6$. The results of these fits are displayed in Table 17.

Using the Equation 25 (p. 50), we can calculate the effective molar ratio (R_e) of DDAO in POPE-POPG bilayer in the sample with $n_{DDAO}:n_{POPE+POPG} = 3$, using the values of $\rho_b/M_L = 1405$ mmol/dm^3 and $K_p = 4800 \pm 500$ (from Chapter 4.4 Partition coefficients) and the known concentrations of lipid and DDAO in this sample. The calculated R_e value is 2.9 ± 0.01, which is close to the value of the effective molar ratio of DDAO at the saturation point (from static light scattering data), $R_e^{SAT} = 3.09 \pm 0.36$. Such proximity to the saturation point might explain higher values of χ^2 for this sample.

Table 17: Parameters of the cylindrical POPE-POPG-DDAO aggregates with elliptical cross section detected at high concentrations of DDAO.

	$n_{DDAO}:n_{LIPID}$ [mol/mol]	r_{minor} [nm]	ν	L [nm]	χ^2
POPE-POPG	3	1.56 ± 0.01	3.19 ± 0.03	191.41 ± 80.30	10.20
	4	1.69 ± 0.01	2.10 ± 0.02	21.09 ± 0.40	2.63
	5	1.74 ± 0.01	1.63 ± 0.02	14.24 ± 0.16	1.38
	6	1.77 ± 0.01	1.49 ± 0.02	10.44 ± 0.09	1.94

r_{minor} – minor radius of the ellipse, ν – axial ratio of the ellipse, L – the length of the cylinder, χ^2 characterises the agreement of the fit with experimental data

The dimensions of the elliptical cross section of the sample with the lowest amount of DDAO ($n_{DDAO}:n_{POPE+POPG}$ = 3) were 3.12 ± 0.02 nm and 9.98 ± 0.02 nm. The former value is similar to the thickness of the POPE-POPG-DDAO bilayer before the liposome-cylinder transition (~ 3 nm). The dimensions are very similar to those observed for DOPC-CHOL-DDAO cylinder with the same molar ratio of $n_{DDAO}:n_{LIPID}$ (3.54 ± 0.02 nm and 10.16 ± 0.02 nm). The changes to the geometrical parameters upon further addition of DDAO were also very reminiscent of the DOPC-CHOL model. Figure 55 shows the comparison of the minor and major radius of the ellipses of DOPC-CHOL-DDAO and POPE-POPG-DDAO cylinders.

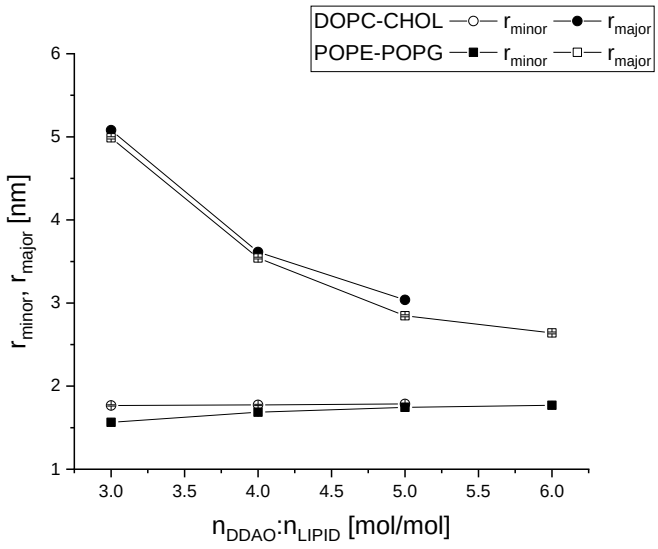

Figure 55: Comparison of the minor (r_{minor}) and major (r_{major}) radius of the ellipse in DOPC-CHOL and POPE-POPG samples fitted with the model of elliptical cylinder.

As observed for mammalian model membranes, the increase in DDAO concentration also caused shortening of POPE-POPG-DDAO cylinders. Therefore, we propose that the solubilisation of our bacterial and mammalian models proceeds in a similar way. The

noticeable difference is that the POPE-POPG liposomes needed more DDAO to undergo those changes (the samples were fitted up to the molar ratio $n_{DDAO}:n_{POPE+POPG} = 2$ using lamellar paracrystal stack model, as opposed to the mammalian model membranes, that could not be fitted with either of the fitting functions at this molar ratio, because of undergoing liposome-micelle transformation), which is consistent with our previous data acquired using nephelometry.

The research involving bacterial model membranes and their interaction with surfactants is mostly oriented on the reconstitution and purification of membrane proteins. The current knowledge on the changes that the lipid part of the membrane goes through during the solubilisation process is not well documented in the literature.

Our SANS experiments have proven that during the solubilisation process induced by DDAO, similar types of aggregates are formed for our mammalian and bacterial model membranes. We observed the transition from lamellar arrangement to cylinders with elliptical cross section. With increasing amount of DDAO, the cylinders become shorter and the difference between the dimensions of the cross-sectional axes is decreasing. SANS results have also shown that the defect in the bilayer caused by the DDAO is larger in case of the mammalian model membrane, as manifested by the change in the bilayer thickness between the neat membrane and the sample with equimolar ratio of DDAO:lipid, which is 0.36 ± 0.04 nm for DOPC-CHOL, in comparison with the bacterial model membrane 0.21 ± 0.04 nm for POPE-POPG. It is in agreement with our solubilisation and fluorescent probe leakage experiments.

4.6 Small-angle neutron diffraction

Using the small-angle neutron diffraction (SAND), we studied the structural properties of bilayer stacks with compositions mimicking mammalian and bacterial membranes. At first, the swelling method was used when measuring lipid membranes without any additives (POPC, POPC-CHOL, POPE-POPG) to analyse the molecular organisation and periodicity as a function of hydration with the intention to reconstruct the neutron scattering length density profiles.

4.6.1 Swelling experiments

4.6.1.1 Mammalian model membranes

The whole procedure regarding the preparation, measuring and evaluation of the data is described in detail in Chapter 3.6 Small-angle neutron diffraction. The samples were

measured at 5 different relative humidities. Figure 56 shows the changes in the repeat spacing for data measured at different RH for POPC (on the left) and POPC-CHOL (on the right).

In case of POPC, negligible changes were observed in the range from 95 – 50% RH. At the lowest humidity (30% RH), a rapid increase in d was observed, which was caused by a phase transition from liquid-crystalline phase (L_α) to a gel phase (L_β). The larger repeat spacing is caused by the hydrocarbon chains being more straightened in the gel phase, resulting in a thicker membrane. Similar transition was observed for a deuterated analogue of POPC by the authors (Binder and Gawrisch, 2001).

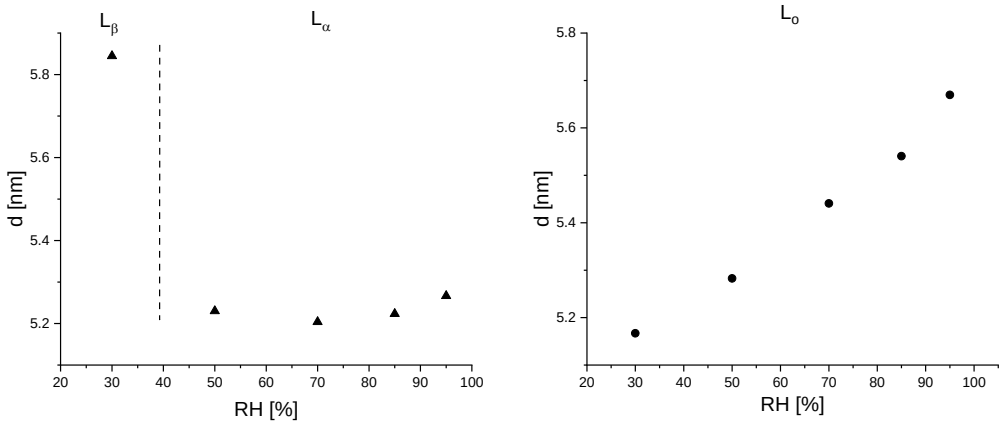

Figure 56: Repeat spacing as a function of RH – POPC (on the left) and POPC-CHOL (on the right). The type of lamellar phase is indicated on top. Dashed line signifies a phase transition.

From our results we assume that the POPC-CHOL (33 mol% of CHOL) mixture created well-organised (given by up to 8 observed diffraction peaks) liquid-ordered phase (L_o), which was stable in the whole range of studied RH. No additional phases occurred. Figure 56 shows that the decrease in the RH is accompanied by decreasing values of the repeat spacing d. This was most probably caused by the reduction of the water layer thickness between the particular bilayers in a stack.

4.6.1.2 Bacterial model membrane

The same procedures were followed with the bacterial type of model membrane, POPE-POPG. Figure 57 shows the results of the swelling experiment with POPE-POPG sample.

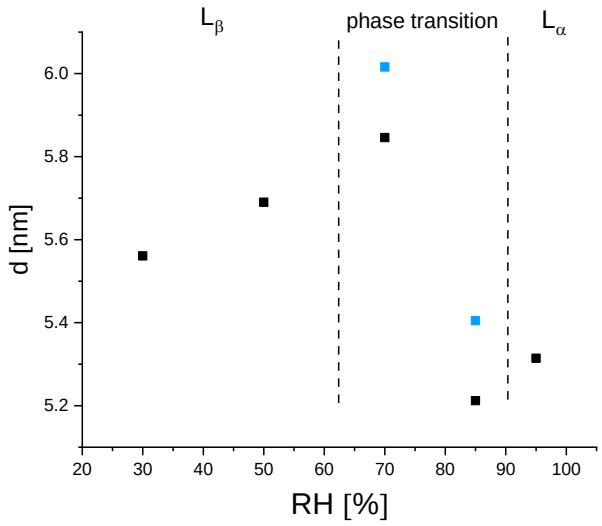

Figure 57: Dependence of repeat spacing d of POPE-POPG bilayer stacks on the RH in the humidity chamber. The type of lamellar phase is indicated on top. Blue points signify an additional phase that appeared during the transition.

On the dependence of repeat spacing on the relative humidity we can see a phase transition from liquid-crystalline phase (L_α), that was present at 95% RH to the gel phase (L_β) at 30% and 50% RH. During the phase transition, an additional lamellar phase appeared, characterised by a larger value of repeat spacing (blue points). In the liquid-crystalline phase, this sample showed only 4 diffraction orders. At RH 30% – 70% we collected up to 8 diffraction orders, which confirms the formation of a gel phase with higher ordering. Because of the phase transition, and the additional phase that appeared, we would not be able to calculate the NSLD profiles using this method. Therefore, we have decided to continue our experiments with the contrast variation technique instead.

4.6.2 Contrast variation experiments

4.6.2.1 Experiments with DDAO

Mammalian model membrane

Up to eight diffraction orders were obtained for the POPC-CHOL and POPC-CHOL-DDAO samples and different conditions, suggesting a well-organised stack of bilayers. Upon the addition of DDAO, the number of Bragg peaks decreased to no less than 4 peaks for the sample with the highest amount of DDAO. This was to be expected since the DDAO is a membrane-disrupting surfactant. The NSLD profiles were reconstructed as described in Chapter 3.6.4 Neutron scattering length density profiles. Table 18 shows the results obtained from the NSLD profiles analysis. Sample containing n_{NaCl}:$n_{POPC+CHOL}$ = 1 was also

measured, but showed only 2 Bragg peaks (d = 7.14 nm), so we were not able to proceed with NSLD profile calculation.

Table 18: Parameters calculated from POPC-CHOL and POPC-CHOL-DDAO bilayer stacks at 25°C and 97 % RH.

n_{DDAO}: $n_{POPC+CHOL}$	d [nm]	d_b [nm]	A_L [nm^2]	d_w [nm]	σ [nm]
0	5.71	3.67	0.58	2.04	0.47
0.2	5.54	3.55	0.65	1.99	0.51
0.5	5.30	3.39	0.75	1.91	0.50
1	5.03	3.04	0.99	1.99	0.47

d – repeat spacing, d_b – bilayer thickness, A_L – area per lipid, d_w – water layer thickness, σ – width of the lipid/water interface.

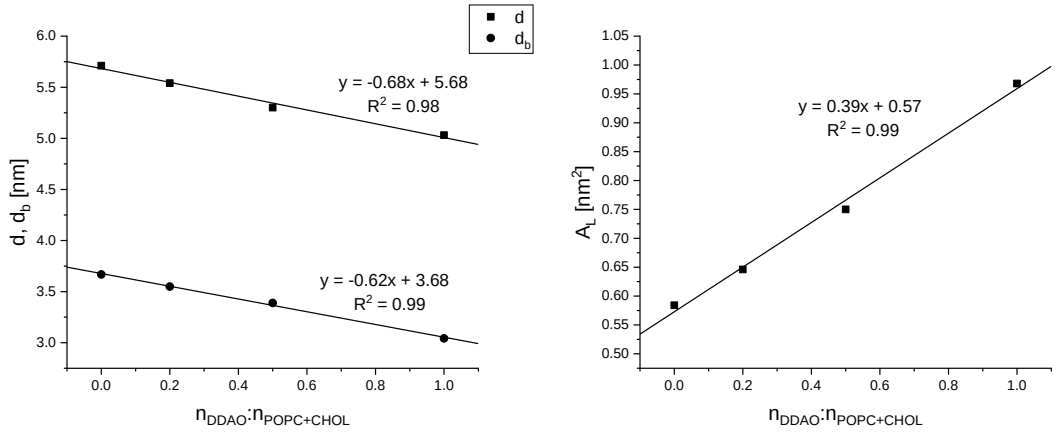

Figure 58: Dependences of repeat spacing d, bilayer thickness d_b (on the left) and area per lipid (on the right) on the amount of added DDAO in POPC-CHOL model membrane.

The ***repeat spacing*** of POPC-CHOL bilayer stack obtained at 97% RH was 5.71 nm. The values of repeat spacings of our POPC-CHOL samples measured in the form of bilayer stacks are lower when compared to repeat spacing of the DOPC-CHOL liposomes obtained from SANS (6.64 ± 0.03 nm). Even though the relative humidity was 97%, the water layer thickness is significantly smaller in comparison with hydration in bulk water phase.

The repeat spacing decreased to the value of 5.03 nm for equimolar mixture with DDAO. As can be seen in Figure 58 (on the left), the repeat spacing and the bilayer thickness decreased with increasing amount of DDAO similarly, suggesting a constant interlipid water layer. Since the repeat spacing is the sum of the water layer and bilayer thickness, the decrease in repeat spacing was caused by the decrease in the bilayer thickness. The differences in repeat spacing of the particular samples measured in different contrasts did not exceed 0.1 nm, suggesting the samples had sufficient time to reach hydration equilibrium.

The ***bilayer thickness*** of POPC-CHOL membrane was found to be 3.67 nm. As observed with our SANS data, DDAO caused decrease in the thickness of the bilayer. The reason is that the difference in the size of lipids compared to DDAO leads to creation of free space in the hydrophobic region, giving more space for *trans-gauche* isomerisation of the chains which lowers their length. From our SANS experiment, equimolar ratio of DDAO:DOPC-CHOL caused decrease in the bilayer thickness by 0.36 nm. From the SAND data, the difference in the bilayer thickness between POPC-CHOL and its equimolar mixture with DDAO was slightly bigger, 0.63 nm.

The ***area per lipid*** was reported to be 0.45 ± 0.01 nm^2 for equimolar mixture of POPC-CHOL and 0.60 ± 0.04 nm^2 for pure POPC by (Leftin et al., 2014). (Kučerka et al., 2011) reported the area per lipid of POPC 0.64 nm^2. The value we obtained for POPC-CHOL (2:1 mol/mol), 0.58 nm^2, fits reasonably with the previous findings. It is well known that CHOL in PC bilayers lowers the *trans-gauche* isomerization of the hydrocarbon chains, causing them to straighten up, which enables more compressed packing in the lateral direction.

Incorporating DDAO into the POPC-CHOL bilayer caused a linear increase (Figure 58, on the right) in area per lipid up to the value of 0.97 nm^2 for the highest DDAO content studied in this thesis. Belička et al. (2014b) calculated a partial lateral molecular area of DDAO in DOPC bilayer to be 0.36 nm^2. The authors suggest that the area per lipid is

$$A_L = A_{POPC-CHOL} + n_{DDAO}: n_{POPC-CHOL} \cdot A_{DDAO} \qquad 58$$

so, from the slope of the dependence $A_L = f(n_{DDAO}: n_{POPC-CHOL})$ in the Figure 58, we can obtain the area per DDAO molecule 0.39 nm^2. Despite the difference in hydration (97% RH in our case), the area per DDAO is very similar to that of Belička et al. (2014b), which was obtained from sample in bulk water.

Figure 59 shows the ***probability of water distribution*** acquired as described in Chapter 3.6.4 Neutron scattering length density profiles, with z = 0 nm being the centre of the bilayer. The calculated water distribution probability reach values from zero (no water) to a value very close to one (pure water). The water layer thickness (d_w) was around 2 nm for all the samples (Table 18). The width of the lipid/water interface (σ) also did not change significantly upon the addition of DDAO, and stayed at a value ~ 0.5 nm. So, the shifting of the water probability that we see with increasing amount of DDAO in Figure 59 is simply caused by the decrease in the thickness of the bilayer.

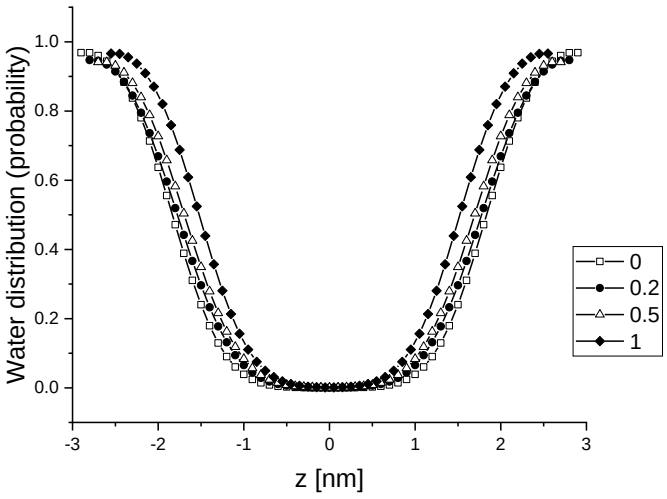

Figure 59: Probability of water distribution for POPC-CHOL samples with DDAO in molar ratios n_{DDAO}:$n_{POPC+CHOL}$ = 0; 0.2; 0.5 and 1.

Bacterial model membrane

We obtained up to five diffraction orders for the POPE-POPG and POPE-POPG-DDAO samples, proving well-organised bilayer stack. No less than four diffraction orders were detected even for the sample with highest amount of DDAO. Unfortunately, we were not able to reconstruct the NSLD profile for the neat POPE-POPG sample, due to the problem with stability of the sample. The sample containing n_{NaCl}:$n_{POPE+POPG}$ = 1 showed 5 diffraction orders.

Because we were not able to reconstruct the NSLD profile for neat membrane, we added the results from the sample containing NaCl, where we were able to do so. The results of the NSLD profile analysis of our bacterial model membrane samples are shown in Table 19.

Table 19: Parameters calculated from POPE-POPG and POPE-POPG-DDAO bilayer stacks at 25°C and 97 % RH. 0 (+NaCl) is the sample with n_{NaCl}:$n_{POPE+POPG}$ = 1.

$\mathbf{n_{DDAO}}$: $\mathbf{n_{POPE+POPG}}$	**d [nm]**	$\mathbf{d_b}$ **[nm]**	$\mathbf{A_L}$ **[nm^2]**	$\mathbf{d_w}$ **[nm]**	**σ [nm]**
0	5.30	-	-	-	-
0 (+NaCl)	5.60	3.62	0.68	1.98	0.45
0.2	5.11	3.37	0.77	1.74	0.45
0.5	4.95	3.13	0.90	1.83	0.51
1	4.70	2.87	1.11	1.83	0.42

d – repeat spacing, d_b – bilayer thickness, A_L – area per lipid, d_w – water layer thickness, σ – width of the lipid/water interface.

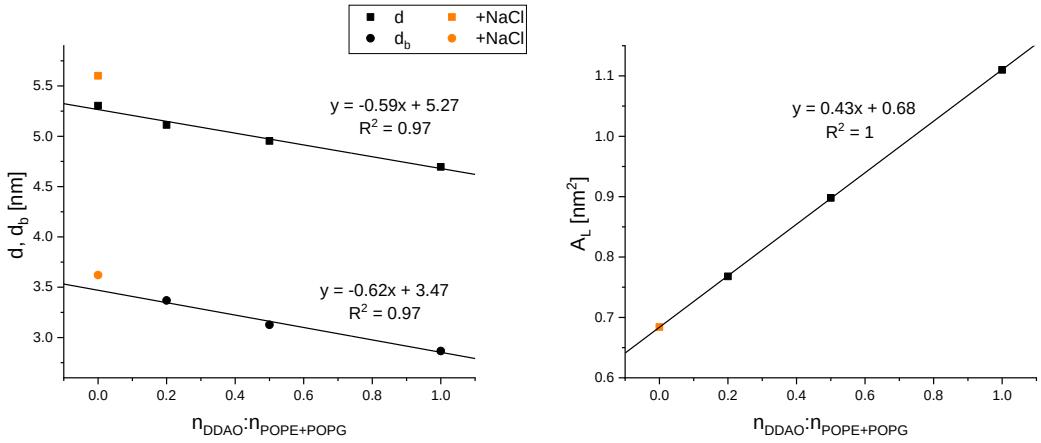

Figure 60: Dependences of repeat spacing d, bilayer thickness d_b (on the left) and area per lipid (on the right) on the amount of added DDAO in POPE-POPG model membrane. The orange points signify the sample with added NaCl, which was excluded from the fitting.

The ***repeat spacing*** of neat POPE-POPG sample was 5.3 nm. The difference in repeat spacing obtained from POPE-POPG OLLs measured using SANS (8.18 ± 0.05 nm) and repeat spacing of SAND samples is even bigger than we reported for the mammalian model membranes, because the negative charge of POPG influences the water layer thickness even more at full hydration. The repeat spacing of POPE-POPG membrane slightly increased to 5.6 nm when NaCl was added to the neat membrane (n_{NaCl}:$n_{POPE+POPG}$ = 1).

Natural and model bacterial membranes were studied previously by (Sebastiani et al., 2012) using the SAND method. The authors have used *Bacillus subtilis* lipid extract and a mixture of lipids mimicking its composition (40% POPE, 20% POPG, 40% CL), as well as pure POPE and POPG. They obtained two Bragg peaks for the synthetic samples and only the first order (d = 11 nm) for the natural one. The pure POPG sample showed a drastic increase in the repeat spacing (from ~5.2 nm to ~7.7 nm) when the RH changed from 92.5% to close to 95% due to electrostatic repulsion. In a small-angle X-ray diffraction study (with liposomes in bulk water) by Pozo Navas et al. (2005), the authors reported increase in repeat spacing from 6.22 nm for pure POPE to 11.3 nm for POPE-POPG sample with X_{POPG} = 0.1. Upon further increase in the amount of POPG, the repeat spacing reached a value of ~ 13 nm at X_{POPG} = 0.4 (our composition). Introducing just a small amount of charged POPG into the MLLs had a significant effect on the repeat spacing in solution. In our case, the bilayer stack of POPE-POPG (X_{POPG} = 0.4) measured at 97% RH was stable with repeat spacing 5.3 nm (averaged for all contrasts). Unfortunately, we were not able to calculate the NSLD profiles, because before the measurement in the last contrast, the sample got equilibrated to 99% RH, which unbeknownst to us at the time probably caused swelling to the point where the bilayers moved on the wafer due to gravitation. We have still observed diffraction, but the integrated intensity was very low, meaning we could not proceed to calculate the NSLD

profiles for this sample. Fortunately, we have measured a sample with the same composition of POPE-POPG, just with added NaCl (n_{NaCl}:$n_{POPE+POPG}$ = 1), without DDAO.

The ***bilayer thickness*** of our POPE-POPG-NaCl sample was 3.62 nm. The thickness of the POPE-POPG bilayer obtained from our SANS experiment was 3.47 ± 0.02 nm. This corresponds well with the theoretical value of POPE-POPG bilayer that can be obtained from our linear dependence in Figure 60 (on the left). The experimentally acquired equation $d_b = -0.62 \times n_{DDAO}: n_{POPE+POPG} + 3.47$, gives us the bilayer thickness value of 3.47 nm if $n_{DDAO}: n_{POPE+POPG} = 0$.

We found the ***area per lipid*** 0.68 nm^2 for the POPE-POPG-NaCl sample. A molecular dynamics simulation of POPE-POPG in a molar ratio 3:1 (ours is 3:2) revealed an area per lipid of 0.58 nm^2. Pure POPE occupies 0.56 nm^2 according to studies of (Rand et al., 1988; Skjevik et al., 2016) and area per POPG lipid was reported to be ~ 0.67 nm^2 (Skjevik et al., 2016; Kučerka et al., 2012). In the study of (Kučerka et al., 2021), it was reported that the presence of divalent cations increased the repeat spacing of DOPC bilayer stack, had thickening effect on the bilayer, as well as tightening and condensing effect in the lateral dimension. Even though an increase in the repeat spacing was observed when comparing the sample with and without added NaCl, our monovalent cation seemed to have no effect on the lateral separation of the lipids, as the area per lipid fits perfectly with the other data (Figure 60, on the right).

Incorporating DDAO into the POPE-POPG bilayer caused a linear increase (Figure 60, on the right) in area per lipid up to the value of 1.11 nm^2 for the highest DDAO content. Similarly, as in the case of the mammalian model membrane, we can calculate the area per DDAO molecule from the slope of the dependence $A_L = f(n_{DDAO}: n_{POPE-POPG})$ in Figure 60:

$$A_L = A_{POPE-POPG} + n_{DDAO}: n_{POPE-POPG} \cdot A_{DDAO} \qquad 59$$

A_{DDAO} = 0.43 nm^2, which does not significantly differ compared to the area per DDAO molecule in POPC-CHOL (0.39 nm^2).

The linear increase was very similar for both the mammalian and bacterial model, even though the area per lipid of the neat bacterial model was higher (by 0.1 nm^2).

The ***probability of water distribution*** is shown in the Figure 61. The water layer thickness (d_w) was slightly below 2 nm for all the samples (Table 19). The width of the lipid/water interface (σ) also did not change significantly upon the addition of DDAO, and stayed at a value ~ 0.45 nm. Therefore, we assume the shifting of the water distribution probability that we see with increasing amount of DDAO in Figure 61 is simply caused by the decrease in the thickness of the bilayer. Similar results were reported for the mammalian model (POPC-CHOL).

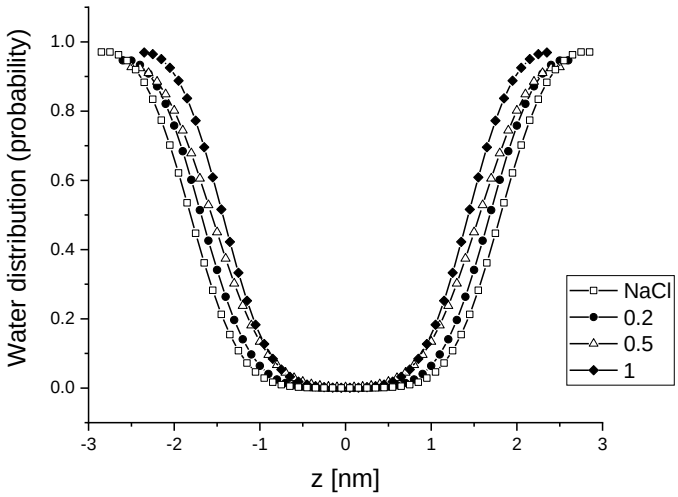

Figure 61: Probability of water distribution for POPE-POPG samples with NaCl (empty squares) and DDAO in molar ratios n_{DDAO}:$n_{POPE+POPG}$ = 0.2; 0.5 and 1.

4.6.2.2 Experiments with DS1

Samples containing partially deuterated phospholipids, dPOPC-CHOL and dPOPE-dPOPG, and their mixture with the antimicrobial peptide dermaseptin S1 (DS1) were measured following procedures identical to the non-deuterated lipids. For these samples, 4 different H_2O/D_2O contrasts were used (8%, 40%, 70% and 100% D_2O). Figure 62 shows the repeat spacing for the dPOPC-CHOL-DS1 samples (on the left) and dPOPE-dPOPG-DS1 samples (on the right).

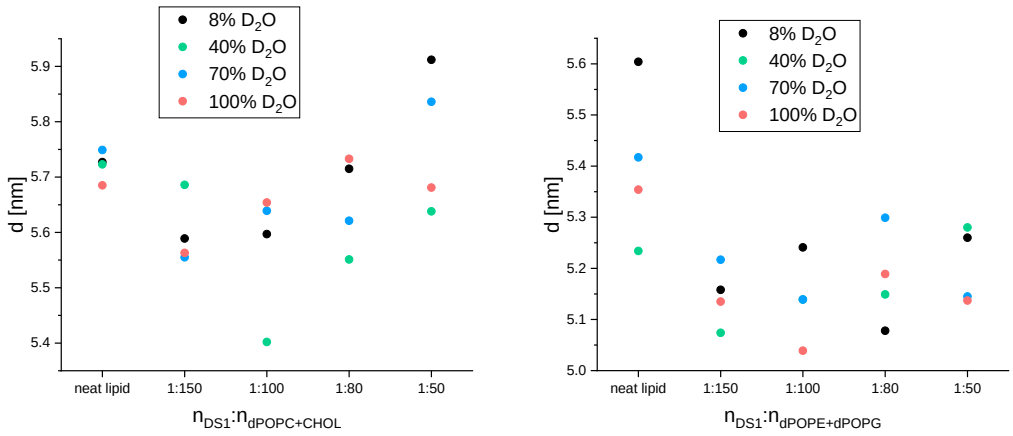

Figure 62: Repeat spacing (d) of samples containing dPOPC-CHOL (on the left) and dPOPE-dPOPG (on the right) and their mixture with DS1 in multiple molar ratios and different contrasts.

We observed unexplainable differences in repeat spacings larger than 0.1 nm between the particular contrasts for most of the samples (except for dPOPC-CHOL). We are unaware of what might have caused these differences, as identical preparation procedures and measurement techniques were employed for all samples, and yet this issue did not occur with the non-deuterated samples. Because of this, we were not able to continue with the calculation of NSLD profiles, with the exception of sample with neat dPOPC-CHOL.

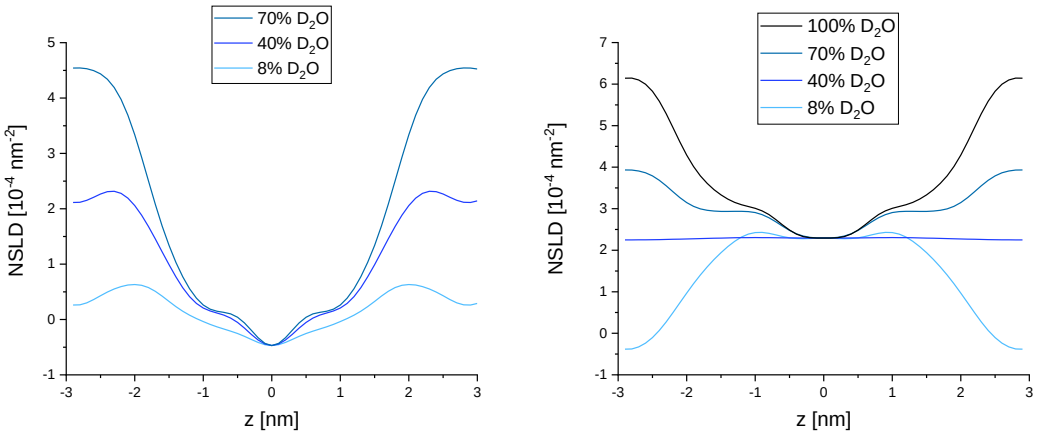

Figure 63: NSLD profiles of POPC-CHOL (on the left) and dPOPC-CHOL (on the right).

Figure 63 shows the NSLD profiles calculated from diffraction data of POPC-CHOL (on the left) and its partially deuterated variant dPOPC-CHOL (on the right). As we can see, the NSLD at the centre of the dPOPC-CHOL bilayer (z = 0 nm), does not acquire negative values (as can be seen on the POPC-CHOL profile), because the SLD of a -CH_3 and -CD_3 group together has a theoretical value of 2.29×10^{-4} nm^{-2}. This is very close to the SLD of 40% D_2O (2.22×10^{-4} nm^{-2}), which is why the profile of the membrane at this contrast is not very pronounced. The SLD of 8% D_2O is close to zero, therefore the profile of the membrane obtained at 8% D_2O contrast seems to be "inverted", if compared to that of POPC-CHOL.

The repeat spacing (averaged across all contrasts) for neat dPOPC-CHOL sample was 5.73 nm, nearly identical to that of its protonated equivalent, POPC-CHOL. Other parameters obtained from the analysis of NSLD profile are also very similar (Table 20). Figure 64 shows that the water distribution probability is also identical for POPC-CHOL and dPOPC-CHOL, despite their different NSLD profiles.

Table 20: Parameters calculated from POPC-CHOL and dPOPC-CHOL bilayer stacks at 25°C and 97 % RH.

	d [nm]	**d_b [nm]**	**A_L [nm^2]**	**d_w [nm]**	**σ [nm]**
POPC-CHOL	5.71	3.67	0.58	2.04	0.47
dPOPC-CHOL	5.73	3.72	0.57	2.02	0.48

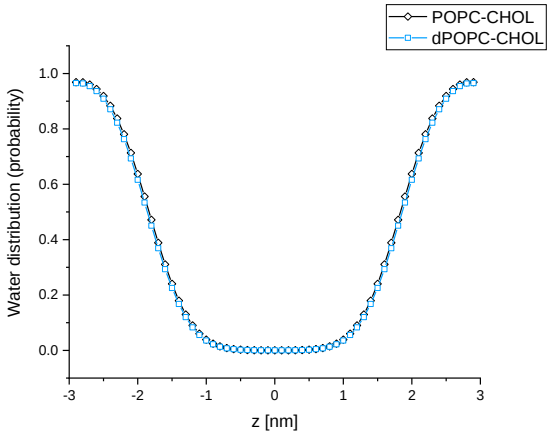

Figure 64: Comparison of water distribution probability between the POPC-CHOL and dPOPC-CHOL membranes.

The dPOPC-CHOL-DS1 samples with molar ratios n_{DS1}:$n_{dPOPC\text{-}CHOL}$ = 1:50 and 1:100 showed indication of phase separation, with a peak at 2θ = 7.7° (example in Figure 65). Similar peak was observed in the study of (Schmitt et al., 2018), attributed to a phase-separated CHOL. (Engelbrecht et al., 2012) reported the first and second order diffraction peaks with 2θ positions 7.49° and 14.84°.

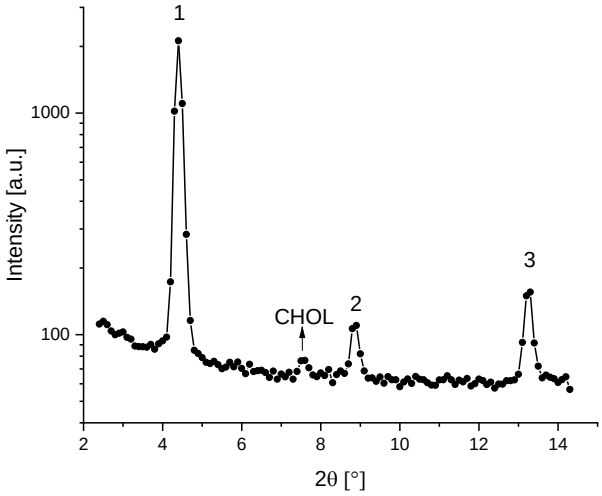

Figure 65: Diffraction data of dPOPC-CHOL-DS1 sample (n_{DS1}:$n_{dPOPC\text{-}CHOL}$ = 1:50) at 100% D_2O with three diffraction orders of the lamellar lipid phase and the first order diffraction peak of phase-separated CHOL.

Even though the interaction of model membranes and antimicrobial peptides has been studied using the small-angle neutron diffraction before (Rehal et al., 2017), we were unfortunately not able to reconstruct the NSLD profiles of DS1-containing samples, due to the differences in repeat spacing obtained from different contrasts caused by an unknown reason.

5 CONCLUSION

The aim of this thesis was to compare the interactions of mammalian and bacterial model membranes with compounds that exert antimicrobial activity – surfactant *N,N*-dimethyl-1-dodecanamine-*N*-oxide (DDAO) and antimicrobial peptide dermaseptin S1 (DS1) using a variety of methods. Amongst the chosen mammalian models were DOPC, DOPC-CHOL and POPC-CHOL (or its partially deuterated form dPOPC-CHOL). POPE-POPG (or its partially deuterated form dPOPE-dPOPG) and POPE-POPG-TOCL were used as the model membranes mimicking the inner membrane of *Escherichia coli*.

To study the interactions, we chose four different experimental methods – static light scattering, fluorescence spectroscopy, small-angle neutron scattering (SANS) and small-angle neutron diffraction (SAND) – together with densitometric study of our lipids/lipid mixtures, to obtain the parameters needed for further evaluation of the other methods.

Static light scattering was used to observe the changes in the size of unilamellar liposomes (ULLs) with increasing concentration of DDAO. Critical concentrations D_t^{SAT} (saturation of the bilayer by DDAO), D_t^{MID} (midpoint of the solubilisation) and D_t^{SOL} (complete liposome-micelle transformation) were evaluated from the dependence of intensity of scattered light on the concentration of DDAO (solubilisation curve). In comparison with the mammalian model membrane (POPC-CHOL), both bacterial model membranes (POPE-POPG, POPE-POPG-TOCL) required more DDAO for complete solubilisation. The cardiolipin containing bacterial model membrane was more stable against the DDAO-induced solubilisation. This is quite significant because many studies on bacterial model membranes tend to neglect the importance of the presence of cardiolipin in model membranes, because of its low occurrence in the bacterial membrane (only 10 w% in *E.coli*).

The creation of defects and pores in the bilayer in the first stage of solubilisation was studied using the fluorescent probe leakage method. ULLs with encapsulated fluorescent probe at a self-quenching concentration were exposed to DDAO, causing the leakage of the probe and increase in fluorescence intensity. Two critical concentrations of DDAO were evaluated D_t^{PERT} (perturbation of the ULLs with intensive leak of the probe) and D_t^{RLS} (complete release of the probe). In contrast to the static light scattering experiments, that were measured three hours after the addition of DDAO, the fluorescent probe leakage had to be measured immediately after the DDAO addition, due to instability of POPE-POPG ULLs to keep the fluorescent probe encapsulated even without adding DDAO. We found that the bacterial model membrane (POPE-POPG) was more resistant against the DDAO-induced leakage than the mammalian model (POPC-CHOL), which corresponds well with the static light scattering-data. The mammalian model membrane showed significant release

of the probe even at $c_{DDAO} < D_t^{PERT}$, while the bacterial model membrane showed little to no leakage before reaching the D_t^{PERT} concentration of DDAO. We suggest that the difference may be caused by the different interactions between the lipid molecules and/or their ordering of the two model membranes.

The leakage of the probe was also observed after the addition of the antimicrobial peptide DS1. DS1 proved to be highly effective in the release of the probe even at small molar ratios of $n_{DS1}:n_{POPE+POPG}$. On the other hand, DS1 was not able to completely release the probe, even at high molar ratio ($n_{DS1}:n_{POPE+POPG} = 1$).

Using the static light scattering, fluorescence spectroscopy and densitometric data, we were able to calculate the partition coefficients of DDAO between the model membranes and the aqueous phase. The partition coefficients were higher in case of the bacterial model membranes (4800 ± 500 for POPE-POPG and 6500 ± 500 for POPE-POPG-TOCL) compared to the mammalian model membrane (2300 ± 300 for POPC-CHOL).The effective molar ratios of the amount of DDAO to the amount of lipid needed for complete solubilisation also much higher in case of bacterial membranes. To conclude, the amount of DDAO in lipid phase is higher when interacting with bacterial model membranes in comparison with mammalian model and the bacterial model membranes need more incorporated DDAO to undergo solubilisation. Multiple factors might cause such differences, for example the strengthening hydrogen bonds in the bacterial model membranes or their charge. Another one might be the tendency of PE molecules to form aggregates with negative curvature, in contrast to the aggregates with positive curvature created by solubilisation. The bacterial membranes are also able to compensate the mismatch in the length of the hydrocarbon chains of phospholipids and DDAO via *trans-gauche* isomerisation, which in case of the mammalian model membrane is suppressed by the presence of cholesterol.

The small-angle neutron scattering method was used to study the structural parameters of the bilayers made of DOPC, DOPC-CHOL and POPE-POPG and the geometry of the aggregates created after the addition of DDAO. An indication of correlation peak was observed for all studied model membranes. Paracrystal lamellar stack model, used to fit the samples with lamellar structure, showed that a part of the liposomes were either oligolamellar with two bilayers on average or some of the ULLs were interacting with each other, causing the visible correlation peak. With increasing amount of DDAO, we observed the bilayer thickness was decreasing. The change in the bilayer thickness between the neat membrane and the sample with equimolar ratio of DDAO:lipid was larger in case of DOPC-CHOL, proving larger defect in the mammalian bilayer caused by the DDAO. Similar types of aggregates are formed during the solubilisation process induced by DDAO for our

mammalian and bacterial model membranes. With the increase of the molar ratio n_{DDAO}:n_{LIPID}, we have observed a transition from liposomes into cylinders with elliptical cross-section. In case of POPE-POPG, this occurred at higher n_{DDAO}:n_{LIPID} molar ratio than for the two mammalian models. The cross-sectional dimensions of the cylinders suggested that the central part of the ellipse is formed by LIPID-DDAO mixed bilayer that is stabilised by a DDAO-rich rim. Further increase in DDAO concentration caused the decrease of the major radius of the ellipse and shortening of the cylinders.

Small-angle neutron diffraction experiments on oriented stacks of bilayers were carried out with the intention of reconstructing the neutron scattering length density profiles of mammalian and bacterial model membranes with the addition of DDAO and DS1. To solve problem of assigning the scattering form factor phases, we first performed swelling experiments with POPC, POPC-CHOL and POPE-POPG membrane. The phase transition of POPE-POPG membrane observed between 70 and 85% relative humidity and the additional phase that was detected during this phase transition ruled out the option of using the swelling experiments to reconstruct the NSLD profiles. POPC-CHOL and POPE-POPG showed similar hydration pressure at low relative humidities.

The contrast variation technique proved to be suitable for NSLD profiles reconstructions of POPC-CHOL and POPE-POPG model membranes mixed with DDAO in various ratios at 97% RH. The samples showed up to 8 orders of diffraction for the neat membranes and the the number did not decrease bellow 4 diffraction peaks, giving us good quality NSLD profiles. We were able to calculate the water distribution probability, area per lipid, thickness of the bilayer, thickness of the water layer and width of the lipid/water interface. As observed with SANS, we observed decrease in the bilayer thickness with increasing amount of DDAO incorporated into the membrane, accompanied by increase in the area per lipid. Membrane-incorporated DDAO did not prove to have an effect on the water distribution probability, as the water layer thickness and the width of the lipid/water interface stayed approximately the same.

Samples containing partially deuterated phospholipids, dPOPC-CHOL and dPOPE-dPOPG, and their mixture with the antimicrobial peptide dermaseptin S1 (DS1) were measured following procedures identical to the experiments with non-deuterated lipids and DDAO. For an unknown reason, the samples did not show stable repeat spacing in different contrasts, with the exception of the neat mammalian model membrane dPOPC-CHOL. Therefore, we could not proceed with the NSLD profile calculation for these samples. Some of the dPOPC-CHOL-DS1 samples even showed phase-separated cholesterol. The parameters obtained from POPC-CHOL and dPOPC-CHOL NSLD profiles, as well as water distribution probability, were almost identical.

Contribution of dissertation to current scientific knowledge:

This dissertation study offers complex knowledge on the topic of the interaction of mammalian and bacterial model membranes with non-ionic surfactant DDAO. With the use of different experimental methods, we have studied all stages of solubilisation, from the partitioning of DDAO into the membranes, creation of defects and pores to complete liposome-mixed micelle transformation. We have proven that the solubilisation proceeds in a similar way for our mammalian and bacterial model membranes, despite the fact that the bacterial model membranes required more DDAO to undergo the particular stages of solubilisation. The fact that mammalian model membranes are more susceptible to solubilisation by DDAO is also very important. It is necessary to monitor the effects of surfactants not only against the bacteria, but also their possibly toxic effect on the environment.

Studying the mechanism of action of compounds with antimicrobial effects is essential for future pharmaceutical development, especially when facing such alarming increase in the number of cases of antibiotic-resistant bacterial infections.

REFERENCES

AHYAYAUCH, H., BENNOUNA, M., ALONSO, A. and GONI, F.M. Detergent effects on membranes at subsolubilizing concentrations: Transmembrane lipid motion, bilayer permeabilization, and vesicle lysis/reassembly are independent phenomena. *Langmuir*. 2010, vol. 26, iss. 10, p. 7307–7313. DOI 10.1021/la904194a.

ANTON PAAR. *Instructions manual DMA 4500M*. Austria: Anton Paar, 2009.

APEL-PAZ, M., DONCEL, G.F. and VANDERLICK, T.K. Impact of membrane cholesterol content on the resistance of vesicles to surfactant attack. *Langmuir*. 2005, vol. 21, iss. 22, p. 9843–9849. DOI 10.1021/la050568r.

BAGATOLLI, L.A., IPSEN, J.H., SIMONSEN, A.C. and MOURITSEN, O.G. An outlook on organization of lipids in membranes: Searching for a realistic connection with the organization of biological membranes. *Progress in Lipid Research*. 2010, vol. 49, iss. 4, p. 378–389. DOI 10.1016/j.plipres.2010.05.001.

BALAZS, D.A. and GODBEY, W. Liposomes for use in gene delivery. *Journal of drug delivery*. 2011, vol. 2011, p. 12. DOI 10.1155/2011/326497.

BALGAVÝ, P. and DEVÍNSKY, F. Cut-off effects in biological activities of surfactants. *Advances in Colloid and Interface Science*. 1996, vol. 66, p. 23–63. DOI 10.1016/0001-8686(96)00295-3.

BARTELS, E.J.H., DEKKER, D. and AMICHE, M. Dermaseptins, multifunctional antimicrobial peptides: A review of their pharmacology, effectivity, mechanism of action, and possible future directions. *Frontiers in Pharmacology*. 2019, vol. 10, p. 1–11. DOI 10.3389/fphar.2019.01421.

BECHINGER, B. and LOHNER, K. Detergent-like actions of linear amphipathic cationic antimicrobial peptides. *Biochimica et Biophysica Acta - Biomembranes*. 2006, vol. 1758, iss. 9, p. 1529–1539. DOI 10.1016/j.bbamem.2006.07.001.

BELIČKA, M., KLACSOVÁ, M., KARLOVSKÁ, J., WESTH, P., DEVÍNSKY, F. and BALGAVÝ, P. Molecular and component volumes of N,N-dimethyl-N-alkylamine N-oxides in DOPC bilayers. *Chemistry and Physics of Lipids*. 2014a, vol. 180, p. 1–6. DOI 10.1016/j.chemphyslip.2014.02.007.

BELIČKA, M., KUČERKA, N., UHRÍKOVÁ, D., ISLAMOV, A.K., KUKLIN, A.I., DEVÍNSKY, F. and BALGAVÝ, P. Effects of N,N-dimethyl-N-alkylamine-N-oxides on DOPC bilayers in unilamellar vesicles: Small-angle neutron scattering study. *European Biophysics Journal*. 2014b, vol. 43, iss. 4–5, p. 179–189. DOI 10.1007/s00249-014-0954-0.

BELIČKA, M., DEVÍNSKY, F. and BALGAVÝ, P. Neutrons in studies of phospholipid bilayers and bilayer-drug interaction. I. Basic principles and neutron diffraction. *Acta Facultatis Pharmaceuticae Universitatis Comenianae*. 2014c, vol. 61, iss. 2, p. 1–11. DOI 10.2478/afpuc-2014-0010.

BENACHIR, T. and LAFLEUR, M. Study of vesicle leakage induced by melittin. *BBA - Biomembranes*. 1995, vol. 1235, iss. 2, p. 452–460. DOI 10.1016/0005-2736(95)80035-E.

BERGSTRÖM, M., PEDERSEN, J.S., SCHURTENBERGER, P. and EGELHAAF, S.U. Small-Angle Neutron Scattering (SANS) Study of Vesicles and Lamellar Sheets Formed from Mixtures of an Anionic and a Cationic Surfactant. *J. Phys. Chem. B*. 1999, vol. 103, p. 9888–9897. DOI 10.1021/jp991846w.

BINDER, H. and GAWRISCH, K. *Effect of unsaturated lipid chains on dimensions, molecular order and hydration of membranes*. 2001.

BRAR, S.K. and VERMA, M. Measurement of nanoparticles by light-scattering techniques. *Trends in Analytical Chemistry*. 2011, vol. 30, iss. 1, p. 4–17. DOI 10.1016/j.trac.2010.08.008.

BROGDEN, K.A. Antimicrobial peptides: pore formers or metabolic inhibitors in bacteria? *Nature reviews. Microbiology*. 2005, vol. 3, p. 238–250. DOI 10.1038/nrmicro1098.

BROWN, D.A. and LONDON, E. Structure of detergent-resistant membrane domains: does phase separation occur in biological membranes? *Biochem. Biophys. Res. Commun.* 1997, vol. 240, iss. 1, p. 1–7. DOI 10.1006/bbrc.1997.7575.

BUKOVSKÝ, M., MLYNARČÍK, D. and ONDRÁČKOVÁ, V. Immunomodulatory activity of amphiphilic antimicrobials on mouse macrophages. *International journal of immunopharmacology*. 1996, vol. 18, iss. 6–7, p. 423–426.

BULLOVÁ, H. and BALGAVÝ, P. Turbidimetric study of unilamellar extruded egg phosphatidylcholine liposomes. *Acta Facultatis Pharmaceuticae Universitatis Comenianae*. 2005, P. 66–72.

CANTOR, R.S. Lateral Pressures in Cell Membranes: A Mechanism for Modulation of Protein Function. *The Journal of Physical Chemistry B*. 1997, vol. 101, iss. 10, p. 1723–1725. DOI 10.1021/jp963911x.

CHANG, D.P., BARAUSKAS, J., DABKOWSKA, A.P., WADSÄTER, M., TIBERG, F. and NYLANDER, T. Non-lamellar lipid liquid crystalline structures at interfaces. *Advances in Colloid and Interface Science*. 2015, vol. 222, p. 135–147. DOI 10.1016/j.cis.2014.11.003.

CHEN, Y.-F. *Phase behaviour of cardiolipin*. Cornell University.

CISSE, A., MARQUETTE, A., ALTANGEREL, M., PETERS, J. and BECHINGER, B. Investigation of the Action of Peptides on Lipid Membranes. *Journal of Physical Chemistry B*. 2021, vol. 125, iss. 36, p. 10213–10223. DOI 10.1021/acs.jpcb.1c06388.

CÓCERA, M., LÓPEZ, O., CODERCH, L., PARRA, J.L. and DE LA MAZA, A. Permeability investigations of phospholipid liposomes by adding cholesterol. *Colloids and Surfaces A: Physicochemical and Engineering Aspects*. 2003, vol. 221, p. 9–17. DOI 10.1016/S0927-7757(03)00104-3.

CRISTIGLIO, V., GIROUD, B., DIDIER, L. and DEMÉ, B. D16 is back to business: more neutrons, more space, more fun. *Neutron News*. 2015, vol. 26, iss. 3, p. 22–24. DOI 10.1080/10448632.2015.1057051.

DALEKE, D.L. Regulation of phospholipid asymmetry in the erythrocyte membrane. *Current Opinion in Hematology*. 2008, vol. 15, iss. 3, p. 191–195. DOI 10.1097/MOH.0b013e3282f97af7.

DE ALMEIDA, R.F.M., FEDOROV, A. and PRIETO, M. Sphingomyelin/phosphatidylcholine/cholesterol phase diagram: Boundaries and composition of lipid rafts. *Biophysical Journal*. 2003, vol. 85, iss. 4, p. 2406–2416. DOI 10.1016/S0006-3495(03)74664-5.

DE LA MAZA, A. and PARRA, J.L. Vesicle-micelle structural transition of phosphatidylcholine bilayers and Triton X-100. *Biochemical Journal*. 1994, vol. 303, iss. 3, p. 907–914. DOI 10.1042/bj3030907.

DEVÍNSKY, F. Amine Oxides. X . Non-aromatic Amine Oxides: Physico-chemical Properties and Some Characteristic Reactions*. *Acta Facultatis Pharmaceuticae Universitatis Comenianae*. 1985, vol. 39, p. 173–195.

DEVÍNSKY, F., ĎURINDA, J., LACKO, I. and VALENTOVÁ, J. *Organická chémia*. 2. Martin: Osveta, 2013. ISBN 978-80- 8063-388-2.

DEVÍNSKY, F., KOPECKÁ-LEITMANOVÁ, A., ŠERŠEŇ, F. and BALGAVÝ, P. Cut-off Effect in Antimicrobial Activity and in Membrane Perturbation Efficiency of the Homologous Series of N , N-Dimethylalkylamine Oxides. *Journal of Pharmacy and Pharmacology*. 1990, vol. 42, p. 790–794. NULL

DOBROTA, D. *Lekárska biochémia*. 1. Martin: Osveta, 2012. ISBN 978-80-8063- 293-9.

DOUCET, M., CHO, J.H., ALINA, G., BAKKER, J., BOUWMAN, W., BUTLER, P., CAMPBELL, K., GONZALES, M., HEENAN, R. and JACKSON, A. *SasView*. 2017. 4.1. Available from: http://www.sasview.org/

DUBNIČKOVÁ, M., KISELEV, M.A., KUTUZOV, S., DEVÍNSKY, F., GORDELIY, V. and BALGAVÝ, P. Effect of N-Lauryl-N,N-Dimethylamine N-Oxide on Dimyristoyl Phosphatidylcholine Bilayer Thickness: A Small-Angle Neutron Scattering Study. *General Physiology and Biophysics*. 1997, vol. 16, iss. 2, p. 175–188.

EDIDIN, M. The state of lipid rafts: from model membranes to cells. *Annual review of biophysics and biomolecular structure*. 2003, vol. 32, p. 257–283. DOI 10.1146/annurev.biophys.32.110601.142439.

EDWARDS, K. and ALMGREN, M. Solubilization of lecithin vesicles by C12E8. *Journal of Colloid and Interface Science*. 1991, vol. 147, iss. 1, p. 1–21. DOI 10.1016/0021-9797(91)90129-v.

EEMAN, M. and DELEU, M. From biological membranes to biomimetic model membranes. *Biotechnology, Agronomy, Society and Environment*. 2010, vol. 14, iss. 4, p. 719–736.

ELIZONDO, E., MORENO, E., CABRERA, I., CÓRDOBA, A., SALA, S., VECIANA, J. and VENTOSA, N. Liposomes and Other Vesicular Systems: Structural Characteristics, Methods of Preparation, and Use in Nanomedicine. *Progress in Molecular Biology and Translational Science*. 2011, vol. 104, p. 1–52. DOI 10.1016/B978-0-12-416020-0.00001-2.

ENGELBRECHT, T.N., DEMÉ, B., DOBNER, B. and NEUBERT, R.H.H. Study of the Influence of the Penetration Enhancer Isopropyl Myristate on the Nanostructure of Stratum Corneum Lipid Model Membranes Using Neutron Diffraction and Deuterium Labelling. *Skin Pharmacology and Physiology*. 2012, vol. 25, p. 200–207. DOI 10.1159/000338538.

ENGELMAN, D.M. Membranes are more mosaic than fluid. *Nature*. 2005, vol. 438, p. 578–580. DOI 10.1038/nature04394.

EPAND, R.M. and EPAND, R.F. Lipid domains in bacterial membranes and the action of antimicrobial agents. *Biochimica et Biophysica Acta - Biomembranes*. 2009, vol. 1788, iss. 1, p. 289–294. DOI 10.1016/j.bbamem.2008.08.023.

EPAND, R.M. and VOGEL, H.J. Diversity of antimicrobial peptides and their mechanisms of action. *Biochimica et Biophysica Acta - Biomembranes*. 1999, vol. 1462, p. 11–28. DOI 10.1016/S0005-2736(99)00198-4.

ESCRIBÁ, P. V. and NICOLSON, G.L. Membrane structure and function: Relevance of lipid and protein structures in cellular physiology, pathology and therapy. *Biochimica et Biophysica Acta*. 2014, vol. 1838, iss. 6, p. 1449–1450. DOI 10.1016/j.bbamem.2014.03.008.

FADEEL, B. and XUE, D. The ins and outs of phospholipid asymmetry in the plasma membrane: Roles in health and disease. *Critical Reviews in Biochemistry and Molecular Biology*. 2009, vol. 44, iss. 5, p. 264–277. DOI 10.1080/10409230903193307.

FATTAL, D.R., ANDELMAN, D. and BEN-SHAUL, A. The Vesicle-Micelle Transiiion in Mixed Lipid-Surfactant Systems: A Molecular Model. *Langmuir*. 1995, vol. 11, iss. 4, p. 1154–1161. DOI 10.1021/la00004a020.

FEDER, R., DAGAN, A. and MOR, A. Structure-activity relationship study of antimicrobial dermaseptin S4 showing the consequences of peptide oligomerization on selective cytotoxicity. *Journal of Biological Chemistry*. 2000, vol. 275, iss. 6, p. 4230–4238. DOI 10.1074/jbc.275.6.4230.

FEIGIN, L.A. and SVERGUN, D.I. *Structure Analysis by Small-Angle X-Ray and Neutron Scattering*. New York: Plenum, 1987.

FRAGNETO, G., DELHOM, R., JOLY, L. and SCOPPOLA, E. Neutrons and model membranes: Moving towards complexity. *Current Opinion in Colloid and Interface Science*. 2018, vol. 38, p. 108–121. DOI 10.1016/j.cocis.2018.10.003.

GALLOVÁ, J., KLACSOVÁ, M., DEVÍNSKY, F. and BALGAVÝ, P. Partial volumes of cholesterol and monounsaturated diacylphosphatidylcholines in mixed bilayers. *Chemistry and Physics of Lipids*. 2015, vol. 190, p. 1–8. DOI 10.1016/j.chemphyslip.2015.06.001.

GALLOVÁ, J., UHRÍKOVÁ, D., KUČERKA, N., DOKTOROVOVÁ, S., FUNARI, S.S., TEIXEIRA, J. and BALGAVÝ, P. The effects of cholesterol and β;-sitosterol on the structure of saturated diacylphosphatidylcholine bilayers. *European Biophysics Journal*. 2010a, vol. 40, iss. 2, p. 153–163. DOI 10.1007/s00249-010-0635-6.

GALLOVÁ, J., UHRÍKOVÁ, D., KUČERKA, N., TEIXEIRA, J. and BALGAVÝ, P. Partial area of cholesterol in monounsaturated diacylphosphatidylcholine bilayers. *Chemistry and Physics of Lipids*. 2010b, vol. 163, iss. 8, p. 765–770. DOI 10.1016/j.chemphyslip.2010.08.002.

GALLOVÁ, J., ŽELINSKÁ, K. and BALGAVÝ, P. Partial volumes of cholesterol and monounsaturated diacylphosphatidylcholines in mixed bilayers. *European Pharmaceutical Journal*. 2017, vol. 1, p. 1–3. DOI 10.1515/afpuc-2017-0012.

GARG, T. and GOYAL, A.K. Liposomes: Targeted and Controlled Delivery System. *Drug Elivery Letters*. 2014, vol. 4, p. 62–71. DOI 10.2174/22103031113036660015.

GARIDEL, P. and BLUME, A. Miscibility of phosphatidylethanolamine-phosphatidylglycerol mixtures as a function of pH and acyl chain length. *European biophysics journal*. 2000, vol. 28, p. 629–638. DOI 10.1007/s002490050003.

GAWRISCH, K., GAEDE, H.C., MIHAILESCU, M. and WHITE, S.H. Hydration of POPC bilayers studied by1H-PFG-MAS-NOESY and neutron diffraction. *European Biophysics Journal*. 2007, vol. 36, iss. 4–5, p. 281–291. DOI 10.1007/s00249-007-0142-6.

GOLTSOV, A.N. and BARSUKOV, L.I. Synergetics of the membrane self-assembly: A micelle-to-vesicle transition. *Journal of Biological Physics*. 2000, vol. 26, iss. 1, p. 27–41. DOI 10.1023/A:1005139631164.

GONI, F.M. The basic structure and dynamics of cell membranes: An update of the Singer-Nicolson model. *Biochimica et Biophysica Acta - Biomembranes*. 2014, vol. 1838, p. 1467–1476. DOI 10.1016/j.bbamem.2014.01.006.

GONI, F.M. and ALONSO, A. Spectroscopic techniques in the study of membrane solubilization, reconstitution and permeabilization by detergents. *Biochimica et Biophysica Acta - Biomembranes*. 2000, vol. 1508, p. 51–68. DOI 10.1016/S0304-4157(00)00011-3.

GONTHIER, J., BARRETT, M.A., AGUETTAZ, O., BAUDOIN, S., BOURGEAT-LAMI, E., DEMÉ, B., GRIMM, N., HAUSS, T., KIEFER, K., LELIÈVRE-BERNA, E., PERKINS, A. and WALLACHER, D. BerILL: The ultimate humidity chamber for neutron scattering. *Journal of Neutron Research*. 2019, vol. 21, p. 65.

GORACCI, L., GERMANI, R., RATHMAN, J.F. and SAVELLI, G. Anomalous behavior of amine oxide surfactants at the air/water interface. *Langmuir*. 2007, vol. 23, iss. 21, p. 10525–10532. DOI 10.1021/la7015726.

HAMANN, S., KIILGAARD, J.F., LITMAN, T., ALVAREZ-LEEFMANS, F.J., WINTHER, B.R. and ZEUTHEN, T. Measurement of Cell Volume Changes by Fluorescence. *Journal of Fluorescence*. 2002, vol. 12, iss. 2, p. 139–145. DOI 10.1023/a:1016832027325.

HANEY, E.F., NATHOO, S., VOGEL, H.J. and PRENNER, E.J. Induction of non-lamellar lipid phases by antimicrobial peptides: a potential link to mode of action. *Chemistry and Physics of Lipids*. 2010, vol. 163, iss. 1, p. 82–93. DOI 10.1016/j.chemphyslip.2009.09.002.

HARROUN, T.A., KATSARAS, J. and WASSALL, S.R. Cholesterol is found to reside in the center of a polyunsaturated lipid membrane. *Biochemistry*. 2008, vol. 45, p. 1227–1233. DOI 10.1021/bi800123b.

HARTL, J., DOLEŽAL, M., MILETÍN, M., OPLETALOVÁ, V. and ZIMČÍK, P. *Farmaceutická chemie IV.* 2. Praha: Karolinum, 2012. ISBN 978-80-246-2129-6.

HARVEY, D. Spectroscopic Methods of analysis. In: HARVEY, David (ed.), *Modern analytical chemistry*. 1. Boston: McGraw-Hill. 2000, p. 369–459. ISBN 0–07–237547–7.

HEERKLOTZ, H. Interactions of surfactants with lipid membranes. *Quarterly Reviews of Biophysics*. 2008, vol. 41, iss. 3/4, p. 205–264. DOI 10.1017/S0033583508004721.

HEERKLOTZ, H. and BLUME, A. Detergent interactions with lipid bilayers and membrane proteins. In: EGELMAN, E.H. (ed.), *Comprehensive Biophysics*. Elsevier. 2012, p. 63–91. ISBN 9780080957180. Available from: http://dx.doi.org/10.1016/B978-0-12-374920-8.00529-4

HELENIUS, A. and SIMONS, K. Solubilization of membranes by detergents. *Biochimica et Biophysica Acta*. 1975, vol. 415, p. 29–79. DOI 10.1016/0304-4157(75)90016-7.

HERRMANN, K.W. Non-Ionic—Cationic Micellar Properties of Dimethyldodecylamine Oxide. *The Journal of Physical Chemistry*. 1962, vol. 66, iss. 4, p. 295–300. DOI 10.1021/j100808a025.

HIMANSHI, S., MAHESH, K.K., AJAY, B., PRABHJOT, K. and SAROJ, B. Liposome : An art for drug delivery. *International Journal of Pharmaceutical Sciences Letters*. 2015, vol. 5, iss. 2, p. 523–530.

HOGG, S. *Essential microbiology*. 1. Chichester: Wiley, 2005. ISBN 0-471-49754-1.

HRUBOVČÁK, P., KONDELA, T., ERMAKOVA, E. and KUČERKA, N. Application of small-angle neutron diffraction to the localization of general anesthetics in model membranes. *European Biophysics Journal*. 2019, vol. 48, iss. 5, p. 447–455. DOI 10.1007/s00249-019-01370-7.

HRUBŠOVÁ, A., KARLOVSKÁ, J., DEVÍNSKY, F., LACKO, I. and BALGAVÝ, P. Solubilization of unilamellar egg yolk phosphatidylcholine liposomes by N-alkyl-N,N-dimethylamine N-oxides. *Česká a slovenská farmacie*. 2003, vol. 52, iss. 6, p. 299–305.

HUANG, H.W. Action of antimicrobial peptides: Two-state model. *Biochemistry*. 2000, vol. 39, iss. 29, p. 8347–8352. DOI 10.1021/bi000946l.

HUANG, K.C., MUKHOPADHYAY, R., WEN, B., GITAI, Z. and WINGREEN, N.S. Cell shape and cell-wall organization in Gram-negative bacteria. *Proceedings of the National Academy of Sciences*. 2008, vol. 105, iss. 49, p. 19282–19287. DOI 10.1073/pnas.0805309105.

HUBČÍK, L., FUNARI, S.S., PULLMANNOVÁ, P., DEVÍNSKY, F. and UHRÍKOVÁ, D. Stimuli responsive polymorphism of C12NO/DOPE/DNA complexes: Effect of pH, temperature and composition. *Biochimica et Biophysica Acta - Biomembranes*. 2015, vol. 1848, iss. 5, p. 1127–1138. DOI 10.1016/j.bbamem.2015.01.020.

HULÁKOVÁ, S., FULIER, B., GALLOVÁ, J. and BALGAVÝ, P. Effect of N-dodecyl-N,N-dimethylamine N-oxide on unilamellar liposomes. *Acta Facultatis Pharmaceuticae Universitatis Comenianae*. 2013, vol. 60, iss. 2, p. 7–13. DOI 10.2478/afpuc-2013-0021.

HULÁKOVÁ, S., GALLOVÁ, J. and DEVÍNSKY, F. Cholesterol protects phosphatidylcholine liposomes from N,N-dimethyl-1-dodecanamine N-oxide influence. *Acta Chimica Slovenica*. 2015, vol. 62, iss. 2, p. 420–427. DOI 10.17344/acsi.2014.750.

ISRAELACHVILI, J.N. *Intermolecular and Surface Forces*. 3. Academic Press, 2011. ISBN 978-0-12-391927-4.

JACKSON, A.J. *Introduction to Small-Angle Neutron Scattering and Neutron Reflectometry*. 2008.

JARSCH, I.K., DASTE, F. and GALLOP, J.L. Membrane curvature in cell biology: An integration of molecular mechanisms. *Journal of Cell Biology*. 2016, vol. 214, iss. 4, p. 375–387. DOI 10.1083/jcb.201604003.

KACÁNI, L., FERENCÍK, M., DEVÍNSKY, F. and DIERICH, M.P. Immunomodulatory effect of some amphiphilic detergents on the human promyelocytic HL-60 cells. *Folia Biol. (Praha)*. 1996, vol. 42, p. 11–16.

KARLOVSKÁ, J., DEVÍNSKY, F. and BALGAVÝ, P. Effect of amphiphilic surfactant LDAO on the solubilization of DOPC vesicles and on the activity of Ca2+-ATPase reconstituted in DOPC vesicles. *General Physiology and Biophysics*. 2007, vol. 26, iss. 4, p. 290–297.

KARLOVSKÁ, J., LOHNER, K., DEGOVICS, G., LACKO, I., DEVÍNSKY, F. and BALGAVÝ, P. Effects of non-ionic surfactants N-alkyl-N,N-dimethylamine-N-oxides on the structure of a phospholipid bilayer: Small-angle X-ray diffraction study. *Chemistry and Physics of Lipids*. 2004a, vol. 129, iss. 1, p. 31–41. DOI 10.1016/j.chemphyslip.2003.11.003.

KARLOVSKÁ, J., DEVÍNSKY, F., LACKO, I., GALLOVÁ, J. and BALGAVÝ, P. Solubilization of multilamellar liposomes by N-dodecyl-N,N-dimethylamine N-oxide. *Acta Facultatis Pharmaceuticae Universitatis Comenianae*. 2004b, P. 119–128.

KARLOVSKÁ, J., UHRÍKOVÁ, D., KUČERKA, N., TEIXEIRA, J., DEVÍNSKY, F., LACKO, I. and BALGAVÝ, P. Influence of N-dodecyl-N,N-dimethylamine N-oxide on the activity of sarcoplasmic reticulum Ca2+-transporting ATPase reconstituted into diacylphosphatidylcholine vesicles: Effects of bilayer physical parameters. *Biophysical Chemistry*. 2006, vol. 119, iss. 1, p. 69–77. DOI 10.1016/j.bpc.2005.09.007.

KATSARAS, J., HARROUN, T.A., PENCER, J., ABRAHAM, T., KUČERKA, N. and NIEH, M.-P. Small-angle neutron scattering and biomolecules. *Physics in Canada*. 2006, P. 233–240.

KAUFMANN, S., ILG, K., MASHAGHI, A., TEXTOR, M., PRIEM, B., AEBI, M. and REIMHULT, E. Supported Lipopolysaccharide Bilayers. *Langmuir*. 2012, vol. 28, p. 12199–12208. DOI 10.1021/la3020223.

KAYSER, F.H. General Bacteriology. In: KAYSER, F.H., BIENZ, K.A., ECKERT, J. and ZINKERNAGEL, R.M. (eds.), *Medical microbiology*. 10. Stuttgart: Thieme. 2005, p. 146–160. ISBN 1-58890-245-5.

KISELEV, M.A., LOMBARDO, D., LESIEUR, P., KISSELEV, A.M., BORBELY, S., SIMONOVA, T.N. and BARSUKOV, L.I. Membrane self assembly in mixed DMPC/NaC systems by SANS. *Chemical Physics*. 2008, vol. 345, p. 173–180. DOI 10.1016/j.chemphys.2007.09.034.

KLACSOVÁ, M., WESTH, P. and BALGAVÝ, P. Molecular and component volumes of saturated n-alkanols in DOPC + DOPS bilayers. *Chemistry and Physics of Lipids*. 2010, vol. 163, iss. 6, p. 498–505. DOI 10.1016/j.chemphyslip.2010.04.004.

KLAUDA, J.B., KUČERKA, N., BROOKS, B.R., PASTOR, R.W. and NAGLE, J.F. Simulation-based methods for interpreting x-ray data from lipid bilayers. *Biophysical Journal*. 2006, vol. 90, iss. 8, p. 2796–2807. DOI 10.1529/biophysj.105.075697.

KOOLMAN, J. and ROEHM, K.-H. *Color Atlas of Biochemistry*. 2. Stuttgart: Thieme, 2005. ISBN 3-13-100372-3.

KOYNOVA, R. and TENCHOV, B.G. Lipids: Phase Transitions. *Wiley Encyclopedia of Chemical Biology*. 2008, No. 4, p. 1–14. DOI 10.1002/9780470048672.wecb287.

KOYNOVA, R. and TENCHOV, B.G. Transitions between lamellar and non-lamellar phases in membrane lipids and their physiological roles. *OA Biochemistry*. 2013, vol. 1, iss. 1, p. 1–9. DOI 10.13172/2052-9651-1-1-602.

KOZLOV, M.M., LICHTENBERG, D. and ANDELMAN, D. Shape of Phospholipid/Surfactant Mixed Micelles: Cylinders or Disks? Theoretical Analysis. *J. Phys. Chem. B*. 1997, vol. 101, p. 6600–6606. DOI 10.1021/jp970295b.

KRAGH-HANSEN, U., LE MAIRE, M. and MØLLER, J. V. The mechanism of detergent solubilization of liposomes and protein-containing membranes. *Biophysical journal*. 1998, vol. 75, iss. 6, p. 2932–46. DOI 10.1016/S0006-3495(98)77735-5.

KUČERKA, N., ERMAKOVA, E., DUSHANOV, E., KHOLMURODOV, K.T., KURAKIN, S., ŽELINSKÁ, K. and UHRÍKOVÁ, D. Cation-zwitterionic lipid interactions are affected by the lateral area per lipid. *Langmuir*. 2021, vol. 37, p. 278–288. DOI 10.1021/acs.langmuir.0c02876.

KUČERKA, N., HOLLAND, B.W., GRAY, C.G., TOMBERLI, B. and KATSARAS, J. The Detailed Scattering Density Profile Model of Pg Bilayers as Determined by Molecular Dynamics Simulations, and Small-Angle Neutron and X-ray Scattering Experiments. *Biophysical Journal*. 2012, vol. 102, iss. 1, p. 504a-505a. DOI 10.1016/j.bpj.2011.11.2764.

KUČERKA, N., NIEH, M.-P. and KATSARAS, J. *Fluid phase lipid areas and bilayer thicknesses of commonly used phosphatidylcholines as a function of temperature*. 2011. ISBN 0006-3002 (Print)n0006-3002 (Linking).

KUČERKA, N., NIEH, M.-P., PENCER, J., SACHS, J.N. and KATSARAS, J. What determines the thickness of a biological membrane. *Gen. Physiol. Biophys.* 2009, vol. 28, p. 117–125. DOI 10.4149/gpb_2009_02_117.

KUČERKA, N., PENCER, J., NIEH, M.-P. and KATSARAS, J. Influence of cholesterol on the bilayer properties of monounsaturated phosphatidylcholine unilamellar vesicles. *European Physical Journal E*. 2007, vol. 23, iss. 3, p. 247–254. DOI 10.1140/epje/i2007-10202-8.

KUČERKA, N., TRISTRAM-NAGLE, S. and NAGLE, J.F. Structure of fully hydrated fluid phase lipid bilayers with monounsaturated chains. *Journal of Membrane Biology*. 2005, vol. 208, iss. 3, p. 193–202. DOI 10.1007/s00232-005-7006-8.

KUKLIN, A.I., ROGACHEV, A. V., SOLOVIOV, D. V., IVANKOV, O., KOVALEV, Y.S., UTROBIN, P.K., KUTUZOV, S., SOLOVIEV, A.G., RULEV, M.I. and GORDELIY, V.I. Neutronographic investigations of supramolecular structures on upgraded small-angle spectrometer YuMO. *Journal of Physics: Conf. Series*. 2017, vol. 848, p. 1–18. DOI 10.1088/1742-6596/848/1/012010.

KULKARNI, C. V. Lipid crystallization: from self-assembly to hierarchical and biological ordering. *Nanoscale*. 2012, vol. 4, iss. 19, p. 5779–5791. DOI 10.1039/c2nr31465g.

LAKOWICZ, J.R. *Principles of Fluorescence Spectroscopy*. 3. New York: Springer, 2006. ISBN 978-0387-31278-1. Zdroje - Knihy - Metódy

LAWLER, D.M. Turbidimetry and Nephelometry. In: WORSFOLD, P.J., TOWNSHEND, A. and POOLE, C.F. (eds.), *Encyclopedia of Analytical Science*. 2. Elsevier. 2005, p. 343–351. ISBN 978-0127641003.

LE MAIRE, M., CHAMPEIL, P. and MØLLER, J. V. Interaction of membrane proteins and lipids with solubilizing detergents. *Biochimica et Biophysica Acta - Biomembranes*. 2000, vol. 1508, iss. 1–2, p. 86–111. DOI 10.1016/S0304-4157(00)00010-1.

LEFTIN, A., MOLUGU, T.R., JOB, C., BEYER, K. and BROWN, M.F. Area per lipid and cholesterol interactions in membranes from separated local-field 13C NMR spectroscopy. *Biophysical Journal*. 2014, vol. 107, iss. 10, p. 2274–2286. DOI 10.1016/j.bpj.2014.07.044.

LICHTENBERG, D., AHYAYAUCH, H., ALONSO, A. and GONI, F.M. Detergent solubilization of lipid bilayers: A balance of driving forces. *Trends in Biochemical Sciences*. 2013a, vol. 38, iss. 2, p. 85–93. DOI 10.1016/j.tibs.2012.11.005.

LICHTENBERG, D., AHYAYAUCH, H. and GONI, F.M. The mechanism of detergent solubilization of lipid bilayers. *Biophysical Journal*. 2013b, vol. 105, iss. 2, p. 289–299. DOI 10.1016/j.bpj.2013.06.007.

LIPOWSKY, R. and SACKMANN, E. *Structure and Dynamics of membranes*. 1. North Holland: Elsevier, 1995. ISBN 9780080541914. Zdroje - knihy - zloženie membrán.jpg

LISKAYOVÁ, G., HUBČÍK, L., ŠIŠKOVÁ, K., PAULIKOVÁ, I., GALLIKOVÁ, D., DEVÍNSKY, F., FUNARI, S.S. and UHRÍKOVÁ, D. PH-sensitive N,N-(dimethyl)-N-alkanamine-N-oxides as gene delivery vectors. *Chemical Papers*. 2017, vol. 71, iss. 9, p. 1739–1748. DOI 10.1007/s11696-017-0171-2.

LOHNER, K. New strategies for novel antibiotics: peptides tagreting bacterial cell membranes. *General physiology and biophysics*. 2009, vol. 28, p. 105–116. DOI 10.4149/gpb. Zlý článok opraviť obidva

LOHNER, K. and BLONDELLE, S.E. Molecular mechanisms of membrane perturbation by antimicrobial peptides and the use of biophysical studies in the design of novel peptide antibiotics. *Combinatorial chemistry & high throughput screening*. 2005, vol. 8, iss. 3, p. 241–56. DOI 10.2174/1386207053764576.

LOPES, S.C., NEVES, C.S., EATON, P. and GAMEIRO, P. Cardiolipin, a key component to mimic the E. coli bacterial membrane in model systems revealed by dynamic light scattering and steady-state fluorescence anisotropy. *Analytical and Bioanalytical Chemistry*. 2010, vol. 398, iss. 3, p. 1357–1366. DOI 10.1007/s00216-010-4028-6.

LOPES, S.C., NEVES, C.S., EATON, P. and GAMEIRO, P. Improved model systems for bacterial membranes from differing species: The importance of varying composition in PE/PG/cardiolipin ternary mixtures. *Molecular Membrane Biology*. 2012, vol. 29, iss. 6, p. 207–217. DOI 10.3109/09687688.2012.700491.

LORENZ, C.D., HSIEH, C.-M., DREISS, C.A. and LAWRENCE, M.J. Molecular dynamics simulations of the interfacial and structural properties of dimethyldodecylamine-N-oxide micelles. *Langmuir*. 2011, vol. 27, iss. 2, p. 546–553. DOI 10.1021/la1031416.

LUCHINI, A. and VITIELLO, G. Mimicking the mammalian plasma membrane: An overview of lipid membrane models for biophysical studies. *Biomimetics*. 2021, vol. 6, iss. 1, p. 1–18. DOI 10.3390/biomimetics6010003.

LUZZATI, V. X-Ray diffraction studies of lipid-water systems. In: CHAPMAN, D. (ed.), *Biological Membranes*. 1. New York: Academic Press. 1968, ISBN 978-0121685409.

MA, Y., GOSH, S.K., BERA, S., JIANG, Z., TRISTRAM-NAGLE, S., LURIO, L.B. and SINHA, S.K. Accurate calibration and control of relative humidity close to 100% by X-raying a DOPC multilayer. *Phys.Chem.Chem.Phys.* 2015, vol. 17, p. 3570–3576.

MACDONALD, R.C., MACDONALD, R.I., MENCO, B.P.M., TAKESHITA, K., SUBBARAO, N.K. and HU, L.R. Small-volume extrusion apparatus for preparation of large, unilamellar vesicles. *Biochimica et Biophysica Acta - Biomembranes*. 1991, vol. 1061, iss. 2, p. 297–303. DOI 10.1016/0005-2736(91)90295-J.

MARCELINO, J., LIMA, J.L.F.C., REIS, S. and MATOS, C. *Assessing the effects of surfactants on the physical properties of liposome membranes*. 2007.

MARQUARDT, D., FRONTZEK, M.D., ZHAO, Y., CHAKOUMAKOS, B.C. and KATSARAS, J. Neutron diffraction from aligned stacks of lipid bilayers using the WAND instrument. *Journal of Applied Crystallography*. 2018, vol. 51, iss. 2, p. 235–241. DOI 10.1107/S1600576718001243.

MARX, L., FREWEIN, M.P.K., SEMERARO, E.F., RECHBERGER, G.N., LOHNER, K., PORCAR, L. and PABST, G. Antimicrobial peptide activity in asymmetric bacterial membrane mimics. *Faraday Discussions*. 2021, vol. 232, p. 435–447. DOI 10.1039/d1fd00039j.

MATTEI, B., FRANCA, A.D.C. and RISKE, K.A. Solubilization of binary lipid mixtures by the detergent triton X-100: The role of cholesterol. *Langmuir*. 2015, vol. 31, iss. 1, p. 378–386. DOI 10.1021/la504004r.

MATTEI, B., LIRA, R.B., PEREZ, K.R. and RISKE, K.A. Membrane permeabilization induced by Triton X-100: The role of membrane phase state and edge tension. *Chemistry and Physics of Lipids*. 2017, vol. 202, p. 28–37. DOI 10.1016/j.chemphyslip.2016.11.009.

MEISTER, A., FINGER, S., HAUSE, G. and BLUME, A. Morphological changes of bacterial model membrane vesicles. *European Journal of Lipid Science and Technology*. 2014, vol. 116, iss. 9, p. 1228–1233. DOI 10.1002/ejlt.201300388. Stabilita mono- a bi-komponentných vezikúl ako modelov bakteriálnych membránPacking charakteristiky

MEMOLI, A., ANNESINI, M.C. and PETRALITO, S. Surfactant-induced leakage from liposomes: A comparison among different lecithin vesicles. *International Journal of Pharmaceutics*. 1999a, vol. 184, iss. 2, p. 227–235. DOI 10.1016/S0378-5173(99)00105-2.

MEMOLI, A., PALERMITI, L.G., TRAVAGLI, V. and ALHAIQUE, F. Effects of surfactants on the spectral behaviour of calcein (II): A method of evaluation. *Journal of Pharmaceutical and Biomedical Analysis*. 1999b, vol. 19, iss. 3–4, p. 627–632. DOI 10.1016/S0731-7085(98)00229-5.

MOR, A., HANI, K. and NICOLAS, P. The vertebrate peptide antibiotics dermaseptins have overlapping structural features but target specific microorganisms. *Journal of Biological Chemistry*. 1994, vol. 269, iss. 50, p. 31635–31641.

MOR, A. and NICOLAS, P. The NH2-terminal alpha-helical domain 1-18 of dermaseptin is responsible for antimicrobial activity. *Journal of Biological Chemistry*. 1994, vol. 269, iss. 3, p. 1934–1939.

MOREIN, S., ANDERSSON, A.-S., RILFORS, L. and LINDBLOM, G. Wild-type Escherichia coli Cells Regulate the Membrane Lipid Composition in a " Window " between Gel and Non-lamellar Sructures. *The Journal of Biological Chemistry*. 1996, vol. 271, iss. 12, p. 6801–6809. DOI 10.1074/jbc.271.12.6801.

MORSE, S.A. and MEITZNER, T.A. Cell Structure. In: BROOKS, G.F., CARROLL, K.C., BUTEL, J.S., MORSE, Stephen A. and MIETZNER, T.A. (eds.), *Jawetz, Melnick and Adelbergs Medical Microbiology*. 26. New York: McGraw-Hill. 2013, p. 11–42. ISBN 978-0-07-179031-4.

MOURITSEN, O.G. *Life - as a matter of fat*. 1. Berlin: Springer, 2005. ISBN 3-540-23248-6.

MURÍN, A., DEVÍNSKY, F., KOLEKOVÁ, A. and LACKO, I. Relation between chemical-structure and biological-activity of N-alkyl dimethylaminoxides series and some other related-compounds. *Biológia*. 1990, vol. 45, p. 521–531.

MURUGOVA, T.N. and BALGAVÝ, P. Molecular volumes of DOPC and DOPS in mixed bilayers of multilamellar vesicles. *Phys.Chem.Chem.Phys.* 2014, vol. 16, p. 18211–18216. DOI 10.1039/c4cp01980f.

MURZYN, K., RÓG, T. and PASENKIEWICZ-GIERULA, M. Phosphatidylethanolamine-phosphatidylglycerol bilayer as a model of the inner bacterial membrane. *Biophysical journal*. 2005, vol. 88, iss. 2, p. 1091–103. DOI 10.1529/biophysj.104.048835. Simulation

NAGAWA, Y. and REGEN, S.L. Membrane-Disrupting Surfactants That Are Highly Selective toward Lipid Bilayers of Varying Cholesterol Content. *Journal of American Chemical Society*. 1991, vol. 113, p. 7237–7240. DOI 10.1021/ja00019a022.

NAGLE, J.F. and TRISTRAM-NAGLE, S. Structure of lipid bilayers. *Biochimica et biophysica acta*. 2000, vol. 1469, p. 159–195. DOI 10.1016/S0304-4157(00)00016-2.

NEIDHARDT, F.C. Bacterial Structures. In: RYAN, K.J. and RAY, C.G. (eds.), *Sherris Medical Microbiology*. 4. New York: McGraw-Hill. 2013, p. 11–25. ISBN 0-83-858529-9.

NICOLAS, P. and EL AMRI, C. The dermaseptin superfamily: A gene-based combinatorial library of antimicrobial peptides. *Biochimica et Biophysica Acta - Biomembranes*. 2009, vol. 1788, iss. 8, p. 1537–1550. DOI 10.1016/j.bbamem.2008.09.006.

NICOLAS, P. and LADRAM, A. Dermaseptins. In: NICOLAS, Pierre and LADRAM, Ali (eds.), *Handbook of Biologically Active Peptides*. 2. Elsevier. 2013, p. 350–363. ISBN 9780123850959. Available from: http://dx.doi.org/10.1016/B978-0-12-385095-9.00050-6

NIKAIDO, H. Molecular Basis of Bacterial Outer Membrane Permeability Revisited. *Microbiology and molecular biology reviews*. 2003, vol. 67, iss. 4, p. 593–656. DOI 10.1128/MMBR.67.4.593–656.2003. Uložené v priečinku Knihy - Mikrobiológia

OHVO-REKILÄ, H., RAMSTEDT, B., LEPPIMÄKI, P. and SLOTTE, J.P. Cholesterol interactions with phospholipids in membranes. *Progress in Lipid Research*. 2002, vol. 41, iss. 1, p. 66–97. DOI 10.1016/S0163-7827(01)00020-0.

OLSON, F., HUNT, C.A., SZOKA, F.C., VAIL, W.J. and PAPAHADJOPOULOS, D. Preparation of liposomes of defined size distribution by extrusion through polycarbonate membranes. *BBA - Biomembranes*. 1979, vol. 557, iss. 1, p. 9–23. DOI 10.1016/0005-2736(79)90085-3.

ORTH, M. and BELLOSTA, S. Cholesterol: Its regulation and role in central nervous system disorders. *Cholesterol*. 2012, vol. 2012, p. 19. DOI 10.1155/2012/292598.

PATEL, H., TSCHEKA, C. and HEERKLOTZ, H. Characterizing vesicle leakage by fluorescence lifetime measurements. *Soft Matter*. 2009, vol. 5, iss. 15, p. 2849. DOI 10.1039/b908524f.

PEDERSEN, J.S. Analysis of small-angle scattering data from colloids and polymer solutions: modeling and least-squares fitting. *Advances in Colloid and Interface Science*. 1997, vol. 70, p. 171–210. DOI 10.3138/9781442674417.

POON, W.C.. K. and ANDELMAN, D. *Soft Condensed Matter Physics in Molecular and Cell Biology*. Boca Raton: CRC Press, 2006. ISBN 0-7503-1023-5.

POUNY, Y., RAPAPORT, D., MOR, A., NICOLAS, P. and SHAI, Y. Interaction of antimicrobial dermaseptin and its fluorescently labeled analogues with phospholipid membranes. *Biochemistry*. 1992, vol. 31, iss. 49, p. 12416–12423. DOI 10.1021/bi00164a017.

POWERS, J.-P.S. and HANCOCK, R.E.W. The relationship between peptide structure and antibacterial activity. *Peptides*. 2003, vol. 24, iss. 11, p. 1681–1691. DOI 10.1016/j.peptides.2003.08.023.

POZO NAVAS, B., LOHNER, K., DEUTSCH, G., SEVCSIK, E., RISKE, K.A., DIMOVA, R., GARIDEL, P. and PABST, G. Composition dependence of vesicle morphology and mixing properties in a bacterial model membrane system. *Biochimica et Biophysica Acta - Biomembranes*. 2005, vol. 1716, iss. 1, p. 40–48. DOI 10.1016/j.bbamem.2005.08.003.

PULLMANNOVÁ, P., BASTOS, M., BAI, G., FUNARI, S.S., LACKO, I., DEVÍNSKY, F., TEIXEIRA, J. and UHRÍKOVÁ, D. The ionic strength effect on the DNA complexation by DOPC — gemini surfactants liposomes. *Biophysical Chemistry*. 2012, vol. 160, p. 35–45. DOI 10.1016/j.bpc.2011.09.002.

PYNN, R. Neutron Scattering - A Non-destructive Microscope for Seeing Inside Matter. In: LIANG, L., RINALDI, R. and SCHOBER, H. (eds.), *Neutron Applocations in Earth, Energy and Environmental sciences*. 2009, p. 15–36. ISBN 978-0-387-09415-1.

QUINN, P.J. Membranes as Targets of Antimicrobial Lipids. In: THORMAR, H. (ed.), *Lipids and Essential Oils as Antimicrobial Agents*. 1. Chichester: Wiley. 2011, p. 1–24. ISBN 9780470741788.

RAND, R.P., FULLER, N., PARSEGIAN, V.A. and RAU, D.C. Variation in Hydration Forces between Neutral Phospholipid Bilayers: Evidence for Hydration Attraction. *Biochemistry*. 1988, vol. 27, iss. 20, p. 7711–7722. DOI 10.1021/bi00420a021.

REHAL, R.P., MARBACH, H., HUBBARD, A.T.M., SACRANIE, A.A., SEBASTIANI, F., FRAGNETO, G. and HARVEY, R.D. The influence of mild acidity on lysyl-phosphatidylglycerol biosynthesis and lipid membrane physico-chemical properties in methicillin-resistant Staphylococcus aureus. *Chemistry and Physics of Lipids*. 2017, vol. 206, p. 60–70. DOI 10.1016/j.chemphyslip.2017.06.007.

ROCHE, H.M. Unsaturated fatty acids. *Proceedings of the Nutrition Society*. 1999, vol. 58, p. 397–401. DOI 10.1017/S002966519900052X.

RUBINSON, K.A. Practical corrections for p(H,D) measurements in mixed H2O/D2O biological buffers. *Analytical Methods*. 2017, vol. 9, iss. 18, p. 2744–2750. DOI 10.1039/c7ay00669a.

RUIZ, J., GONI, F.M. and ALONSO, A. Surfactant-induced release of liposomal contents. A survey of methods and results. *BBA - Biomembranes*. 1988, vol. 937, iss. C, p. 127–134. DOI 10.1016/0005-2736(88)90234-9.

SALDITT, T., LI, C. and SPAAR, A. Structure of antimicrobial peptides and lipid membranes probed by interface-sensitive X-ray scattering. *Biochim Biophys Acta*. 2006, vol. 1758, p. 1483–1498. DOI 10.1016/j.bbamem.2006.08.002.

SAVOIA, D., DONALISIO, M., CIVRA, A., SALVADORI, S. and GUERRINI, R. In vitro activity of dermaseptin S1 derivatives against genital pathogens. *Apmis*. 2010, vol. 118, iss. 9, p. 674–680. DOI 10.1111/j.1600-0463.2010.02637.x.

SAVOIA, D., GUERRINI, R., MARZOLA, E. and SALVADORI, S. Synthesis and antimicrobial activity of dermaseptin S1 analogues. *Bioorganic and Medicinal Chemistry*. 2008, vol. 16, iss. 17, p. 8205–8209. DOI 10.1016/j.bmc.2008.07.032.

SCHLAME, M., REN, M., XU, Y., GREENBERG, M.L. and HALLER, I. Molecular symmetry in mitochondrial cardiolipins. *Chemistry and Physics of Lipids*. 2005, vol. 138, iss. 1–2, p. 38–49. DOI 10.1016/j.chemphyslip.2005.08.002.

SCHMITT, T., LANGE, S., DOBNER, B., SONNENBERGER, S., HAUSS, T. and NEUBERT, R.H.H. Investigation of a CER[NP]- and [AP]-Based Stratum Corneum Modeling Membrane System: Using Specifically Deuterated CER Together with a Neutron Diffraction Approach. *Langmuir*. 2018, vol. 34, p. 1742–1749. DOI 10.1021/acs.langmuir.7b01848.

SCHNITZER, E., KOZLOV, M.M. and LICHTENBERG, D. The effect of cholesterol on the solubilization of phosphatidylcholine bilayers by the non-ionic surfactant Triton X-100. *Chemistry and Physics of Lipids*. 2005, vol. 135, iss. 1, p. 69–82. DOI 10.1016/j.chemphyslip.2005.02.002.

SEBASTIANI, F., HARVEY, R., KHANNICHE, S., ARTERO, J.-B., HAERTLEIN, M. and FRAGNETO, G. Diffraction studies on natural and model lipid bilayers. *The European Physical Journal Special Topics*. 2012, vol. 213, iss. 1, p. 355–365. DOI 10.1140/epjst/e2012-01682-3.

SEKAR, P.C. and RAJASEKARAN, R. Could Dermaseptin Analogue be a Competitive Inhibitor for ACE2 Towards Binding with Viral Spike Protein Causing COVID19?: Computational Investigation. *International Journal of Peptide Research and Therapeutics*. 2021, vol. 27, iss. 2, p. 1043–1056. DOI 10.1007/s10989-020-10149-w.

ŠERŠEŇ, F., GABUNIA, G., KREJČÍROVÁ, E. and KRÁĽOVÁ, K. The relationship between lipophilicity of N-alkyl-N,N-dimethylamine oxides and their effects on the thylakoid membranes of chloroplasts. *Photosynthetica*. 1992, vol. 26, p. 205–212.

SHAI, Y. Mode of action of membrane active antimicrobial peptides. *Biopolymers - Peptide Science Section*. 2002, vol. 66, iss. 4, p. 236–248. DOI 10.1002/bip.10260.

SILHAVY, T.J., KAHNE, D. and WALKER, S. The bacterial cell envelope. *Cold Spring Harbor perspectives in biology*. 2010, vol. 2, iss. 5. DOI 10.1101/cshperspect.a000414.

SILVA, T., CLARO, B., SILVA, B.F.B., VALE, N., GOMES, P., GOMES, M.S., FUNARI, S.S., TEIXEIRA, J., UHRÍKOVÁ, D. and BASTOS, M. Unravelling a Mechanism of Action for a Cecropin A-Melittin Hybrid Antimicrobial Peptide: The Induced Formation of Multilamellar Lipid Stacks. *Langmuir*. 2018, vol. 34, iss. 5, p. 2158–2170. DOI 10.1021/acs.langmuir.7b03639.

SIMONS, K. and IKONEN, E. Functional rafts in cell membranes. *Nature*. 1997, vol. 387, iss. 6633, p. 569–72. DOI 10.1038/42408.

SIMONS, K. and VAZ, W.L.C. Model systems, lipid rafts, and cell membranes. *Annual Review of Biophysics and Biomolecular Structure*. 2004, vol. 33, p. 269–295. DOI 10.1146/annurev.biophys.32.110601.141803.

SINGER, S.J. and NICOLSON, G.L. The fluid mosaic model of the structure of cell membranes. *Science*. 1972, vol. 175, p. 720–731. DOI 10.1017/CBO9781107415324.004.

SKJEVIK, Å.A., MADEJ, B.D., DICKSON, C.J., LIN, C., TEIGEN, K., WALKER, R.C. and GOULD, I.R. Simulation of lipid bilayer self-assembly using all-atom lipid force fields. *Physical Chemistry Chemical Physics*. 2016, vol. 18, iss. 15, p. 10573–10584. DOI 10.1039/c5cp07379k.

SOLOVIEV, A.G., SOLOVJEVA, T.M., IVANKOV, O., SOLOVIOV, D. V., ROGACHEV, A. V. and KUKLIN, A.I. SAS program for two-detector system: seamless curve from both detectors. *Journal of Physics: Conf. Series*. 2017, vol. 848, p. 1–7. DOI 10.1088/1742-6596/848/1/012020.

SOT, J., COLLADO, M.I., ARRONDO, J.L.R., ALONSO, A. and GONI, F.M. Triton X-100-resistant bilayers: Effect of lipid composition and relevance to the raft phenomenon. *Langmuir*. 2002, vol. 18, iss. 7, p. 2828–2835. DOI 10.1021/la011381c.

TRISTRAM-NAGLE, S. *Preparation of oriented, fully hydrated lipid samples for structure determination using X-ray scattering*. 2007. ISBN 1597455199.

UHRÍKOVÁ, D. Biologické membrány a fosfolipidová dvojvrstva. In: UHRÍKOVÁ, Daniela (ed.), *Biofyzika – Vybrané kapitoly*. 1. Bratislava: Univerzita Komenského v Bratislave. 2015, p. 1–28. ISBN 978-80-223-3800-4.

UHRÍKOVÁ, D., KUČERKA, N., ISLAMOV, A., GORDELIY, V. and BALGAVÝ, P. Small-angle neutron scattering study of N-dodecyl-N,N-dimethylamine N-oxide induced solubilization of dioleoylphosphatidylcholine bilayers in liposomes. *General Physiology and Biophysics*. 2001, vol. 20, iss. 2, p. 183–189.

VALEUR, B. *Molecular fluorescence: Principles and Applications*. 1. Weinheim: Wiley, 2002. ISBN 3-527-29919-X.

VAN MEER, G., VOELKER, D.R. and FEIGENSON, G.W. Membrane lipids: where they are and how they behave. *Nature Reviews Molecular Cell Biology*. 2009, vol. 9, iss. 2, p. 112–124. DOI 10.1038/nrm2330.Membrane.

VAN SWAAY, D. and DEMELLO, A. Microfluidic methods for forming liposomes. *Lab on a Chip*. 2013, vol. 13, iss. 5, p. 752. DOI 10.1039/c2lc41121k.

VANOUNOU, S., PAROLA, A.H. and FISHOV, I. Phosphatidylethanolamine and phosphatidylglycerol are segregated into different domains in bacterial membrane. A study with pyrene-labelled phospholipids. *Molecular Microbiology*. 2003, vol. 49, iss. 4, p. 1067–1079. DOI 10.1046/j.1365-2958.2003.03614.x. Membránové domény

VOET, D. and VOET, J.G. *Biochemistry*. 4. New York: Wiley, 2010. ISBN 978-0-470-91745-9.

VOLLMER, W., BLANOT, D. and DE PEDRO, M.A. Peptidoglycan structure and architecture. *FEMS Microbiology Reviews*. 2008, vol. 32, iss. 2, p. 149–167. DOI 10.1111/j.1574-6976.2007.00094.x.

WILLIS, B.T.M. and CARLILE, C.J. *Experimental neutron scattering*. 1st. Oxford: Oxford University Press, 2009. ISBN 978-0-19-967377-3.

ZASLOFF, M. Antimicrobial peptides of multicellular organisms. *Nature*. 2002, vol. 415, p. 389–395. DOI 10.1038/415389a.

ŽELINSKÁ, K., GALLOVÁ, J., HULÁKOVÁ, S., UHRÍKOVÁ, D. and IVANKOV, O. Solubilisation of model membrane by DDAO surfactant – partitioning, permeabilisation and liposome-micelle transition. *General physiology and biophysics*. 2020, vol. 39, p. 107–122. DOI 10.4149/gpb_2019056.

https://avantilipids.com/product-category/natural-lipids/extracts, [12.4.2022]

https://www.sasview.org/docs/user/qtgui/Perspectives/Fitting/models/index.html, [12.4.2022].